Molecular Diagnostics of Uncommon Soft Tissue and Bone Tumors

Song, Wangzhao

DOI:
10.33612/diss.127007579

Molecular Diagnostics of Uncommon Soft Tissue and Bone Tumors

Wangzhao Song

Cover design Wangzhao Song
Layout Wangzhao Song
Print Gildeprint
ISBN: 978-94-034-2713-3 (print)
ISBN: 978-94-034-2714-0 (digital)

The PhD project was financially supported by:
China Scholarship Council (201606940023)
Graduate School of Medical Sciences of the University of Groningen

Printing of this thesis was supported by:
University of Groningen

university of groningen

Molecular Diagnostics of Uncommon Soft Tissue and Bone Tumors

PhD thesis

to obtain the degree of PhD at the
University of Groningen
on the authority of the
Rector Magnificus Prof. C. Wijmenga
and in accordance with
the decision by the College of Deans.

This thesis will be defended in public on

Wednesday 17 June 2020 at 11.00 hours

by

Wangzhao Song

born on 16 March 1989
in Henan, China

Supervisors

Prof. A.J.H. Suurmeijer

Prof. J.V.M.G. Bovée

Assessment Committee

Prof. P. Van Der Valk

Prof. W.N.M. Dinjens

Prof. H. Hollema

Paranymphs

Pei Meng

Geok Wee Tan

Contents

Chapter 1

General introduction

Chapter 1

General introduction

Tumors arising in soft tissue and bone (STB) locations comprise a very heterogeneous group of tumors of mesenchymal or neuroectodermal origin. Although STB tumors may occur in many different anatomic locations, they are more common in the extremities. STB tumors are classified according to histologic differentiation, e.g. resembling cells in fatty tissue, smooth or striated muscle, blood or lymph vessels, peripheral nervous system, cartilage and bone. The 2013 World Health Organization (WHO) classification of soft tissue tumors[1] recognizes more than 60 benign tumors, 30 intermediate (locally aggressive or rarely metastasizing) tumors and 50 malignant tumors. According to biological behavior, bone tumor categories include 20 benign tumors, 10 tumors with intermediate behavior and 28 malignant tumors. The frequent histological types of soft tissue sarcoma include pleomorphic undifferentiated sarcoma, myxofibrosarcoma, liposarcoma and leiomyosarcoma. The more common malignant bone tumors include chondrosarcoma, osteosarcoma, and Ewing sarcoma.

A. Epidemiology of STB tumors

Tumors arising in soft tissue and bone (STB) are rare. The true incidence of benign STB tumors (e.g. soft tissue lipoma and skeletal chondroma) is unknown[2,3], because these lesions are often asymptomatic and remain untreated. Malignant soft tissue and bone tumors, the sarcomas, are very rare. The relative proportion of soft tissue sarcomas is about 1% of all adult malignancies and 20% of all pediatric malignancies[4]. Bone sarcomas are even more uncommon and account for only 0.2% of all neoplasms[2]. In 2018, 744 new cases of soft tissue sarcoma and 205 new cases of bone sarcoma were diagnosed in the Netherlands[5] (Figure 1). Compared to new cases of invasive breast cancer (14963) and lung cancer (13262), the incidence of malignant STB tumors is very low and only slightly increasing over the past ten years.

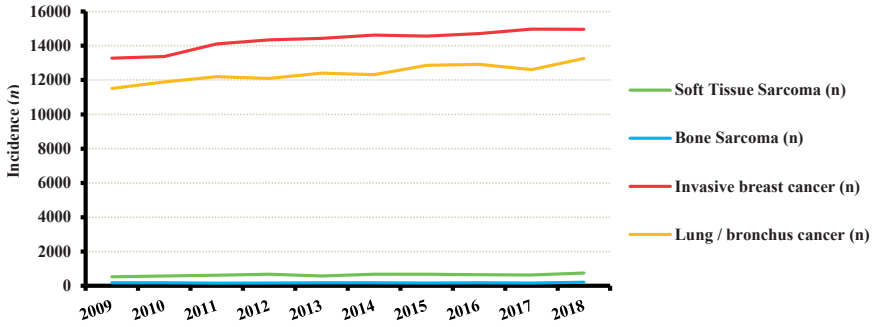

Figure 1. Incidence of STB tumors, breast and lung cancer in the Netherlands (www.iknl.nl)

Table 1. Incidence of STB sarcoma in the Netherlands 2009-2018 (www.iknl.nl)

Year	Soft Tissue Sarcoma (*n*)	Bone Sarcoma (*n*)
2009	522	175
2010	566	168
2011	620	153
2012	677	164
2013	576	171
2014	677	174
2015	670	162
2016	644	177
2017	636	166
2018	744	205

B. Clinical presentation of STB tumors

The large majority of benign soft tumors are relatively small and superficial tumors that arise in dermis and subcutis. In contrast, deep-seated and large (> 5 cm) tumors more likely represent soft tissue sarcoma. More than half of all soft tissue sarcomas occur in the extremities, especially in the thigh. Figure 2 recapitulates the anatomical distribution of soft tissue tumors. Soft tissue sarcomas usually present in adults and elderly. Certain soft tissue sarcomas are more typically or only encountered in the pediatric age group, e.g. embryonal and alveolar rhabdomyosarcoma and infantile fibrosarcoma. The most common benign soft tissue tumor is lipoma, the most common sarcoma is liposarcoma[6,7 8-10].

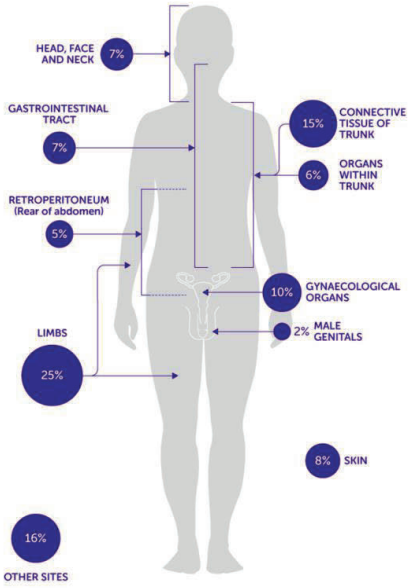

Figure 2. Soft tissue sarcoma incidence by anatomical site (source: https://www.cancerresearchuk.org)

Bone tumors may occur in many different bone types, although long bones are most commonly affected. About half of all malignant bone tumors occur around the knee. Within a long tubular bone, e.g. the femur or tibia, each bone tumor has a more or less specific site of origin. Thus, Ewing sarcoma usually involves the diaphysis, whereas conventional osteosarcoma normally originates in the metaphysis[1,11]. Figure 3 depicts the common spatial distribution of several benign and malignant bone tumors when occurring in a long bone. Some bone tumors have a predilection for a certain age group. Giant cell tumor of bone, for instance is exceptionally rare before puberty. The age-specific incidence rates of osteosarcomas have a bimodal distribution, with a first peak in the second decade of life and a second peak in elderly people older than 60 years of age. Osteochondroma and enchondroma are the most frequently benign bone tumors. Chondrosarcoma is the most common malignant bone tumor and accounts for one-third of all malignant bone neoplasms[2]. Bone sarcoma (like soft tissue sarcoma) is slightly more common in males than females[2,12,13].

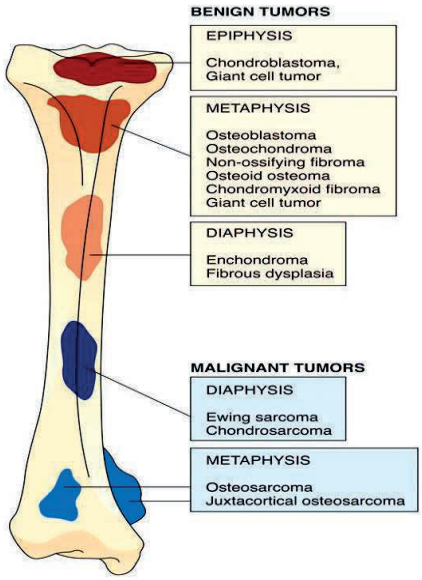

Figure 3. The anatomical location of bone tumors within a long bone (source: Rubin's Pathology: Rubin's Pathology: Clinicopathologic Foundations of Medicine, 6th edition, Figure 26-38).

C. Diagnosis of STB tumors

Imaging studies, in particular computer tomography (CT) and magnetic resonance imaging (MRI) are of paramount importance during the work-up of a STB tumor. In soft tissue tumors, MRI may be of great value in deciphering tumor tissue composition and, thus, diagnose fatty tumors or myxoid tumors. In bone tumors, matrix deposition (cartilage or bone matrix) may become evident with CT scanning. In malignant STB tumors imaging also provides information about tumor size and tumor location, in addition to extent of invasion, an important issue for treatment decisions, e.g. (limb-salvage or joint-sparing) surgery.

To render a histopathological diagnosis, the next step is to take histological biopsies ("tissue is the issue"). Nowadays, histological needle biopsies are routinely taken during the work-up of (large) STB tumors. A complete excision may be considered with small and superficial tumors. Using routine hematoxylin and eosin stained microscopic slides, even pathologists with special interest and expertise in STB pathology, are faced with a great challenge to arrive at an accurate diagnosis, since STB tumors display a wide

spectrum of overlapping microscopic features[14]. In general, the goal in STB pathology is to identify the tumor cell-type or cell-lineage, e.g. adipocytic soft tissue tumors or cartilaginous bone tumors. In this respect, immunohistochemical (IHC) detection of certain proteins and transcription factors is an indispensable tool. Some STB tumors harbor relatively specific IHC markers, e.g. MDM2 and CDK4 overexpression in well differentiated / dedifferentiated liposarcoma or mutated histone protein (H3G34W) in giant cell tumor of bone. However, even when applying diagnostic marker panels with IHC, many tumors may show nonspecific, overlapping or absent marker expression[8,15,16]. In this scenario, the morphologic appearance of a tumor becomes descriptive, e.g. a STB tumor with benign or malignant cytomorphology and spindle cell, round cell, epithelioid or pleomorphic features[17].

D. Examples illustrating the importance of molecular pathology in diagnosis and therapy of STB tumors

Scientific advances often drive medical science. In the past decades, advances in the field of molecular genetics have translated into several diagnostic tests, in particular reverse transcriptase polymerase chain reaction (RT-PCR), fluorescence in situ hybridization (FISH), and (targeted) next generation sequencing (NGS). With these novel molecular techniques, gene fusions and mutations were discovered in many tumor types. Fortunately, many new fusion genes proved to be specific for a certain STB tumor. Examples of more recently discovered and diagnostically important molecular genetic abnormalities are *VGLL2* or *NCOA2*-related fusions in spindle cell rhabdomyosarcomas, a tumor with relatively favorable clinical outcome, when compared to other types of rhabdomyosarcoma[18,19], and *EML4-ALK* gene fusions in inflammatory myofibroblastic tumors (IMT), allowing therapy with ALK inhibitors[20]. As studied in this thesis *CTNNB1* gene mutations may assist in discriminating (benign) desmoplastic fibroma from low-grade malignant central osteosarcoma[21]. Another novel finding is the presence of neurotrophic tropomyosin-related kinase (*NTRK*) fusion genes in solid tumors. Unfortunately, *NTRK* rearrangements are very rare in (spindle cell) sarcomas[22] (<5%, except for infantile fibrosarcoma, with *ETV6-NTRK3)*[14,23]. Importantly, tumors with *NTRK* fusions often respond to the blocking agent Larotrectinib. FISH or RT-

PCR are the most cost-effective methods to detect of *NTRK* fusions[22]. Alternatively, a two-step strategy may be applied, using IHC to screen for *NTRK* expression followed by NGS to validate gene partners. Technically, each method has its limitations in daily practice, and awareness of their mechanisms, sensitivity, specificity, cost and turn-around time, as summarized in Table 2.

Table 2. Comparison of 5 molecular tests for the detection of *NTRK* fusions

Method	Sensitivity	Specificity	Detection of all fusion genes	Detection of gene partner	Detection of (gene) expression	Cost	Turn-around time (days)
IHC	High[1]	High[2]	Yes	No	Yes	Low	1-2
FISH	High	High	One per probe	No	No	Low	5-8
NanoString	Unknown[3]	Unknown[4]	One per probe	Yes	No	Low	1-3
RT-PCR	High	High	One per probe	Yes	No	Low	5-8
RNA seq NGS	High	High	Yes	Yes	Yes	High	5-10

1: False negatives with *NTRK3* fusions[24,25]. 2: lacking smooth muscle differentiation. 3-4: no data.

Needless to say, an accurate histopathological diagnosis of STB tumors is key in medical management. Treatment decisions (surgery, radiotherapy, chemotherapy or targeted therapy) heavily rely on a proper pathological diagnosis. It has been suggested that the design of clinical trials for soft tissue tumors should based on specific genetic abnormalities[26]. Noteworthy, in several STB tumors, treatment strategy had to be adjusted after including molecular findings in diagnostics[27,28]. As a consequence, some patients did not benefit from (unnecessary) chemotherapy, whereas others were prescribed targeted therapy. For instance, the small-molecule *ALK* inhibitor crizotinib has a durable respons IMT[29,30] , the *PDGFB* inhibitor imatinib reduces tumor size and may improve surgical outcome in dermatofibrosarcoma protuberans[31,32] (DFSP), and the emerging selective *TRK* inhibitor larotrectinib for (soft tissue tumors) with *NTRK* fusions[33].

E. Molecular pathology and tumor prognostication

In general, the prognosis of STB tumors (in terms of overall survival) related to tumor type, tumor grade, and tumor stage. In addition to tumor typing, tumor grading is mandatory for treatment decisions. Interestingly, at the DNA level, the CINSARC gene expression signature may serve as a novel prognostic tool. In soft tissue sarcomas, CINSARC proved to be superior to FNCLCC tumor grading[34-39]. The genes

in the CINSARC profile are involved in chromosome biogenesis, mitosis control or chromosome segregation, mechanisms that play a vital role in tumorigenesis. Some ongoing projects are aiming at optimization of molecular techniques for application of CINSARC with STB tumors[34,39].

F. Techniques applied for the diagnosis of STB tumors (Part 1 of this thesis)

The diagnosis of STB tumors depends on examination of adequate histologic (needle) biopsies. Cytology (in combination with imaging studies) is only used in very few sarcoma centers around the world. However, cytology can be an accurate method in certain circumstances[40,41]. First, to diagnose recurrent or metastatic sarcoma when the primary diagnosis has been already established; Second, e.g. with mediastinal or retroperitoneal tumors, when fine-needle aspiration cytology (FNAC) is assisted by ultrasound in combination with endoscopy (EUS-FNA), cytology can be applied with a cell block method, which allows the study of minibiopsies by routine H&E staining, IHC staining, and molecular analysis. In **Chapter 2**, we studied the value of the Cellient™ cell block method, studying a cohort of 20 STB tumors. Pros and cons of different cell block techniques were studied in the literature and discussed. This is the first study applying the Cellient™ cell block method for the successful diagnosis of STB tumors.

At the genetic level, STB tumors can be divided into two separate categories[16,42]. The first group of STB tumors has complex genetic alterations, thought to occur after chromothripsis, whereas the second group harbors (often specific) gene mutations and translocations. As discussed earlier (see Table 2), several molecular techniques are available to detect these genetic abnormalities in STB tumors. In **Chapter 3** we studied the accuracy of the NanoString nCounter platform for the investigation of 174 fusion variants in 104 soft tissue tumors (22 histologic types). NanoString results were compared with FISH, RT-PCR or Archer NGS, when available. The Nanostring hybridization method uses RNA probes that recognize specific gene fusion sites. Three target-specific probes are included in the system: a capture probe, a reporter probe and a protector probe. After hybridization, labeled barcodes can be automatically calculated with the nCounter® Digital Analyzer. Thus, amplification steps are not necessary. Moreover, Nanostring can be applied with FFPE material and requires only very small amounts (100 ng) of RNA input for

analysis[43,44]. Multiple fusion genes can be detected in a single run, a laborsaving and cost-effective approach. As such, NanoString has high sensitivity and is technically reproducible and reliable.

G. Examples illustrating molecular techniques in the diagnosis of rare STB tumors (Part 2 of this thesis)

C**hapter 4** contains a review article on myoepithelial tumors (MET) of bone (BMET). (B)MET represent a rare group of STB tumors with highly variable morphology and clinical behavior. Therefore, (B)MET nicely illustrate the challenge for (expert) pathologists face in daily diagnostic work, trying to arrive at a correct diagnosis. Microscopically, the appearance of tumor cells is highly diverse and include bland eosinophilic spindle cells, clear cells, epithelioid cells or plasmacytoid cells, which may be arranged in bundles, cohesive cell nests, cords or reticular formations, and embedded in myxohyaline stroma. By IHC, the (so-called) prototypical IHC staining profile of BMET consists of combined expression of cytokeratins and/or epithelial membrane antigen (EMA) together with S100 protein and/or glial fibrillary acidic protein (GFAP)[1]. Clearly, due to highly variable morphology and rather unspecific immunoprofile, the differential diagnosis of BMETs is broad. Moreover, only around half of all BMET harbor specific *EWSR1* (and rare *FUS*) gene fusions, which may assist in arriving at the correct diagnosis[45]. Thus, in half of the cases pathologists often cannot make a definitive conclusive diagnosis.

Among the many tumors considered in the differential diagnosis of (B)MET is ossifying fibromyxoid tumor (OFMT), a rare soft tissue neoplasm of unknown origin and intermediate malignant potential[46]. This tumor has a local recurrence rate of 10-20% and a low risk of metastatic disease (up to 2% of cases). Macroscopically, OFMT has a nodular architecture and thick fibrous capsule sometimes with a thin bone shell. Tumors cells may be spindle-shaped or oval / epithelioid, and are typically arranged in nests, sheets, cords or lace-like patterns, and surrounded by ample fibromyxoid stroma, hence its name. By IHC, most (typical) OFMTs display S100 and/or desmin expression[47]. OFMT is a translocation-positive soft tissue neoplasm. *PHF1* rearrangements have been detected in more than 80% cases with *EP400* as a partner in 44% of cases[48]. In a collaborative international study described in **Chapter 5** of this thesis, we performed

RNA sequencing (RNA seq) and/or FISH in a small cohort of selected cases of OFMT with an unusual IHC profile and *PHF1* rearrangements, but lacking a known gene partner. We identified a novel *PHF1-TFE3* fusion, an observation that was recently confirmed by another research group[49].

In **Chapter 6**, we discuss the rare soft tissue aneurysmal bone cyst (STABC) in a small series from the archives of the Dutch Committee for Bone Tumors. In bone, ABC represents a benign but expansile tumor that mainly affects young adult patients. ABC may occur in any bone, but usually presents in the metaphysis of long tubular bones or the posterior part of vertebrae. Like many bone tumors, ABC also has a soft tissue counterpart. Only up to 30 STABC cases were reported in the English literature to date and in only 6 cases imaging details have been provided in the literature. The morphology of STABC may overlap with myositis ossificans. In a study of six new cases, we evaluated imaging results and histopathological features. FISH and/or anchored multiplex PCR-based targeted NGS (Archer) were applied to study the presence of genetic alterations (USP6 fusion genes).

In **Chapter 7** we elaborate on the differential diagnosis of two morphologic mimickers in bone pathology, namely desmoplastic fibroma (DF) of bone and low-grade central osteosarcoma. DF is a very rare, locally aggressive bone tumor. DF incidence was calculated to be only 0.003%[50] (in a cohort of 4692 cases). With respect to clinicopathologic features, morphologic features and imaging features, DF strongly resembles low-grade central osteosarcoma (LGCOS). Both tumors may present in one of the long bones. Histologically, both consist of spindle-shaped cells with abundant collagenous tissue. By IHC, DF may show nuclear staining of beta-catenin. Overexpression of MDM2 and CDK4 may be found in LGCOS.

References

1. Fletcher CDM, Bridge JA, Hogendoorn PCW, Mertens F, eds. *WHO classification of tumours of soft tissue and bone*. Lyon, France: IARC Press; 2013.
2. Franchi A. Epidemiology and classification of bone tumors. *Clin Cases Miner Bone Metab.* 2012;9(2):92-95.

3. Church DJ, Krumme J, Kotwal S. Evaluating Soft-Tissue Lumps and Bumps. *Mo Med.* 2017;114(4):289-294.
4. Corey RM, Swett K, Ward WG. Epidemiology and survivorship of soft tissue sarcomas in adults: a national cancer database report. *Cancer Med.* 2014;3(5):1404-1415.
5. www.iknl.nl.
6. Kransdorf MJ. Benign soft-tissue tumors in a large referral population: distribution of specific diagnoses by age, sex, and location. *AJR Am J Roentgenol.* 1995;164(2):395-402.
7. Katenkamp K, Katenkamp D. Soft tissue tumors: new perspectives on classification and diagnosis. *Dtsch Arztebl Int.* 2009;106(39):632-636.
8. Oda Y, Yamamoto H, Kohashi K, et al. Soft tissue sarcomas: From a morphological to a molecular biological approach. *Pathol Int.* 2017;67(9):435-446.
9. Fletcher CD. The evolving classification of soft tissue tumours: an update based on the new WHO classification. *Histopathology.* 2006;48(1):3-12.
10. Sbaraglia M, Dei Tos AP. The pathology of soft tissue sarcomas. *Radiol Med.* 2019;124(4):266-281.
11. Muscolo DL, Campaner G, Aponte-Tinao LA, Ayerza MA, Santini-Araujo E. Epiphyseal primary location for osteosarcoma and Ewing sarcoma in patients with open physis. *J Pediatr Orthop.* 2003;23(4):542-545.
12. Rosenberg AE. Bone Sarcoma Pathology: Diagnostic Approach for Optimal Therapy. *Am Soc Clin Oncol Educ Book.* 2017;37:794-798.
13. Jackson TM, Bittman M, Granowetter L. Pediatric Malignant Bone Tumors: A Review and Update on Current Challenges, and Emerging Drug Targets. *Curr Probl Pediatr Adolesc Health Care.* 2016;46(7):213-228.
14. Mertens F, Antonescu CR, Mitelman F. Gene fusions in soft tissue tumors: Recurrent and overlapping pathogenetic themes. *Genes Chromosomes Cancer.* 2016;55(4):291-310.

15. Puls F, Niblett AJ, Mangham DC. Molecular pathology of bone tumours: diagnostic implications. *Histopathology.* 2014;64(4):461-476.

16. Marino-Enriquez A, Bovee JV. Molecular Pathogenesis and Diagnostic, Prognostic and Predictive Molecular Markers in Sarcoma. *Surg Pathol Clin.* 2016;9(3):457-473.

17. Cloutier JM, Charville GW. Diagnostic classification of soft tissue malignancies: A review and update from a surgical pathology perspective. *Curr Probl Cancer.* 2019;43(4):250-272.

18. Mosquera JM, Sboner A, Zhang L, et al. Recurrent NCOA2 gene rearrangements in congenital/infantile spindle cell rhabdomyosarcoma. *Genes Chromosomes Cancer.* 2013;52(6):538-550.

19. Alaggio R, Zhang L, Sung YS, et al. A Molecular Study of Pediatric Spindle and Sclerosing Rhabdomyosarcoma: Identification of Novel and Recurrent VGLL2-related Fusions in Infantile Cases. *Am J Surg Pathol.* 2016;40(2):224-235.

20. Antonescu CR, Suurmeijer AJ, Zhang L, et al. Molecular characterization of inflammatory myofibroblastic tumors with frequent ALK and ROS1 gene fusions and rare novel RET rearrangement. *Am J Surg Pathol.* 2015;39(7):957-967.

21. Song W, van den Berg E, Kwee TC, et al. Low-grade central fibroblastic osteosarcoma may be differentiated from its mimicker desmoplastic fibroma by genetic analysis. *Clin Sarcoma Res.* 2018;8:16.

22. Marchio C, Scaltriti M, Ladanyi M, et al. ESMO recommendations on the standard methods to detect NTRK fusions in daily practice and clinical research. *Ann Oncol.* 2019;30(9):1417-1427.

23. Suurmeijer AJ, Dickson BC, Swanson D, et al. The histologic spectrum of soft tissue spindle cell tumors with NTRK3 gene rearrangements. *Genes Chromosomes Cancer.* 2019;58(11):739-746.

24. Hechtman JF, Benayed R, Hyman DM, et al. Pan-Trk Immunohistochemistry Is an Efficient and Reliable Screen for the Detection of NTRK Fusions. *Am J Surg Pathol.* 2017;41(11):1547-1551.

25. Rudzinski ER, Lockwood CM, Stohr BA, et al. Pan-Trk Immunohistochemistry Identifies NTRK Rearrangements in Pediatric Mesenchymal Tumors. *Am J Surg Pathol.* 2018;42(7):927-935.

26. Verweij J. Soft tissue sarcoma trials: one size no longer fits all. *J Clin Oncol.* 2009;27(19):3085-3087.

27. Yen CC, Chen TW. Next frontiers in systemic therapy for soft tissue sarcoma. *Chin Clin Oncol.* 2018;7(4):43.

28. Nakano K, Takahashi S. Current Molecular Targeted Therapies for Bone and Soft Tissue Sarcomas. *Int J Mol Sci.* 2018;19(3).

29. Theilen TM, Soerensen J, Bochennek K, et al. Crizotinib in ALK(+) inflammatory myofibroblastic tumors-Current experience and future perspectives. *Pediatr Blood Cancer.* 2018;65(4).

30. Gambacorti-Passerini C, Orlov S, Zhang L, et al. Long-term effects of crizotinib in ALK-positive tumors (excluding NSCLC): A phase 1b open-label study. *Am J Hematol.* 2018;93(5):607-614.

31. Allen A, Ahn C, Sangueza OP. Dermatofibrosarcoma Protuberans. *Dermatol Clin.* 2019;37(4):483-488.

32. Navarrete-Dechent C, Mori S, Barker CA, Dickson MA, Nehal KS. Imatinib Treatment for Locally Advanced or Metastatic Dermatofibrosarcoma Protuberans: A Systematic Review. *JAMA Dermatol.* 2019;155(3):361-369.

33. Doebele RC, Drilon A, Paz-Ares L, et al. Entrectinib in patients with advanced or metastatic NTRK fusion-positive solid tumours: integrated analysis of three phase 1-2 trials. *Lancet Oncol.* 2019.

34. Chibon F, Lesluyes T, Valentin T, Le Guellec S. CINSARC signature as a prognostic marker for clinical outcome in sarcomas and beyond. *Genes Chromosomes Cancer.* 2019;58(2):124-129.

35. Bertucci F, De Nonneville A, Finetti P, et al. The Genomic Grade Index predicts postoperative clinical outcome in patients with soft-tissue sarcoma. *Ann Oncol.* 2018;29(2):459-465.

36. Bertucci F, Finetti P, Monneur A, Birnbaum D. Pathological grade-independent prediction of chemosensitivity by CINSARC should rehabilitate adjuvant chemotherapy in soft tissue sarcomas of any grade. *Ann Oncol.* 2019;30(2):342-343.

37. Lesluyes T, Delespaul L, Coindre JM, Chibon F. The CINSARC signature as a prognostic marker for clinical outcome in multiple neoplasms. *Sci Rep.* 2017;7(1):5480.

38. Lesluyes T, Perot G, Largeau MR, et al. RNA sequencing validation of the Complexity INdex in SARComas prognostic signature. *Eur J Cancer.* 2016;57:104-111.

39. Le Guellec S, Lesluyes T, Sarot E, et al. Validation of the Complexity INdex in SARComas prognostic signature on formalin-fixed, paraffin-embedded, soft-tissue sarcomas. *Ann Oncol.* 2018;29(8):1828-1835.

40. Domanski HA. Fine-needle aspiration cytology of soft tissue lesions: diagnostic challenges. *Diagn Cytopathol.* 2007;35(12):768-773.

41. van Hemel BM, Suurmeijer AJ. Effective application of the methanol-based PreservCyt() fixative and the Cellient() automated cell block processor to diagnostic cytopathology, immunocytochemistry, and molecular biology. *Diagn Cytopathol.* 2013;41(8):734-741.

42. Lam SW, Cleton-Jansen AM, Cleven AHG, et al. Molecular Analysis of Gene Fusions in Bone and Soft Tissue Tumors by Anchored Multiplex PCR-Based Targeted Next-Generation Sequencing. *J Mol Diagn.* 2018;20(5):653-663.

43. Sheth J, Arnoldo A, Zhong Y, et al. Sarcoma Subgrouping by Detection of Fusion Transcripts Using NanoString nCounter Technology. *Pediatr Dev Pathol.* 2019;22(3):205-213.

44. Chang KTE, Goytain A, Tucker T, et al. Development and Evaluation of a Pan-Sarcoma Fusion Gene Detection Assay Using the NanoString nCounter Platform. *J Mol Diagn.* 2018;20(1):63-77.

45. Antonescu CR, Zhang L, Chang NE, et al. EWSR1-POU5F1 fusion in soft tissue myoepithelial tumors. A molecular analysis of sixty-six cases, including soft tissue, bone, and visceral lesions, showing common involvement of the EWSR1 gene. *Genes Chromosomes Cancer.* 2010;49(12):1114-1124.

46. Enzinger FM, Weiss SW, Liang CY. Ossifying fibromyxoid tumor of soft parts. A clinicopathological analysis of 59 cases. *Am J Surg Pathol.* 1989;13(10):817-827.

47. Folpe AL, Weiss SW. Ossifying fibromyxoid tumor of soft parts: a clinicopathologic study of 70 cases with emphasis on atypical and malignant variants. *Am J Surg Pathol.* 2003;27(4):421-431.

48. Gebre-Medhin S, Nord KH, Moller E, et al. Recurrent rearrangement of the PHF1 gene in ossifying fibromyxoid tumors. *Am J Pathol.* 2012;181(3):1069-1077.

49. Hofvander J , Jo VY, Fletcher CDM, et al. PHF1 Fusions Cause Distinct Gene Expression and Chromatin Accessibility Profiles in Ossifying Fibromyxoid Tumors and Mesenchymal Cells. *Mod Pathol.* doi:10.1038/s41379-020-0457-8.

50. Evans S, Ramasamy A, Jeys L, Grimer R. Desmoplastic fibroma of bone: A rare bone tumour. *J Bone Oncol.* 2014;3(3-4):77-79.

Part 1

Novel technology in diagnosis soft tissue and bone tumors

Chapter 2

Suitability of the Cellient™ cell block method for diagnosing soft tissue and bone tumors

This chapter is based on the publication: **Song W**, van Hemel BM, Suurmeijer AJH. Suitability of the Cellient™ cell block method for diagnosing soft tissue and bone tumors. Diagn Cytopathol. 2018 Apr;46(4):299-305.

Suitability of the Cellient™ cell block method for diagnosing soft tissue and bone tumors

W. Song MD | B. M. van Hemel MD | A. J. H. Suurmeijer MD, PhD

Department of Pathology and Medical Biology, University Medical Center Groningen, University of Groningen, P.O. Box 30.001, RB Groningen, 9700, The Netherlands

Correspondence
A. J. H. Suurmeijer, Department of Pathology and Medical Biology, University Medical Center Groningen, University of Groningen, P.O. Box 30.001, 9700RB Groningen, The Netherlands.
E-mail: a.j.h.suurmeijer@umcg.nl

Funding information
China Scholarship Council (CSC) program, Grant/Award Number: 201606940023

BACKGROUND: The diagnosis of tumors of soft tissue and bone (STB) heavily relies on histological biopsies, whereas cytology is not widely used. Cellient™ cell blocks often contain small tissue fragments. In addition to Hematoxylin and Eosin (H&E) interpretation of histological features, immunohistochemistry (IHC) can be applied after optimization of protocols. The objective of this retrospective study was to see whether this cytological technique allowed us to make a precise diagnosis of STB tumors.

METHODS: Our study cohort consisted of 20 consecutive STB tumors, 9 fine-needle aspiration (FNAC) samples, and 11 endoscopic ultrasonography (EUS) FNACs and included 8 primary tumors and 12 recurrences or metastases of known STB tumors.

RESULTS: In all 20 cases, H&E stained sections revealed that diagnostically relevant histological and cytological features could be examined properly. In the group of 8 primary tumors, IHC performed on Cellient™ material provided clinically important information in all cases. For instance, gastrointestinal stromal tumor (GIST) was positive for CD117 and DOG-1 and a PEComa showed positive IHC for actin, desmin, and HMB-45. In the group of 12 secondary tumors, SATB2 was visualized in metastatic osteosarcoma, whereas expression of S-100 was present in 2 secondary chondrosarcomas. Metastatic chordoma could be confirmed by brachyury expression. Two metastatic alveolar rhabdomyosarcomas were myf4 positive, a metastasis of a gynecologic leiomyosarcoma was positive for actin and estrogen receptor (ER) and a recurrent dermatofibrosarcoma protuberans expressed CD34.

CONCLUSION: In the proper clinical context, including clinical presentation with imaging studies, the Cellient™ cell block technique has great potential for the diagnosis of STB tumors.

KEYWORDS
cell block, Cellient, cytopathology, immunochemistry, soft tissue and bone tumors

1 | INTRODUCTION

Soft tissue and bone (STB) tumors are rare malignancies, which comprise approximately 2% of all neoplasms. Because of this low incidence, patients with STB tumors are usually referred to expert sarcoma centers, where multidisciplinary teams, according to well-established protocols and latest developments, can perform diagnostic procedures and treatment. The clinical diagnosis of primary STB tumors relies on imaging studies and an adequate biopsy. Imaging, in particular with computed tomography (CT) and magnetic resonance imaging (MRI), provides insight into the location, size, margins, and tissue composition and heterogeneity of STB tumors. Although cytology has been applied in just a few sarcoma centers,[1–7] the primary diagnosis of STB tumors is usually made on histological (needle or open) biopsies, since these malignancies are morphologically heterogeneous and several histological types have overlapping microscopic features. Moreover, for a conclusive diagnosis of STB tumors, additional immunohistochemistry (IHC) and molecular pathology (fluorescent in situ hybridization (FISH),

TABLE 1 The 20 STB tumors included in this study

Primary tumor	Localization	Material	Diagnostic antibodies	Diagnosis
1	Stomach	EUS	CD117, DOG1	GIST
2	Stomach	EUS	CD117, DOG1	GIST
3	Peripancreatic	EUS	CD117, DOG1	GIST
4	Stomach	EUS	DOG1	GIST
5	Rectum	EUS	CD117, DOG1	GIST
6	Pararectal	EUS	Beta-catenin	Desmoid fibromatosis
7	Rectum	EUS	Actin, desmin, HMB-45	PEComa
8	Retroperitoneum	EUS	Desmin, caldesmon, SMA	Leiomyosarcoma
Secondary tumor				Metastasis or recurrence of
1	Mediastinum	EUS	Desmin, ER	Uterine leiomyosarcoma
2	Pancreas	EUS	SATB2	Osteosarcoma of bone
3	Mediastinum	EUS	S-100	Chondrosarcoma of bone
4	Inguinal node	FNAC	Brachyury	Chordoma of sacrum bone
5	Inguinal node	FNAC	...	Pleomorphic sarcoma NOS
6	Orbit	FNAC	myf4	Alveolar rhabdomyosarcoma
7	Cheek	FNAC	myf4	Alveolar rhabdomyosarcoma
8	Neck	FNAC	...	Radiation-induced MPNST
9	Inguinal node	FNAC	...	Pleomorphic sarcoma NOS
10	Paranasal	FNAC	CD-34	Dermatofibrosarcoma (DFSP)
11	Hip	FNAC	S-100	Chondrosarcoma of bone
12	Supraclavicular	FNAC	...	Pleomorphic radiation sarcoma

Abbreviations: DFSP, dermatofibrosarcoma protuberans; GIST, gastrointestinal stromal tumor; MPNST, malignant peripheral nerve sheath tumor; NOS, not otherwise specified.

polymerase chain reaction (PCR), and next generation sequencing (NGS)) often have to be administered, requiring special expertise.

Typing and grading of STB tumors is mandatory for treatment decisions. In this clinical context, in our and most other sarcoma teams, cytology is only applied in selected cases. Firstly, in cases with an established diagnosis of the primary STB tumor, cytology can be effectively used to diagnose recurrent or metastatic sarcoma. Secondly, for deep-located STB tumors, cell material can be collected by fine-needle aspiration (FNAC) during endoscopic ultrasonography (EUS-FNA) or by endobronchial ultrasound-guided transbronchial needle aspiration (EBUS). In our sarcoma team there is ample experience with these techniques.[2,4,8] Compared with histological biopsies, it is more easy to sample different tumor areas with fine-needle aspiration (FNA), and this may result in increased diagnostic accuracy, in particular when dealing with STBs with heterogeneous features on clinical imaging (CT and MRI).

Several different cell block methods can be used to process cell material thus collected.[9] As an adjunct to routinely prepared smears or cell sediments, cytoblock techniques allow the application of IHC and molecular methods, expanding the diagnostic armamentarium. For this purpose, we and others[8,10–14] have used the Cellient™ automated cell block system, by which cytotechnicians can make an automated cell block within 1 hour, albeit with higher costs than that of traditional cell block techniques. As described previously, with the Cellient™ method, using methanol fixation instead of formalin, a broad array of diagnostically important antibodies can be applied to IHC after optimization of IHC protocols. In clinical cytology, the Cellient™ method has been used successfully for the characterization of tumor cells in serous fluids and FNAC material, for example, to characterize different carcinoma types or to diagnose metastatic melanoma.[12]

In this article, we report our first experience on the suitability of the Cellient™ method to diagnose several types of STB tumors, 8 primary lesions (5 of which were gastrointestinal stromal tumors) and 12 secondary recurrences or metastases, applying 9 diagnostically relevant antibodies that were not described in our earlier article of the Cellient™ method.

2 | MATERIAL AND METHODS

2.1 | Ethics statement

The study met the criteria of the code of conduct for responsible use of human tissue that is used in the Netherlands (Dutch federation of biomedical scientific societies; http://www.federa.org).

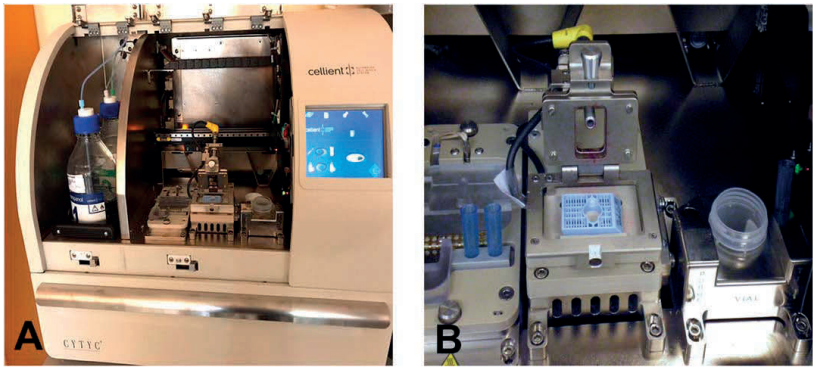

FIGURE 1 A closer look at the Cellient™ processor. Further details are found on the website: http://www.hologic.com/products/clinical-diagnostics/instrument-systems/cellient-automated-cell-block-system [Color figure can be viewed at wileyonlinelibrary.com]

2.2 | Cell samples

Cell samples of aspirations from soft tissue and bone tumors processed with the Cellient™ processor (Hologic, Marlborough, Massachusetts) between 2013 and 2016 were retrieved from the archives of the cytology laboratory of the pathology department of University Medical Center Groningen. Our cohort consisted of 20 consecutive cases, shown in Table 1, and included 12 EUS guided aspirations of deep-seated tumors (in the abdomen, retroperitoneal space, and mediastinum) and 9 FNAC specimens of superficial lesions. All but 1 EUS guided aspirations were performed with an EProCore needle (ECHO-HD-22-C; Echo Tip Ultra; Cook Medical, Bloomington, Indiana). In all EUS procedures and most FNAC aspirations, specimen cellularity had been checked on site by our cytotechnicians and in case of low cellularity, repeated aspirations were done. The study cohort comprised 16 soft tissue tumor cases (5 were gastrointestinal stromal tumors) and 4 bone tumor cases (2 chondrosarcomas and 2 osteosarcomas). For evaluation of diagnostic performance, the cohort was divided in 2 groups, 8 primary lesions, and 12 secondary lesions (metastases or recurrences of tumors of which the histologic diagnosis was known). Histologic follow-up was available for all primary tumors, allowing correlation of cytological and histological diagnosis.

2.3 | Cellient™ cell block technique

Before being loaded into the Cellient™ processor (Figure. 1A,B), materials were washed in 1 mL Cytolyt™ Wash, centrifuged at 1000 g for 5 minutes, dissolved in 20 mL PreservCyt™ fluid and fixed for 20 minutes. One drop of the cell sediment was used to

TABLE 2 The 14 antibodies applied with Cellient™ cell block specimens

Antibody	Clone type	Clone	Manufacturer	Dilution	Pretreatment
Actin-SMA	Monoclonal	1A4	Ventana	R.T.U	No
Beta-catenin	Monoclonal	14	Ventana	R.T.U	CC1 52 min
Brachyury	Monoclonal	EPR18113	Abcam	1:400	CC1 36 min
Caldesmon	Monoclonal	h-CD	Dako	1:800	No
CD-117	Polyclonal	C-KIT	Dako	1:100	No
CD-34	Monoclonal	QBEND10	Ventana	R.T.U	CC1 92 min
CK-AE1/3	Monoclonal	AE1/AE3	Ventana	R.T.U	CC1 36 min + protease 4 min
Desmin	Monoclonal	DE-R-11	Ventana	R.T.U	CC1 64 min
DOG1	Monoclonal	SP 31	Ventana	R.T.U.	no
ER	Monoclonal	SP-1	Ventana	R.T.U.	No
HMB-45	Monoclonal	HMB45	Ventana	R.T.U	No
myf-4	Monoclonal	LO26	Monosan	1:25	CC1 64 min
S-100	Monoclonal	4C4.9	Ventana	R.T.U	No
SATB2	Monoclonal	4B10	Abcam	1:100	CC1 64 min

CC1, cell conditioning solution (Ventana), pre-treatment buffer, pH 8.4.

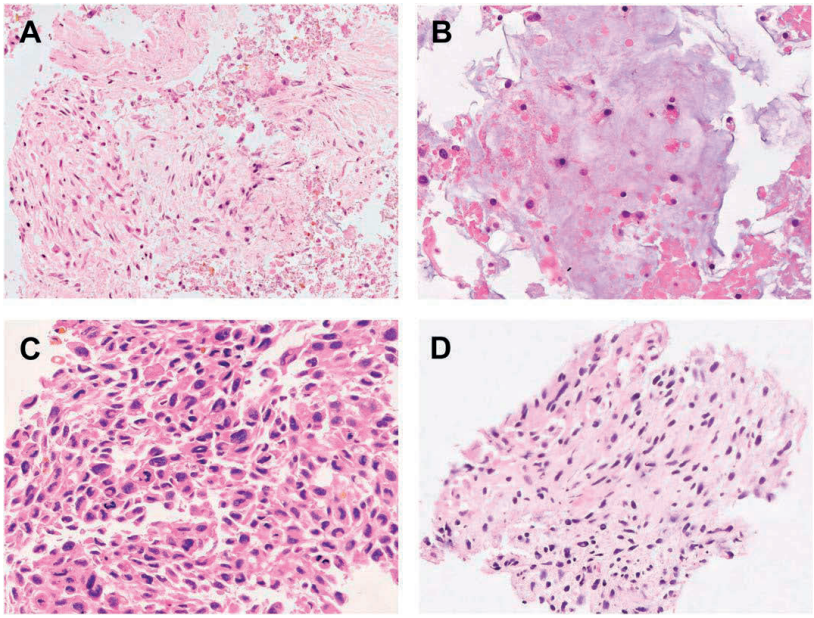

FIGURE 2 Microphotographs of H&E slides obtained from CellientTM cell blocks. (A) collagen rich tissue with fibroblastic tumor cells in desmoid fibromatosis. (B) cartilaginous matrix with atypical hyperchromatic tumor cells in grade 2 chondrosarcoma. (C) pleomorphic tumor cells in pleomorphic undifferentiated sarcoma. (D) hyperchromatic spindled tumor cells in malignant peripheral nerve sheath tumor (original ×200) [Color figure can be viewed at wileyonlinelibrary.com]

prepare a Giemsa-stained smear. In addition, 6 drops of the cell sediment were washed for 20 minutes in 1 mL Cytolyt Wash™ (Hologic), a low-dose methanol-based solution used to lyse erythrocytes and dissolve mucus. From this sediment, a Papanicolaou-stained microscopic thin layer slide was prepared with the ThinPrep T5000 processor. The remaining part of the cell suspension was rinsed twice in Cytolyt Wash™ solution and centrifuged again for 5 minutes at 1200 g, after which the pellet was fixed with PreservCyt™ fluid for 20 minutes before the sample vial with PreservCyt™ was put in the automated Cellient™ processor. The Cellient™ Automated Cell Block System is fully automated. It creates a paraffin-embedded cell block in <1 hour by means of a controlled vacuum that concentrates a layer of cells on a specially designed filter. Dehydrating and clearing reagents, including propranolol and xylene, are vacuum-drawn through the sample, which is subsequently embedded in paraffin and finished in an additional layer of paraffin; this makes it ready for histological sectioning. The vacuum-assisted filtration concentrates available cells within the final paraffin block. Eosin staining is used for visualization of the cell layer during sectioning. During sectioning of the Cellient™ cell blocks 10 paraffin sections of 4-mm thickness were prepared, and these were mounted on aminopropyltriethoxysilane (APES)-coated microscopic slides. One section was routinely stained with Hematoxylin and Eosin (H&E) for microscopic evaluation of specimen cellularity. The remaining unstained slides were available for IHC.

2.4 | Immunohistochemistry

The 14 antibodies (13 monoclonal, 1 polyclonal) applied in this study, including their commercial source, clone, and working dilution, as summarized in Table 2. Five diagnostically relevant antibodies had been evaluated in our earlier study of the Cellient™ method (CD117, AE1/3, ER, HMB-45, S-100). The 9 additional antibodies used to diagnose the STB tumors in this cohort were actin, beta-catenin, brachyury, caldesmon, CD-34, desmin, DOG-1, myf4, and SATB2. All IHC stains were performed in the Benchmark Ultra automated immunostainer (Ventana, Tuscon, Arizona) using the Ultraview detection system and validated by testing proper dilution of the antibody, need for CC1 antigen retrieval, and need for an 8 minutes amplification step in the IHC staining protocol, respectively (Table 2). All antibodies had been tested with at least 3 different Cellient™ cell blocks prepared from 3 different specimens. IHC results obtained with Cellient ™ cell blocks were compared with IHC results obtained with corresponding formalin-fixed, paraffin-embedded (FFPE) tissue tumor material from the same patient as reference standard. Several antibodies required antigen retrieval with CC1 (cell conditioning buffer, pH 8.4) for optimal staining. CC1 with protease pretreatment proved to give to best results for cytokeratin antibody AE1–3. For all IHC staining, the Ventana Ultraview DAB detection kit was used with an amplification step of 8 minutes. Hematoxylin was used as a counterstain.

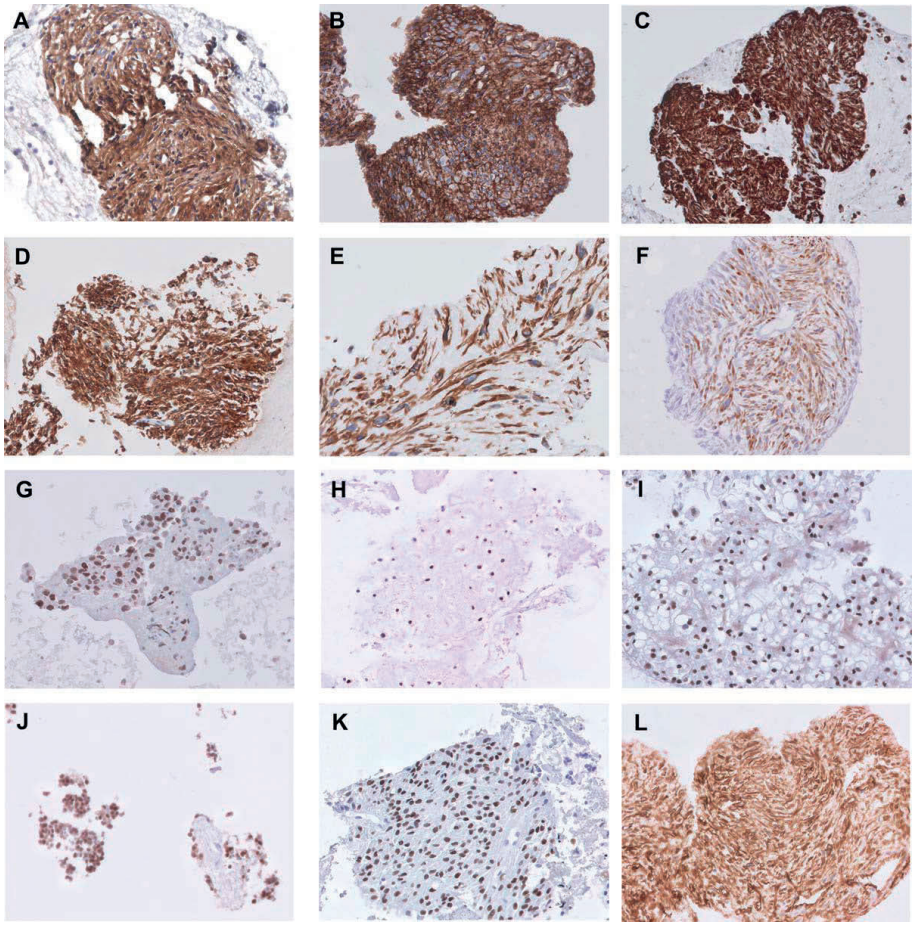

FIGURE 3 Microphotographs of IHC using 12 diagnostically relevant antibodies with the CellientTM method. CD117 (A) and DOG-1 (B) in GIST. Desmin (C) and HMB-45 (D) in PEComa. SMA (E) and caldesmon (F) in leiomyosarcoma. Nuclear staining of osteosarcoma cells with SATB2 (G), S-100 (H) in chondrosarcoma, brachyury (I) in chordoma, myf4 (J) in alveolar rhabdomyosarcoma, and ER (K) in gynecologic leiomyosarcoma. CD34 (L) in dermatofibrosarcoma protuberans (original ×200) [Color figure can be viewed at wileyonlinelibrary.com]

3 | RESULTS

In all 20 cases, the H&E stained sections of the Cellient™ material contained small tissue fragments. H&E histology of these small tissue fragments (microbiopsies) revealed that diagnostically relevant histological and cytological features could be examined properly, as shown in Figure 2. Fragments of desmoid fibromatosis consisted of collagen rich tissue with haphazardly arranged fibroblastic cells with round nuclei, nucleoli, and tapering eosinophilic cytoplasm (Figure 2A). Fragments of a grade 2 myxoid chondrosarcoma contained tumor cells with moderately atypical, hyperchromatic, single and double nuclei embedded in myxochondroid matrix (Figure 2B), whereas cellular fragments with pleomorphic and hyperchromatic tumor cells were encountered in recurrences of pleomorphic undifferentiated sarcoma and radiation sarcoma (malignant peripheral nerve sheath tumor (MPNST)) (Figure 2C,D).

In the group of 8 primary tumors, we specifically diagnosed 5 spindle cell gastrointestinal stromal tumors (GISTs) by positive IHC for both CD117 and DOG-1. A PEComa of the rectum could be diagnosed after positive IHC for actin, desmin and HMB-45, and a mesenteric desmoid fibromatosis in a patient with familial adenomatosis polyposis (FAP) syndrome showed focal nuclear positivity for beta-catenin, whereas a retroperitoneal leiomyosarcoma was diagnosed as it showed expression of the smooth muscle markers actin (SMA), desmin, and caldesmon. Thus, in all primary STB tumors, IHC performed on Cellient™ material provided clinically important information.

In the group of 12 secondary tumors of known STB primaries, we managed to confirm the presence of a local recurrence or metastasis in

TABLE 3 Comparison of commonly used cell block methods, as reviewed by Jain et al.[9]

Method	Advantage	Disadvantage	Utility	IHC	Molecular studies
Agar method	Inexpensive Better orientation of cell block	Inconvenient heat treatment process Heat-related artefacts possible, if not cooled as recommended	For any fluid or FNA	Optimum results for cytoplasmic and nuclear antigens	Suitable
Histogel method	Good cellular preservation and architecture	Tedious process as HistoGel needs to be converted and maintained in liquid state Possible heat-related artefacts	Useful in specimens with no visible sediment after centrifugation	Suitable	Suitable
Collodion bag method	Good cellular yield	Time-consuming preparation of bags Toxic ether fumes for storage	Friable tissues and fragments, specimens of scanty cellularity	Appropriate results	Suitable
Cellient method	Good cellular yield Uniformly distributed cells Improved cellular architecture and nuclear features Consistent results Automated method with reduced procedural time No cross contamination Minimal cell loss	Expensive machines and consumables Requires trained staff for cutting thin sections	Limited studies Useful in low-cellularity specimens Useful in cervical LBC	Good results with optimized IHC protocols, adjusted to methanol fixation (see Refs. 8 and 13)	High quality of DNA and RNA

Abbrevitions: FNA, fine needle aspiration; IHC, immunohistochemistry; LBC, liquid-based cytology.

all cases. This group included 4 bone sarcomas. A metastasis of an osteosarcoma was positive for SATB2 and 2 secondary chondrosarcomas showed expression of S-100, whereas an inguinal lymph node metastasis of a sacral chordoma was confirmed by IHC for the transcription factor brachyury. The 8 secondary manifestations of soft tissue sarcomas included 2 radiation-induced sarcomas and 2 pleomorphic undifferentiated sarcomas (diagnosed solely on H&E morphology), 2 metastatic alveolar rhabdomyosarcomas (which were myf4 positive), a metastatic leiomyosarcoma of the uterus (in which actin and ER were positive), and a recurrent dermatofibrosarcoma protuberans (CD34 positive). Thus, in addition to H&E morphology, in 8 out of 12 cases, IHC on CellientTM material provided incremental diagnostic information.

In both groups (primary and secondary tumors), IHC results in Cellient slides were concordant with those obtained in FFPE tumor biopsies or excisions/resections from the same patient.

Figure 3 depicts IHC results of all antibodies applied: CD117 (Figure 3A) and DOG-1 (Figure 3B) in GIST, desmin (Figure 3C) and HMB-45 (Figure 3D) in PEComa, SMA (Figure 3E) and caldesmon (Figure 3F) in leiomyosarcoma, SATB2 in osteosarcoma (Figure 3G), S-100 in chondrosarcoma (Figure 3H), brachyury in chordoma (Figure 3I), myf4 in alveolar rhabdomyosarcoma (Figure 3J), ER (Figure 3K) in metastatic gynecologic leiomyosarcoma, and CD34 (Figure 3L) in dermatofibrosarcoma protuberans.

4 | DISCUSSION

The Cellient™ is a fully automated device that produces a cell block within 1 hour based on a standardized protocol. This allows rapid diagnosis on the same day the specimen arrives in the lab instead of the following day, which is convenient in selected cases. A methanol-based PreservCyt ™ solution is used instead of formalin. Several research groups have mentioned that the cellularity of Cellient™ material is at least comparable to that in traditional cell blocks, whereas cytomorphological details, in particular chromatin structure, appear to be better.[10,12,14] Advantages and disadvantages of commonly used cell block methods including Cellient™ have been amply reviewed by Jain et al.[9] and are summarized in Table 3. We have noted that the Cellient™ cell blocks often contain small tissue fragments. In addition to H&E interpretation of histological features, IHC and molecular methods, for example, FISH or NGS, can be applied.[8] In the cytology laboratory, immunostaining can be applied to cell smears, ThinPrep specimens, cytospin specimens, and cell blocks. In a UK NEQUAS quality control study, testing commonly used antibodies for a diagnosis of carcinoma, mesothelioma, melanoma, and lymphoma, it was found that the highest sensitivity was provided by cell blocks, followed by cytospin specimens, liquid-based cytology slides, and cell smears.[15]

Although cellular DNA and RNA are well preserved by methanol fixation, at the protein level, IHC protocols that are routinely used for FFPE material, have to be optimized and validated. We[8] and Sauter et al.[13] have extensively tested many different antibodies for Cellient™ material using the automated Ventana Benchmark immunostainer. In our initial study published in 2013, we showed that IHC performed on Cellient™ cell blocks could be applied to diagnostic algorithms that proved to be helpful in the discrimination of major tumor types (carcinoma, lymphoma, melanoma, and germ cell tumors), discrimination of carcinoma subtypes (adenocarcinoma, squamous-cell carcinoma, and neuroendocrine carcinoma), and determination of primary tumor site (eg, lung and breast) in cases of metastatic carcinoma. Notably, in a consecutive series of 100 cases, additional and clinically relevant information was obtained in 25% of serous fluid specimens and 29% of FNA specimens.[8]

To our knowledge, this is the first report on the use of Cellient™ cell blocks for the diagnosis of soft tissue and bone tumors. We stress that, in our and most sarcoma centers, cytology is only rarely applied for diagnosing tumors of soft tissue and bone. For the tumors in this series, EUS-FNA was tried to render a diagnosis of deep-seated primary tumors and FNA was used for superficially located metastatic or recurrent tumors of which the histologic diagnosis was known. We showed that by combining clinical presentation (including imaging studies), H&E morphology, and IHC, a diagnosis could be made in all 20 consecutive cases of tumors of soft tissue and bone. We evaluated 14 antibodies, 9 of which were not tested in our initial study. After optimization of factors influencing IHC results (in particular antigen retrieval conditions, amplification steps in the detection system kit) we managed to obtain excellent staining results for both cytoplasmic (eg, the smooth muscle markers, actin, desmin, and caldesmon) as well as nuclear antigens (eg, brachyury, myf4, and SATB2). In all 16 cases (all 8 primary tumors and 8 secondary tumors) where IHC was applied, a specific diagnosis could be made. For instance, brachyury, myf4, and SATB2, which are markers for notochordial, myogenic, and osteoblastic cell differentiation, respectively, allowed or confirmed a diagnosis of chordoma, alveolar rhabdomyosarcoma, and osteosarcoma.

Finally, cost considerations and budgetary constraints will determine the extent to which cytology laboratories use the rapid automated processing or more time-consuming traditional manual FFPE method to prepare cell blocks for H&E, IHC and/or FISH. Costs of the Cellient™ technique include purchase (50 000 US$) and reagents (10 US$ per specimen). Although the cost of the Cellient™ block technique is higher than that of a traditional cell block technique, we estimated that saved technician time is 30 minutes per specimen, using the time required to prepare an agar cell block as a reference standard. However, in our opinion, the cost of a new laboratory technique should be judged in the context of total cost of patient health care, including reduction of other diagnostic tests and patient life years saved, a cost analysis which is beyond the scope of this article.

In summary, we have shown that routine H&E staining and IHC of cell material processed with Cellient™ processor has the potential to accurately diagnose tumors of soft tissue and bone. In all 20 consecutive cases, important clinical information was provided, which translated into improved patient care. However, due to the small sample size, statistical analysis was not feasible, and a future study, testing appropriate antibodies on a larger number of cases, is needed to assess the real value of this method.

CONFLICT OF INTEREST

The authors have no conflict of interest.

DISCLOSURES

The authors made no disclosures.

ORCID

A. J. H. Suurmeijer http://orcid.org/0000-0003-1361-9454

REFERENCES

[1] Domanski HA. Fine-needle aspiration cytology of soft tissue lesions: diagnostic challenges. *Diagn Cytopathol.* 2007;35:768–773.

[2] Kramer H, Sanders J, Post WJ, Groen HJ, Suurmeijer AJ. Analysis of cytological specimens from mediastinal lesions obtained by endoscopic ultrasound-guided fine-needle aspiration. *Cancer* 2006;108:206–211.

[3] Layfield LJ, Baloch Z. Cytologic diagnosis of osseous lesions: a review with emphasis on the diagnosis of primary neoplasms of bone. *Diagn Cytopathol.* 2009;37:299–310.

[4] van Hemel BM, Lamprou AA, Weersma R, Plukker JT, Suurmeijer AJ, van Dullemen HM. Procedure-related, false-positive cytology results during EUS-guided FNA in patients with esophageal cancer. *Gastrointest Endosc.* 2010;71:1130–1133.

[5] Domanski HA, Akerman M, Carlén B, et al. Core-needle biopsy performed by the cytopathologist: a technique to complement fine-needle aspiration of soft tissue and bone lesions. *Cancer* 2005;105:229–239.

[6] Klijanienko J, Pierron G, Sastre-Garau X, Theocharis S. Value of combined cytology and molecular information in the diagnosis of soft tissue tumors. *Cancer Cytopathol.* 2015;123:141–151.

[7] Layfield LJ, Armstrong K, Zaleski S, Eckardt J. Diagnostic accuracy and clinical utility of fine-needle aspiration cytology in the diagnosis of clinically primary bone lesions. *Diagn Cytopathol.* 1993;9:168–173.

[8] van Hemel BM, Suurmeijer AJH, Aisner D. Effective application of the methanol-based PreservCyt(™) fixative and the Cellient(™) automated cell block processor to diagnostic cytopathology, immunocytochemistry, and molecular biology. *Diagn Cytopathol.* 2013;41:734–741.

[9] Jain D, Mathur SR, Iyer VK. Cell blocks in cytopathology: a review of preparative methods, utility in diagnosis and role in ancillary studies. *Cytopathology* 2014;25:356–371.

[10] Kruger AM, Stevens MW, Kerley KJ, Carter CD. Comparison of the Cellient(™) automated cell block system and agar cell block method. *Cytopathology* 2014;25:381–388.

[11] Montgomery E, Gao C, de Luca J, Bower J, Attwood K, Ylagan L. Validation of 31 of the most commonly used immunohistochemical antibodies in cytology prepared using the Cellient(®) automated cell block system. *Diagn Cytopathol.* 2014;42:1024–1033.

[12] Prendeville S, Brosnan T, Browne TJ, McCarthy J. Automated Cellient(™) cytoblocks: better, stronger, faster? *Cytopathology* 2014;25:372–380.

[13] Sauter JL, Grogg KL, Vrana JA, Law ME, Halvorson JL, Henry MR. Young investigator challenge: validation and optimization of immunohistochemistry protocols for use on Cellient cell block specimens. *Cancer Cytopathol.* 2016;124:89–100.

[14] Wagner DG, Russell DK, Benson JM, Schneider AE, Hoda RS, Bonfiglio TA. Cellient automated cell block versus traditional cell block preparation: a comparison of morphologic features and immunohistochemical staining. *Diagn Cytopathol.* 2011;39:730–736.

[15] Kirbis IS, Maxwell P, Fležar MS, Miller K, Ibrahim M. External quality control for immunocytochemistry on cytology samples: a review of UK NEQAS ICC (cytology module) results. *Cytopathology* 2011;22:230–237.

Chapter 3

Diagnostic yield of NanoString nCounter FusionPlex profiling in soft tissue tumors

This chapter is based on the publication: **Wangzhao Song**, Inge Platteel, Albert J. H. Suurmeijer et.al. Diagnostic yield of NanoString nCounter FusionPlex profiling in soft tissue tumors. Genes Chromosomes Cancer, 2020 May; 59(5): 318–324.

Diagnostic yield of NanoString nCounter FusionPlex profiling in soft tissue tumors

Wangzhao Song | Inge Platteel | Albert J. H. Suurmeijer | Léon C. van Kempen

Department of Pathology and Medical Biology, University Medical Center Groningen, University of Groningen, Groningen, The Netherlands

Correspondence
Léon C. van Kempen, Department of Pathology and Medical Biology, University Medical Center Groningen, University of Groningen, P.O. Box 30.001, 9700 RB Groningen, The Netherlands.
Email: l.van.kempen@umcg.nl

Funding information
China Scholarship Council (CSC) program, Grant/Award Number: 201606940023

Abstract

Diagnostic histopathology of soft tissue tumors can be troublesome as many entities are quite rare and have overlapping morphologic features. Many soft tissue tumors harbor tumor-defining gene translocations, which may provide an important ancillary tool for tumor diagnosis. The NanoString nCounter platform enables multiplex detection of pre-defined gene fusion transcripts in formalin-fixed and paraffin-embedded tissue. A cohort of 104 soft tissue tumors representing 20 different histological types was analyzed for the expression of 174 unique gene fusion transcripts. A tumor-defining gene fusion transcript was detected in 60 cases (58%). Sensitivity and specificity of the NanoString assay calculated against the result of an alternative molecular method were 85% and 100%, respectively. Highest diagnostic coverage was obtained for Ewing sarcoma, synovial sarcoma, myxoid liposarcoma, alveolar rhabdomyosarcoma, and desmoplastic small round cell tumor. For these tumor types, the NanoString assay is a rapid, cost-effective, sensitive, and specific ancillary screening tool for molecular diagnosis. For other sarcomas, additional molecular testing may be required when a translocation transcript is not identified with the current 174 gene fusion panel.

KEYWORDS
fusion genes, molecular pathology, NanoString, sarcoma, soft tissue tumor

1 | INTRODUCTION

Soft tissue tumors represent a remarkably heterogeneous group of neoplasms, with many subtypes being exceptionally rare. More than 100 different soft tissue tumors have been described in the latest 2013 WHO classification.[1] The proper histological classification of soft tissue tumors is grounded in the microscopic analysis of tumor growth patterns and their cytological features, which may be a difficult exercise, since many tumors have overlapping morphologic features. Although tumor-associated protein markers may be visualized by ancillary immunohistochemistry (IHC), many tumors show non-specific, overlapping or absent marker expression. Thus, it may be difficult or impossible to render an objective accurate diagnosis, in particular when studying small biopsy specimens with a limited amount of tumor tissue.

Fortunately, a significant number of soft tissue tumors, in particular those with monomorphic round cell, spindle cell or epithelioid morphology, harbor recurrent gene translocations, which are often tumor-specific. These unique recurrent translocations were first discovered in the early 1990s by chromosomal banding techniques, for example, the *t(X;18)(p11;q11)* translocation in synovial sarcoma, which results in the tumor specific *SS18-SSX* fusion genes.[2] At the molecular level, with knowledge of the exon regions involved in fusion genes, RT-PCR and Fluorescence In Situ

Hybridisation (FISH, using break-apart probes) methods became available to detect these particular gene fusions and rearrangements. In the past decade, pathologists have witnessed the rapid development of next generation sequencing (NGS) techniques, which allow simultaneous detection of multiple fusion transcripts. This translated into more accurate classification and also prognostication of soft tissue tumors.[3] At present, the two novel molecular multiplex methods commonly used in Dutch sarcoma centers are the anchored multiplex PCR (AMP)-based NGS (Archer FusionPlex Sarcoma assay)[4] and the NanoString nCounter platform.[5] The Archer AMP PCR method targets exons of 26 genes commonly involved in fusion genes of soft tissue tumors, whereas the NanoString assay is a high-throughput hybridization technique, which uses specific probes that target 174 unique gene fusion junctions in 22 soft tissue tumor types.[6]

In this quality control study, we evaluated the sensitivity and specificity of the NanoString nCounter platform for gene fusion detection in 22 different soft tissue tumors, adding our results to the initial report on this method.[7]

2 | MATERIALS AND METHODS

2.1 | Case selection

Case selection included 106 soft tissue tumors derived from the archives of the Department of Pathology in the University Medical Center Groningen and diagnosed between 1988 and 2018. The series comprised 22 different translocation-associated tumor types. All cases were reviewed by a pathologist with special expertise in diagnostic pathology of soft tissue tumors (A.S.). In all cases, Formalin-Fixed and Paraffin-embedded (FFPE) material was available, in the large majority of cases from tumor excision or resection specimens. In two tumor specimens (one undifferentiated round cell sarcoma and one desmoplastic small round cell tumor), RNA quantity was too low to allow proper analysis. Thus, 104 tumors were eventually included in the study, of which 59 tumors had been tested previously by an alternative molecular method (Figure 1), including FISH (36 cases), RT-PCR (12 cases), FISH and RT-PCR (7 cases), or Archer NGS (4 cases). Fifty-two out of fifty-nine cases were fusion positive by alternative

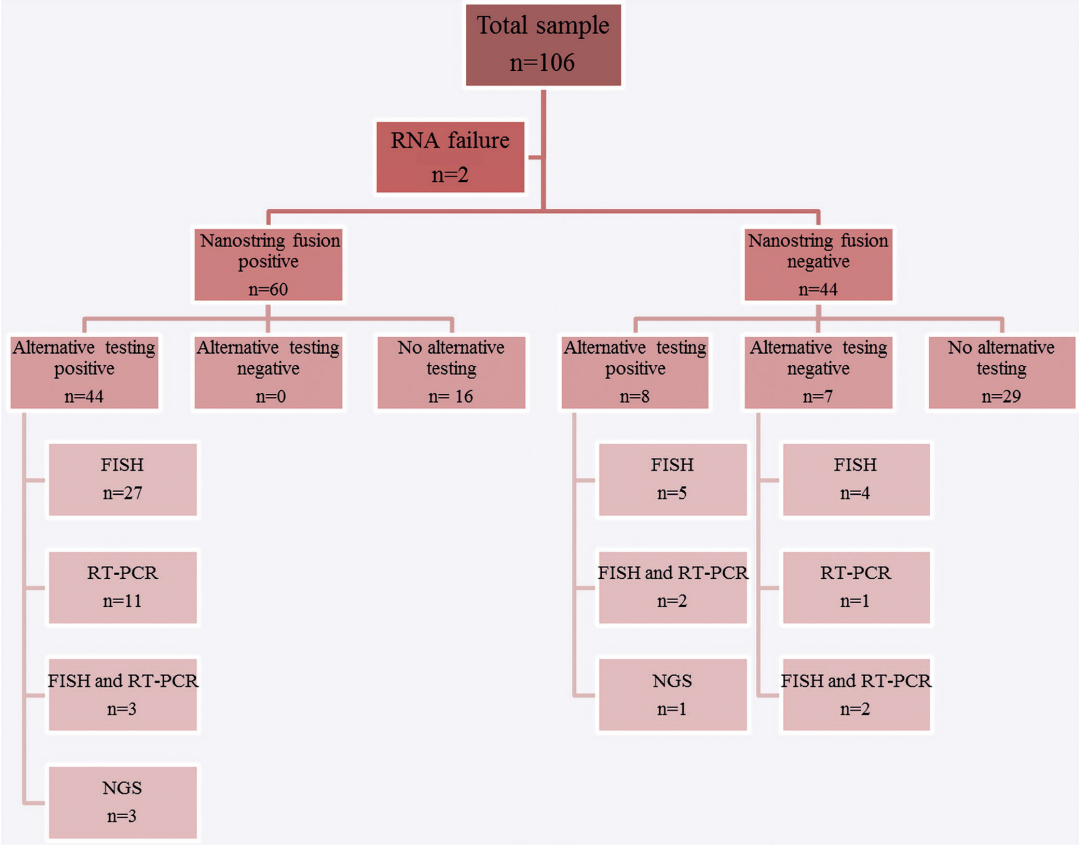

FIGURE 1 Overview of Nanostring nCounter FusionPlex results [Color figure can be viewed at wileyonlinelibrary.com]

molecular tests. In the remaining 45 cases, in which no molecular methods had been applied, the tumor diagnosis was based on clinical presentation and histologic features in combination with IHC.

The study was approved by the UMCG institutional ethical review board (P18-116) and performed in accordance with the code of conduct for responsible use of human tissue that is used in the Netherlands (Dutch Federation of Biomedical Scientific Societies; http://www.federa.org).

2.2 | NanoString gene expression profiling

RNA was isolated from four 5-μm-thick formalin-fixed and paraffin-embedded tissue sections containing at least 50% tumor cells using the RNeasy mini kit (Qiagen) according to suppliers instructions. Total RNA was quantified with Qubit (ThermoFisher).

The soft tissue and bone tumor probe set as described by Chang et al.[7] was ordered from IDT Technologies (Leuven, Belgium). In contrast to the initial study, our panel did not contain probes for the detection of *COL1A1-PDGFB* gene fusion transcripts, as can be found in dermatofibrosarcoma protuberans. Probes were hybridized with 100 ng RNA overnight in a thermocycler at 67°C with a heated-lid at 72°C. The RNA-probe complexes were loaded on an nCounter cartridge, and hybridized, washed and read on a nCounter SPRINT platform according to suppliers instructions (NanoString nCounter Technologies, Seattle, WA).

2.3 | Data analysis

The platform-generated Reporter Code Count (RCC) files containing the raw data were analyzed. Samples with a geometric mean of the raw counts of the four reference genes (*ACTB*, *GAPDH*, *SDHA*, *UBC*) of <500 were excluded from the analysis due to low RNA input or poor RNA quality. Subsequent data normalization were performed with the nSolver Analysis Software (NanoString nCounter Technologies) to correct for differences in hybridization efficiency using the respective control probes. Counts were not corrected for RNA input. Following a $\log^2$ transformation of the normalized data, the interquartile range (IQR) of counts for each probe across all samples in the run was calculated. Outliers in each sample, that is, positive signal for a gene fusion transcript, were determined as counts larger than 1.5*IQR, and which exceed the background threshold of 40 counts. The counts were not compared to the median of the counts across all the probes within a sample as reported by Chang et al.[7] A comparison of both methods did not alter the results for the sample set described in this work (data not shown).

3 | RESULTS

As shown in Figure 1 and Table 1, the NanoString assay detected gene fusions in 60/104 cases suitable for analysis. In 44/60 NanoString positive cases, a similar gene fusion had already been detected by previous alternative molecular testing. In the other 16/60 cases, no previous molecular testing had been performed. The detected fusion genes are summarized in Table S1.

In 44/104 cases, no fusion was detected by the NanoString assay, whereas in 8/44 cases, a gene rearrangement or fusion had been found by prior alternative molecular testing (5 by FISH, 2 by FISH and RT-PCR, and 1 by targeted NGS). Thus, there were no false-positive NanoString results and eight false-negative NanoString results. Overall, fusion gene detection by NanoString had a sensitivity of 85% and specificity of 100%.

3.1 | Concordant and discordant (false-negative) cases

Of the 52/104 cases, in which a gene rearrangement or fusion had been detected by prior molecular testing, NanoString was positive (concordant) in 44 cases and negative (discordant) in 8 cases. With respect to soft tissue tumor type, concordant cases included all eight Ewing sarcomas (four with *EWSR1-FLI1*, three with *EWSR1-ERG*, and one with *EWSR1-FEV*), all eight synovial sarcomas with *SS18-SSX1/2*, all seven myxoid liposarcomas with *FUS/EWSR1-DDIT*, and all three desmoplastic small round cell tumors (DSRCT) with *EWSR1-WT1*.

Table 2 summarizes the eight discordant cases, in which NanoString failed to detect gene fusions that were detected by other molecular methods. These discordant cases included one single BCOR-rearranged sarcoma (with a *BCOR* (exon 15)-*CCNB3* (exon 5) fusion gene detected by Archer) and one single CIC-rearranged sarcoma (with *CIC* rearrangement detected by FISH). Moreover, NanoString was negative in 1/4 clear-cell sarcomas (positive by FISH *EWSR1* break-apart assay), 2/5 epithelioid hemangioendotheliomas (positive by FISH for *WWTR1-CAMTA1*), and 2/4 inflammatory myofibroblastic tumors (one with *ALK* rearrangement by FISH and one with *EML4* (exon2)-*ALK1* (exon20) by RT-PCR).

3.2 | Positive NanoString results in cases without prior molecular testing

As shown in Table 1, 16 fusion-positive cases were detected by NanoString, which had no previously molecular testing, including 2/3 alveolar soft part sarcomas, 3/5 alveolar rhabdomyosarcomas, 1/6 aneurysmal bone cysts, 1/5 angiomatoid fibrous histiocytomas, 3/6 mesenchymal chondrosarcomas, 2/7 myxoid liposarcomas, 3/5 cases of nodular fasciitis, and 1/5 extraskeletal myxoid chondrosarcomas.

3.3 | The relative value of the NanoString assay is strongly associated with the level of diagnostic evidence in daily practice

In order to determine the usefulness of NanoString testing in daily pathology practice, we divided the 104 soft tissue and bone (STB)

TABLE 1 Overview soft tissue tumors evaluated with NanoString

Diagnosis	Total cases	NanoString fusion positive			NanoString fusion negative		
		Prior testing +	Prior testing –	No prior testing	Prior testing +	Prior testing –	No prior testing
Alveolar soft part sarcoma	3	–	–	2	–	–	1
Alveolar rhabdomyosarcoma	5	2	–	3	–	–	–
Aneurysmal bone cyst	6[a]	2	–	1	–	–	3
Angiomatoid fibrous histiocytoma	5	3	–	1	–	–	1
BCOR-rearranged sarcoma	1[b]	–	–	–	1	–	–
Biphenotypic sinonasal sarcoma	3	1	–	–	–	–	2
CIC-rearranged sarcoma	1	–	–	–	1	–	–
Clear-cell sarcoma	4	3	–	–	1	–	–
Congenital/infantile fibrosarcoma	3	2	–	–	–	–	1
Desmoplastic small round cell tumor	3	3	–	–	–	–	–
Epithelioid hemangioendothelioma	5	2	–	–	3	–	–
Ewing sarcoma	8[c]	8	–	–	–	–	–
Undiff. round cell sarcoma	7	–	–	–	–	5	2
Extraskeletal myxoid chondrosarcoma	5	2	–	1	–	1	1
Inflammatory myofibroblastic tumor	7	2	–	–	2	–	3
Lipoblastoma	3	–	–	–	–	–	3
Mesenchymal chondrosarcoma	6	1	–	3	–	–	2
Myoepithelial tumor	4	–	–	–	–	1	3
Myxoid liposarcoma	7	5	–	2	–	–	–
Nodular fasciitis	5	–	–	3	–	–	2
Synovial sarcoma	8	8	–	–	–	–	–
Tenosynovial giant cell tumor	5	–	–	–	–	–	5
Total cases	104	44	0	16	8	7	29

[a]Two soft tissue tumors, four bone tumors.
[b]A bone tumor.
[c]Four soft tissue tumors, four bone tumors.

TABLE 2 Summarize of eight discordant cases

Tumor	Case (*n*)	Alternative testing results
BCOR-rearranged sarcoma	1	NGS found BCOR (exon15)—CCNB3 (exon 5)
CIC-rearranged sarcoma	1	FISH found CIC-DUX4
Clear-cell sarcoma	1	FISH found EWS break
Epithelioid hemangioendothelioma	3	FISH found WWTR1-CAMTA1
Inflammatory myofibroblastic tumor	2	1 case RT-PCR found EML4 (exon2)—ALK1 (exon20), 1 case FISH found ALK positive

tumors in three groups according to their level of diagnostic evidence, as shown in Figure 2. Group 1 consisted of 52 STB tumors in which the histological diagnosis was confirmed by prior alternative molecular testing. Fusion genes transcripts were detected by NanoString in 44 cases (85%). Group 2 consisted of 36 STB tumors in which the histological diagnosis was based on typical histological features, often in combination with IHC findings. Fusion gene transcripts were detected by NanoString in 15 cases (42%). Group 3 consisted of 16 STB tumors, in which the histological diagnosis was uncertain, due to overlapping or undifferentiated morphologic features and lack of specific IHC markers. In this group, a fusion gene transcript was detected by NanoString in only one case (6%), an extraskeletal myxoid chondrosarcoma with an *EWSR1-NR4A3* fusion.

3.4 | Estimated diagnostic coverage of NanoString in STB tumors

By combining the results of this study (Table 1) with those obtained by Chang et al.[7] (as shown in their Table 2), it may be concluded that the NanoString nCounter assay has an excellent diagnostic coverage for five tumor types. In both studies, specific fusion genes were detected in all cases of Ewing sarcoma (n = 28), synovial sarcoma

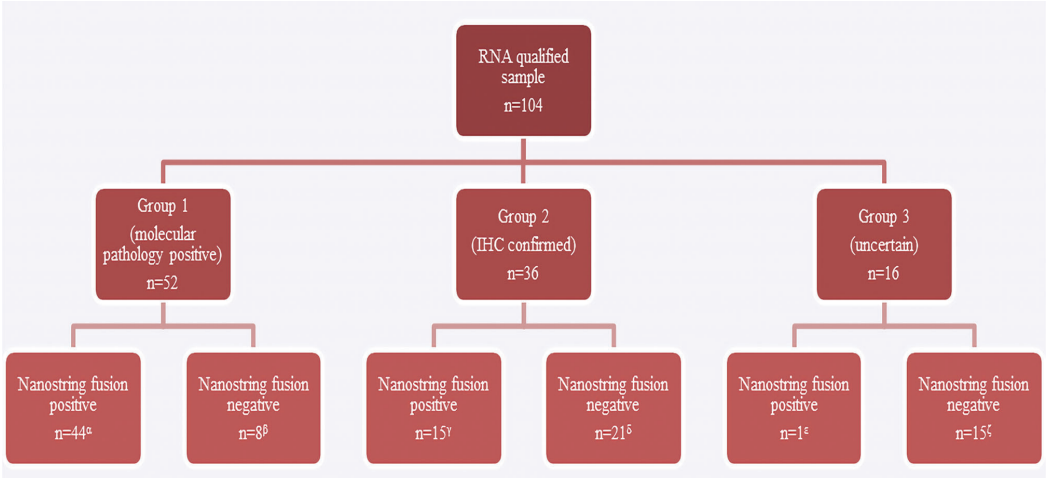

FIGURE 2 Diagnostic value of Nanostring nCounter FusionPlex in different fusion-associated tumor types. α: Two alveolar rhabdomyosarcomas, two aneurysmal bone cysts, three angiomatoid fibrous histiocytomas, one biphenotypic sinonasal sarcoma, three clear cell sarcomas, two infantile fibrosarcomas, three desmoplastic small round cell tumors, two epithelioid hemangioendotheliomas, eight Ewing sarcomas, two extraskeletal myxoid chondrosarcomas, two inflammatory myofibroblastic tumors, one mesenchymal chondrosarcoma, five myxoid liposarcomas, and eight synovial sarcomas. β: One BCOR-rearranged sarcoma, one CIC-rearranged sarcoma, one clear cell sarcoma, three epithelioid hemangioendotheliomas, and two inflammatory myofibroblastic tumors. γ: Two alveolar soft part sarcomas, three alveolar rhabdomyosarcomas, one aneurysmal bone cyst, one angiomatoid fibrous histiocytoma, three mesenchymal chondrosarcomas, two myxoid liposarcomas, and three nodular fasciitis. δ: One alveolar soft part sarcoma, three aneurysmal bone cysts, one angiomatoid fibrous histiocytoma, two biphenotypic sinonasal sarcomas, one infantile fibrosarcoma, one inflammatory myofibroblastic tumor, three lipoblastomas, two mesenchymal chondrosarcomas, two nodular fasciitis, and five tenosynovial giant cell tumors. ε: One extraskeletal myxoid chondrosarcoma. ζ: Seven undifferentiated round cell sarcomas, two extraskeletal myxoid chondrosarcomas, two inflammatory myofibroblastic tumors, and four myoepithelial tumors [Color figure can be viewed at wileyonlinelibrary.com]

(n = 19), myxoid liposarcoma (n = 12), alveolar rhabdomyosarcoma (n = 10), and desmoplastic small round cell tumor (n = 5). Moreover, five out of six infantile fibrosarcomas were diagnosed.

Tumors with an estimated diagnostic coverage of 50% to 75% included nodular fasciitis (10/17), clear cell sarcoma (8/13), alveolar soft part sarcoma (6/8), mesenchymal chondrosarcoma (6/8), angiomatoid fibrous histiocytoma (5/7), extraskeletal myxoid chondrosarcoma (4/6), and BCOR-rearranged sarcoma (3/4).

Tumors with a low diagnostic coverage of less than 50% included epithelioid hemangioendothelioma (4/11), myoepithelial tumors (3/9), aneurysmal bone cyst (3/9), inflammatory myofibroblastic tumor (2/9), CIC-rearranged sarcoma (1/4), and biphenotypic sinonasal sarcoma (1/3).

Tumors in which no fusion genes were detected included (CD99 negative) undifferentiated round cell sarcomas (13), tenosynovial giant cell tumors (6), and lipoblastomas (4).

4 | DISCUSSION

Soft tissue tumors are highly heterogeneous in histological and molecular subtypes. The identification of tumor type-specific gene translocations has enabled a molecular classification with diagnostic and prognostic value.[8] In this study, we demonstrate that NanoString fusion gene transcript profiling can reliably identify five molecularly defined soft tissue tumors: Ewing sarcoma, synovial sarcoma, myxoid liposarcoma, alveolar rhabdomyosarcoma, and desmoplastic small round cell tumor. Further improvement of the assay can likely extend its diagnostic value to other sarcoma subtypes.

The diagnostic coverage of the current design of the NanoString panel for the other relatively rare tumor types included in this study is limited. The most likely reason for this is the lack of probes for known and unknown gene fusion events. Furthermore, lack of performance was demonstrated for a few probes in the current design. The probe for *EML4* (exon2)-*ALK* (exon 20) did not identify this gene fusion event in two inflammatory myofibroblastic tumors that were previously determined by RT-PCR and FISH. However, analysis of these samples with the commercially available lung carcinoma fusion gene panel did demonstrate this transcript in these tumors (data not shown).

For other previously identified translocations that could not be confirmed with the current NanoString panel, it is unknown whether this is due to a lack of performance of the fusion gene probes or a lack of probes for other known and unknown fusion. For example, this study included one CIC-rearranged sarcoma in which a *CIC* rearrangement was demonstrated by FISH previously. However, a

CIC-DUX4 fusion gene transcript could not be detected. It is estimated that *CIC-DUX4* fusions can be observed in approximately 60% of CIC-rearranged sarcomas, with lower incidence of others fusion partner such as *FOXO4* and *NUTM1*.[9,10] Chang et al.[7] demonstrated that the current NanoString panel identified one *CIC-DUX4* fusion transcript in four CIC-rearranged sarcomas, indicating that at least one of the probes is working. Therefore, and in contrast to well-studied soft tissue tumors such as Ewing sarcoma and synovial sarcoma, the current panel design has a high false negative rate for rare tumors in which the gene-fusion partners and exact location of the break are poorly characterized. The combined analysis of the current and previously published study[7] indicates, with the exception Ewing sarcoma, synovial sarcoma, myxoid liposarcoma, alveolar rhabdomyosarcoma, and desmoplastic small round cell tumors, a moderate to high risk of a false negative result (25% and higher, depending on tumor type).

The current panel appears not suitable for the molecular analysis of undifferentiated round cell carcinoma, lipoblastoma, and tenosynovial giant-cell tumors. Despite the inclusion of probes for fusion genes frequently detected in these tumors, none were positive in the NanoString analysis.

In addition to the tumor type-specific performance of this NanoString test, the percentage of tumor cells in a sample as well as RNA quality can contribute to a false-negative test result. Although the minimal percentage of tumor cells in a sample that is required for a confident detection of a gene fusion transcript was not determined, only samples with >50% tumor cellularity were included. Furthermore, only samples from which at least 15 ng RNA/μL could be extracted were analyzed with NanoString using 100 ng RNA input. Some samples were analyzed with 300 ng RNA input, but that did not result in a higher diagnostic yield (data not shown). Despite a high RNA yield from one desmoplastic small round cell tumor and one undifferentiated round cell sarcoma, counts for the reference genes were insufficient for analyses. Re-examination of both tissues revealed extensive necrosis that was presumably causal to poor RNA quality. Therefore, irrespective of sufficient tumor cellularity and RNA yield, a NanoString analysis can fail due to poor RNA quality.

The cost effectiveness and short turn-around time of a NanoString analysis is a strong argument for the replacement of FISH and RT-PCR as the initial screening test for sarcomas.[5] Turnaround time for FISH and a NanoString assay in a diagnostic setting is comparable, yet a NanoString assay is less labor intensive. In agreement with Chang et al.,[7] the cost per sample of a FISH analysis (one target-one sample) is comparable to one multiplex NanoString analysis when analyzing 12 samples simultaneously. NanoString thus significantly reduces the cost per sample while maintaining a short turnaround time. However, when no fusion event is identified, additional molecular profiling based on, for example, multiplex PCR (AMP)-based NGS may be necessary. This will be required for those tumors for which the current NanoString panel has a low diagnostic yield. For these tumor types, analysis Archer RNA-seq NGS is likely more effective,[11] but is associated with higher costs and longer turnaround times that are comparable to NGS sequencing of large targeted panels.

In conclusion, the NanoString nCounter FusionPlex assay is a screening tool with high sensitivity and specificity[5-7,12,13] for the detection of sarcoma-defining fusion gene transcripts in Ewing sarcoma, synovial sarcoma, myxoid liposarcoma, alveolar rhabdomyosarcoma, and desmoplastic small round cell tumors. Its diagnostic yield for rare soft tissue tumors is limited and might require additional or alternative testing.

DATA AVAILABILITY STATEMENT

The data that support the findings of this study are available on request from the corresponding author. The data are not publicly available due to privacy or ethical restrictions.

ORCID

Wangzhao Song https://orcid.org/0000-0002-7935-6493

REFERENCES

1. Fletcher CDM, Bridge JA, Hogendoorn PCW, Mertens F, eds. *WHO classification of tumours of soft tissue and bone*. Lyon, France: IARC Press; 2013.
2. Sreekantaiah C, Ladanyi M, Rodriguez E, Chaganti RS. Chromosomal aberrations in soft tissue tumors. Relevance to diagnosis, classification, and molecular mechanisms. *Am J Pathol*. 1994;144(6):1121-1134.
3. Cloutier JM, Charville GW. Diagnostic classification of soft tissue malignancies: a review and update from a surgical pathology perspective. *Curr Probl Cancer*. 2019;43(4):250-272.
4. Lam SW, Cleton-Jansen AM, Cleven AHG, et al. Molecular analysis of gene fusions in bone and soft tissue tumors by anchored multiplex PCR-based targeted next-generation sequencing. *J Mol Diagn*. 2018; 20(5):653-663.
5. Tsang HF, Xue VW, Koh SP, Chiu YM, Ng LP, Wong SC. NanoString, a novel digital color-coded barcode technology: current and future applications in molecular diagnostics. *Expert Rev Mol Diagn*. 2017;17 (1):95-103.
6. Sheth J, Arnoldo A, Zhong Y, et al. Sarcoma subgrouping by detection of fusion transcripts using NanoString nCounter technology. *Pediatr Dev Pathol*. 2019;22(3):205-213.
7. Chang KTE, Goytain A, Tucker T, et al. Development and evaluation of a pan-sarcoma fusion gene detection assay using the NanoString nCounter platform. *J Mol Diagn*. 2018;20(1):63-77.
8. Antonescu CR. The role of genetic testing in soft tissue sarcoma. *Histopathology*. 2006;48(1):13-21.
9. Antonescu CR, Owosho AA, Zhang L, et al. Sarcomas with CIC-rearrangements are a distinct pathologic entity with aggressive outcome: a clinicopathologic and molecular study of 115 cases. *Am J Surg Pathol*. 2017;41(7):941-949.
10. Watson S, Perrin V, Guillemot D, et al. Transcriptomic definition of molecular subgroups of small round cell sarcomas. *J Pathol*. 2018;245 (1):29-40.
11. Marino P, Touzani R, Perrier L, et al. Cost of cancer diagnosis using next-generation sequencing targeted gene panels in routine practice: a nationwide French study. *Eur J Hum Genet*. 2018;26(3): 314-323.
12. Leal LF, Evangelista AF, de Paula FE, et al. Reproducibility of the NanoString 22-gene molecular subgroup assay for improved prognostic prediction of medulloblastoma. *Neuropathology*. 2018;38(5): 475-483.
13. Veldman-Jones MH, Brant R, Rooney C, et al. Evaluating robustness and sensitivity of the NanoString technologies nCounter platform to enable multiplexed gene expression analysis of clinical samples. *Cancer Res*. 2015;75(13):2587-2593.

Part 2

Molecular Pathology of soft tissue and bone tumors

Chapter 4

Myoepithelial Tumors of Bone

This chapter is based on the publication: **Song W**, Flucke U, Suurmeijer AJH, et.al. Myoepithelial Tumors of Bone. Ann Diagn Pathol. 2016 Dec;25:37-41.

Myoepithelial Tumors of Bone

Wangzhao Song, MD[a], Uta Flucke, MD, PhD[b], Albert J.H. Suurmeijer, MD, PhD[a,*]

KEYWORDS

• Myoepithelioma • Myoepithelial carcinoma • Bone • Pathology • Immunohistochemistry • EWSR1 • FUS • Fusion gene

ABSTRACT

Myoepithelial tumors (METs) of bone (BMETs) are a rare but distinct tumor entity. METs that are cytologically benign are termed myoepitheliomas; METs with malignant histologic features are called myoepithelial carcinomas. BMETs have a wide age range, may involve any part of the skeleton, and have a variable spindle cell and epithelioid morphology. Bone tumors to be considered in the differential diagnosis are discussed. Additional techniques are indispensable to correctly diagnose BMETs. By immunohistochemistry, BMETs often express cytokeratins and/or EMA together with S100, GFAP, or calponin. Half of BMETs harbor EWSR1 (or rare FUS) gene rearrangements with different gene partners.

OVERVIEW, HISTORICAL PERSPECTIVE

To the novice in musculoskeletal pathology who was taught in medical school that the most common bone tumors differentiate along mesenchymal or neuroectodermal lines, it may come as a surprise that some bone tumors show myoepithelial differentiation.

Myoepithelial tumors (METs) of bone (BMETs) are rare. To date, up to 30 cases have been described in the literature.[1–12] BMETs were recognized as a distinct clinicopathological entity only after their initial description in soft tissue.

In 1997, Kilpatrick and colleagues[13] first proposed the unifying concept that METs morphologically resembling myoepithelial counterparts presenting as skin adnexal or salivary gland tumors, may also occur in soft tissue. Hornick and Fletcher[14] described a series of 101 soft tissue METs in 2003, after which Gleason and Fletcher[15] reported a series of 29 soft tissue METs presenting in childhood in 2007. Soft tissue METs represent a wide histologic spectrum with cases showing benign and malignant histomorphology and clinical behavior. In the 2013 World Health Organization (WHO) classification of tumors of soft tissue and bone,[16] the terms myoepithelioma and mixed tumor are used for the benign variants and myoepithelial carcinoma is the proper name for the malignant phenotypes. Myoepithelioma is mainly composed of myoepithelial cells, whereas mixed tumor also shows clear-cut ductal differentiation. The older term parachordoma, which was still used as a synonym for myoepithelioma in the 2002 WHO classification,[16] reflects the morphologic resemblance of some METs to chordoma, but clearly chordoma is a completely different tumor entity, as shown by nuclear immunostaining for the T-box transcription factor brachyury.[17]

Only in the past decade have molecular pathologic studies revealed that the molecular genetic pathogenesis of METs of soft tissue and bone is different from those occurring in skin and salivary glands.

EPIDEMIOLOGY, SITES OF INVOLVEMENT, AND GROSS FEATURES

BMETs have a wide age distribution and show an almost equal sex distribution. Most patients are adults and adolescents, but BMETs also arise in teenagers. The elderly are seldom affected.

Disclosure statements: the authors have no commercial or financial conflicts of interest. W. Song receives funding from the China Scholarship Council (CSC) program (grant no: 201606940023).

[a] Department of Pathology and Medical Biology, University Medical Center Groningen, University of Groningen, PO Box 30.001, Groningen 9700RB, The Netherlands; [b] Department of Pathology, Nijmegen Medical Center, Radboud University, PO Box 9101, Nijmegen 6500HB, The Netherlands

* Corresponding author.

E-mail address: a.j.h.suurmeijer@umcg.nl

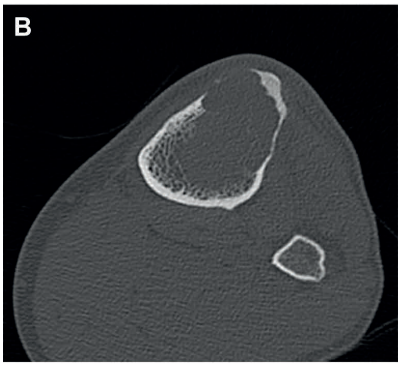

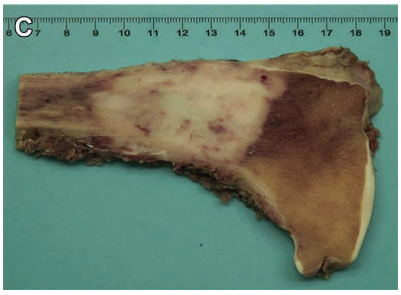

By location, BMETs have a variable distribution. The tumors most often present in long tubular bones (femur, tibia, fibula, humerus), but also occur in small tubular bones (phalanges), and axial skeleton (iliac bone, sacrum, vertebra, ribs, skull, and maxilla).

Although BMETs are usually intraosseous tumors, juxtacortical lesions also have been reported.[8]

By imaging studies (radiographs, computed tomography [CT], MRI) BMETs are well-demarcated, lytic tumors that may have aggressive features and show invasion of surrounding soft tissue (**Fig. 1**). By gross examination of surgical specimens, BMETs are solid, nodular tumors. Cortical destruction and extension in surrounding soft tissue may be present (see **Fig. 1**, **Fig. 2**).

Grossly, BMETs are well-demarcated, nodular, lobulated masses. On cut surface, color and consistency are proportionate to cellularity, collagenization, and myxoid change or hemorrhage. Commonly, BMETs are solid and gray-white, whereas myxochondroid areas are gelatinous and glistening.

MICROSCOPIC FEATURES AND DIAGNOSIS

The histology of benign BMETs (myoepitheliomas) is variable and resembles their salivary gland counterparts (**Fig. 3**). Microscopically, myoepithelial tumor cells can have different features,[18] with areas consisting of bland eosinophilic spindle cells, epithelioid cells, clear cells, squamous cells, or plasmacytoid cells (**Figs. 4–7**). Some tumors are predominantly composed of spindle cells arranged in bundles (**Fig. 8**), whereas other BMETs show foci with epithelioid cells and clear or vacuolated tumor cells that form cohesive cell nests and cords (**Figs. 9** and **10**). Myxoid areas with spindle or epithelioid cells can show a reticular architectural pattern (**Fig. 11**). These neoplastic myoepithelial cells are embedded in a variable amount of fibrous, hyaline fibrous, myxoid, or myxohyaline stroma (see **Figs. 9–11**, **Fig. 12**). Frank cartilaginous or osseous differentiation is rather rare.

Fig. 1. Myoepithelioma of the proximal tibia. (*A*) The plain radiograph and (*B*) MRI both show an intramedullary lytic lesion that is well demarcated, but destroys the cortical bone (*arrows*). (*C*) Gross examination of the cut surface of the resection specimen reveals a well-demarcated, solid, gray-white tumor that is located intramedullary but destroys cortical bone.

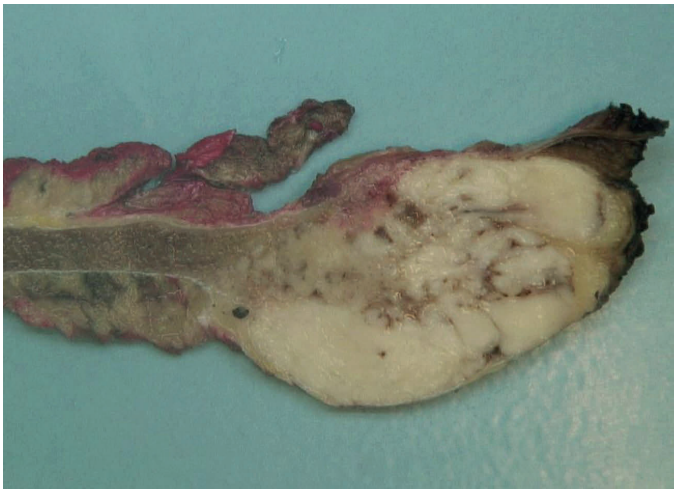

Fig. 2. Myoepithelioma of the scapula. This gross specimen shows a myoepithelioma that breaks through cortical bone and invades the surrounding soft tissue.

Malignant BMETs (myoepithelial carcinomas) show cytonuclear atypia, prominent nucleoli, increased mitotic activity, and areas of necrosis. Morphologic features that distinguish benign myoepitheliomas of bone from malignant variants are not well established.[7] In soft tissue locations, nuclear atypia and prominent nucleoli are currently considered to be the sole histologic features of (potential) malignant behavior. A subset of myoepithelial carcinomas is composed of solid sheets of round tumor cells with nuclear atypia with prominent nucleoli (**Fig. 13**).

The myoepithelial phenotype of BMETs can be demonstrated by immunohistochemistry (IHC) using an appropriate panel of antibodies (**Fig. 14**). The large majority of METs show combined expression of cytokeratins and/or epithelial membrane antigen (EMA) together with S100 and/or

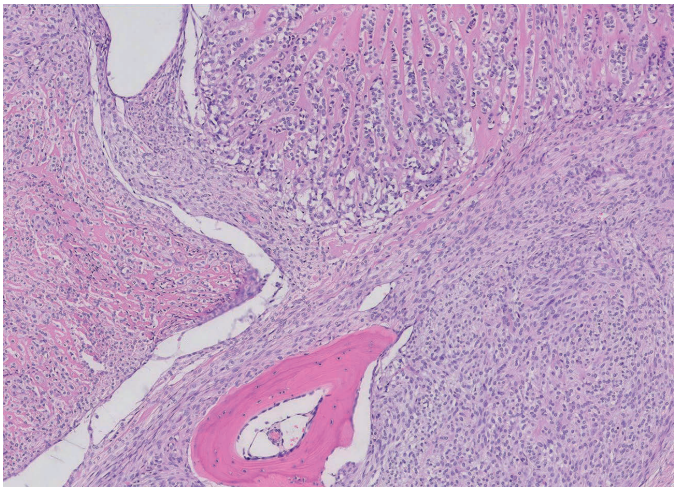

Fig. 3. Myoepithelioma of bone. Hematoxylin and eosin (H&E, original magnification, ×50) microphotograph illustrating the variable histology of myoepithelioma with bundles of spindle cells (lower right) and cords of epithelioid cells embedded in hyalinized fibrous stroma (upper left and right).

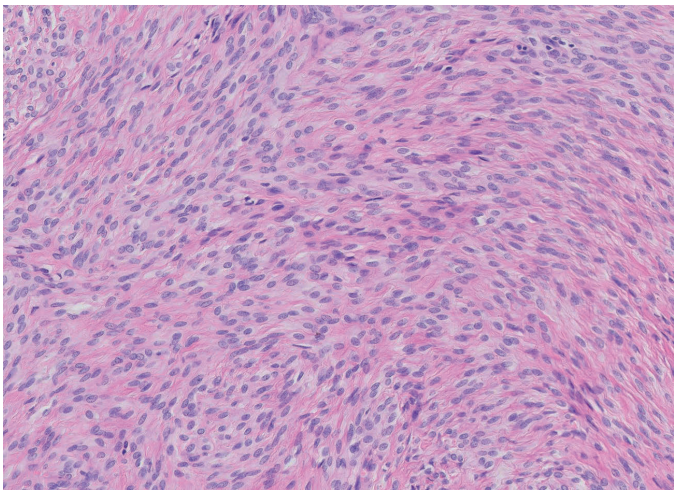

Fig. 4. Myoepithelioma of bone. H&E microphotograph showing an area of spindled tumor cells with monomorphic oval nuclei with fine chromatin and inconspicuous nucleoli. The tumor cells are surrounded by a small amount of fibrillary collagen (H&E, original magnification, ×200).

glial fibrillary acidic protein (GFAP), an immunophenotype required to make a confirmatory diagnosis (**Fig. 15**). Sox-10 is another useful marker for myoepithelial tumors.[19] Smooth muscle markers that have proven to be useful are calponin, smooth muscle actin (SMA), or smooth muscle myosin heavy chain (SMMS-1). A small percentage of myoepithelial carcinomas show loss of SMARCB1/INI1 in tumor cell nuclei.

Nearly half of the BMETs harbor recurrent EWSR1 (and rare FUS) gene fusions, that can be demonstrated using a break-apart fluorescence in situ hybridization (FISH) assay or, more specifically, by reverse-transcriptase polymerase chain reaction (RT-PCR) or next-generation sequencing (NGS). Several different fusion partners have been found in METs (**Fig. 16**). In BMETs, EWSR1 (or FUS) fusion partners described to date are

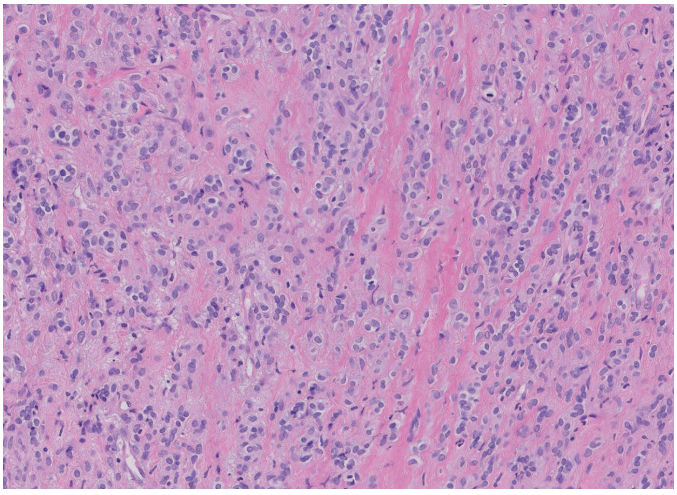

Fig. 5. Myoepithelioma of bone. H&E microphotograph showing an area in which the tumor is composed of epithelioid cells with monomorphic round nuclei with fine chromatin and inconspicuous nucleoli (H&E, original magnification, ×200).

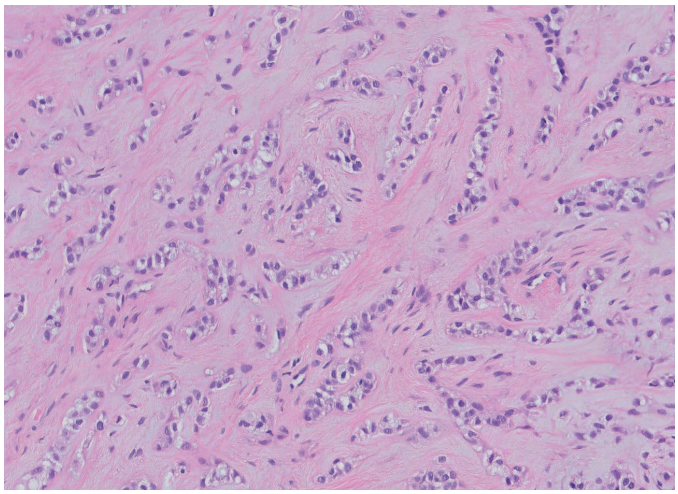

Fig. 6. Myoepithelioma of bone. H&E microphotograph showing an area in which the tumor is composed of clusters and cords of epithelioid tumor cells with clear and vacuolated cytoplasm. The tumor cells are embedded in myxohyaline stroma (H&E, original magnification, ×200).

POU5F1, PBX1, PBX3, and KLF17.[4,9,10,20] Additional fusion partners detected in soft tissue tumors are ZNF444 and ATF1.[10,21]

The molecular pathology of METs of bone and soft tissue is different from METs in salivary glands that lack EWSR1 fusion genes and often show PLAG1 rearrangements. Hence, despite morphologic overlap between these counterparts, METs in bone or soft tissue and salivary gland METs appear to be separate clinicopathological entities.

DIFFERENTIAL DIAGNOSIS

Given their rarity, occurrence in almost any bone, and variable histologic features, it is not surprising that the differential diagnosis of BMETs can be difficult and troubling. Moreover, in daily practice, needle bone biopsies taken for diagnostic histopathology of bone tumors may contain only a limited amount of tumor tissue. Therefore, IHC and molecular pathology are indispensable for an accurate diagnosis.

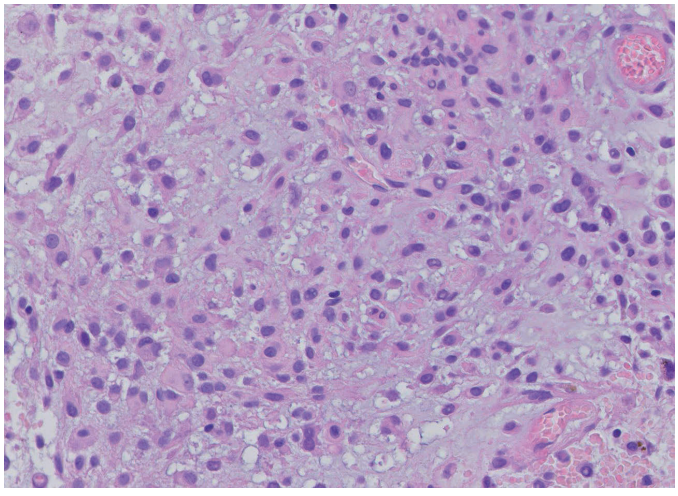

Fig. 7. Myoepithelioma of bone. H&E microphotograph showing an area in which the tumor is composed of plasmacytoid tumor cells with eccentric eosinophilic cytoplasm. The tumor cells are embedded in myxohyaline stroma (H&E, original magnification, ×200).

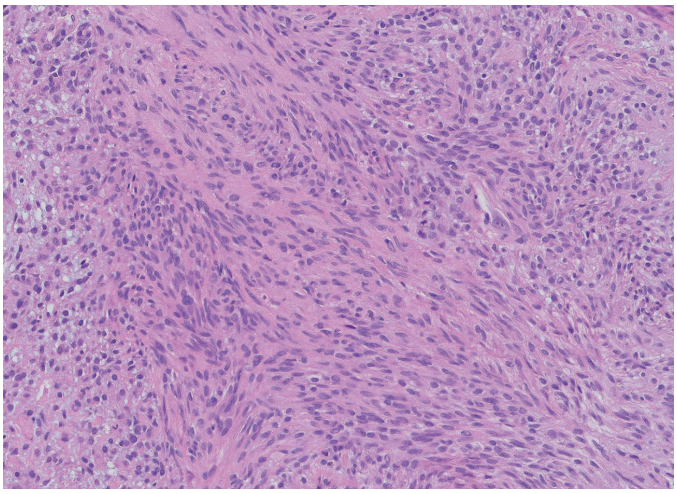

Fig. 8. Myoepithelioma of bone. H&E microphotograph illustrating that myoepithelioma may be predominantly composed of bundles of eosinophilic spindle cells, by which the tumor may be confused with a smooth muscle tumor (H&E, original magnification, ×200).

Herein, we focus on the differential diagnosis of METs presenting as bone tumors.

In the differential diagnosis, we consider the variable histologic appearance of BMETs and discuss bone tumors with relatively bland spindle cells and/or epithelioid cells that are embedded in a variable amount of fibrous, myxoid, or myxohyaline stroma.

Spindle cell bone tumors that enter the differential diagnosis of myoepithelioma are fibrous dysplasia, fibro-osseous dysplasia, desmoplastic fibroma, chondromyxoid fibroma, smooth muscle tumors, and myxoma of jawbones.

Fibrous dysplasia (FD) can present as a solitary nonaggressive and expansile bone lesion. FD often has a typical ground glass appearance on radiographs or CT images, whereas BMETs are lytic and radiolucent. Histologically, FD is easily discriminated from BMETs when areas of metaplastic woven bone are seen. However, needle

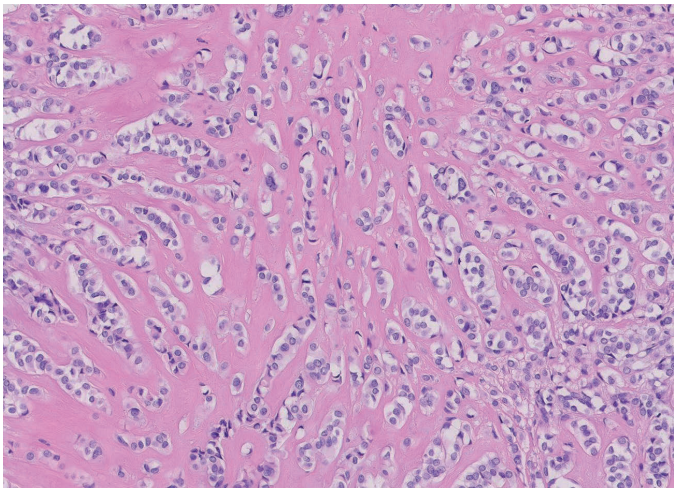

Fig. 9. Myoepithelioma of bone. H&E microphotograph showing an area in which the tumor is composed of hyaline stroma with radiating cords of cohesive tumor cells with eosinophilic and clear cytoplasm, by which the tumor may be confused with chordoma or extraskeletal myxoid chondrosarcoma (H&E, original magnification, ×200).

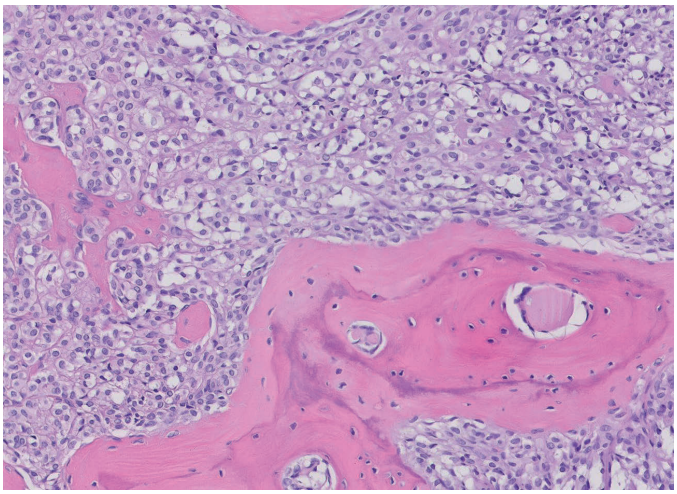

Fig. 10. Myoepithelioma of bone. H&E microphotograph showing an area in which the tumor invades bone marrow and is composed of tumor cells with eosinophilic and strongly vacuolated cytoplasm that is arranged in nests, by which the tumor may be confused with metastatic adenocarcinoma (H&E, original magnification, ×200).

biopsies may contain only the cellular component, woven bone being absent. The bland fibroblastic spindle cells in FD may be arranged in short storiform bundles, a growth pattern that is uncommon in BMETs. IHC expression of keratins and EMA does not occur in FD. Most FD lesions harbor GNAS1 gene mutations that may be detected by PCR, which is a very useful tool when confronted with diagnostically difficult cases.

Osteofibrous dysplasia (OFD) and the closely related OFD-like adamantinoma are bone tumors that predominantly occur in children. The typical location is the diaphysis of the tibia, with few cases presenting in the fibula. OFD and OFD-like

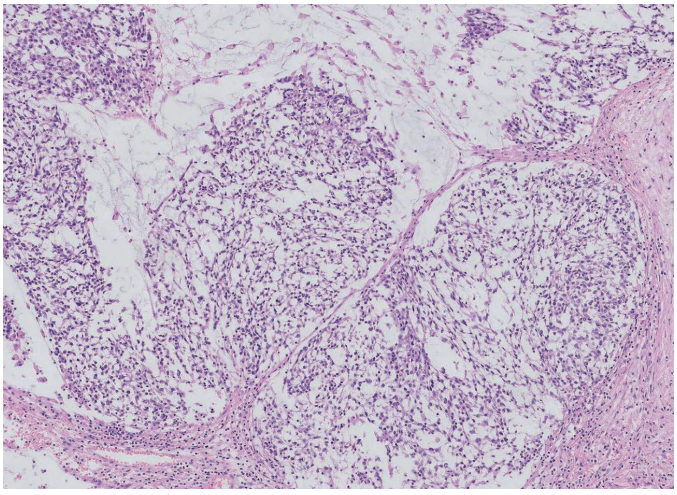

Fig. 11. Myoepithelioma of bone. H&E microphotograph, showing a myxoid area in which the tumor has a reticular architecture, reminiscent of extraskeletal myxoid chondrosarcoma (H&E, original magnification, ×100).

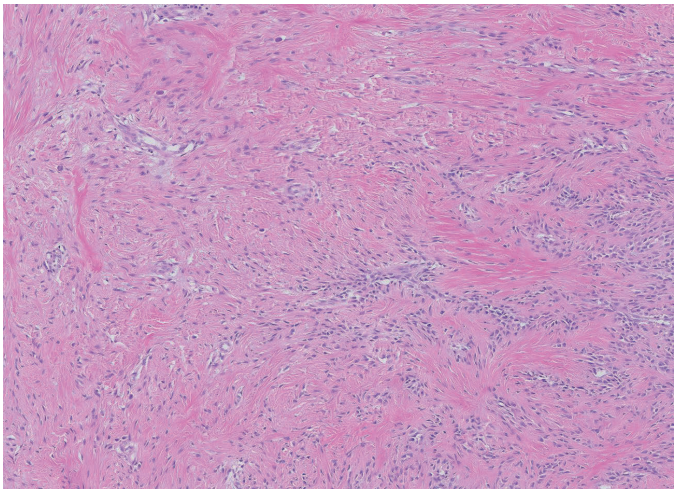

Fig. 12. Myoepithelioma of bone. H&E microphotograph showing an area in which the tumor has abundant fibrous stroma with spindle cells, by which the tumor may be confused with FD, fibro-osseous dysplasia, or DF (H&E, original magnification, ×50).

adamantinoma are intracortical lesions, clearly different from the intramedullary location of BMETs. Confusion may arise, however, because OFD and OFD-like adamantinoma contain single or grouped spindle cells that are positive for (basal type) cytokeratins and EMA. Importantly, IHC for S100, GFAP, and calponin is negative.

The clinical and radiologic presentation of desmoplastic fibroma (DF) and BMETs show much overlap, as both lesions may present as expansile, lytic lesions with cortical breakthrough. DF is most common in the mandible, but also may occur in other bones. Microscopically, DF is usually composed of bundles of fibroblastic spindle cells with tapering cytoplasm arranged in a collagenous stroma, by which the tumor resembles desmoid-type fibromatosis of soft tissue. Approximately half of DF cases show cytoplasmic staining for

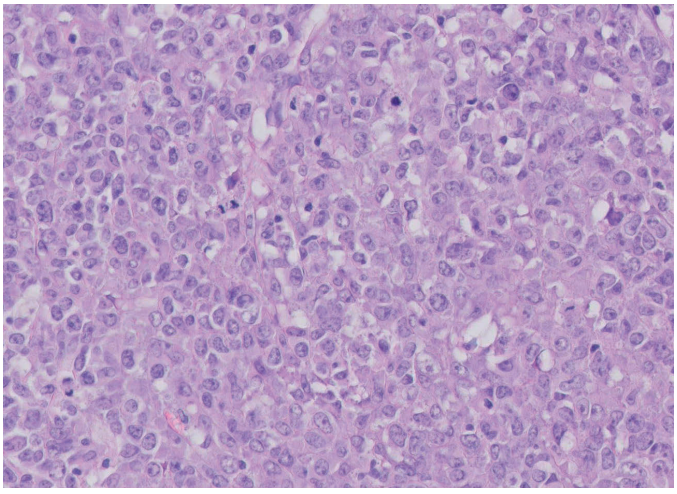

Fig. 13. Myoepithelial carcinoma. H&E microphotograph showing sheets of round tumor cells with hyperchromatic nuclei, prominent nucleoli, and mitotic activity (H&E, original magnification, ×200).

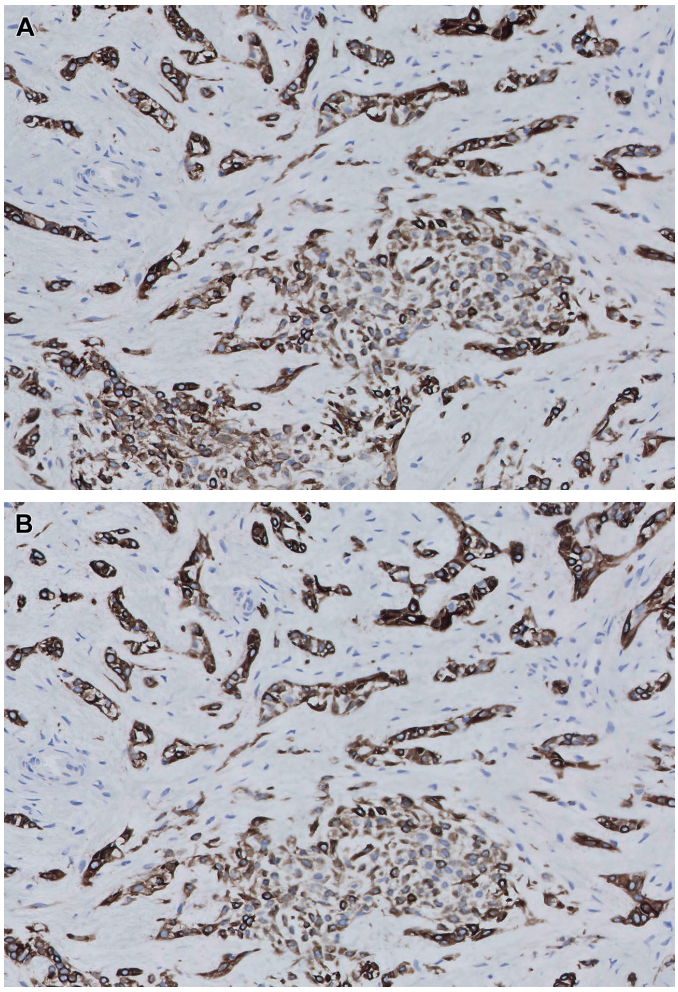

Fig. 14. Myoepithelioma of bone. IHC. Epithelioid areas are usually strongly positive for (*A*) cytokeratins and (*B*) EMA, whereas spindle cell areas show variable staining for (*C*) cytokeratins, (*D*) EMA, (*E*) S100, (*F*) calponin, and (*G*) SMA (H&E, original magnification, ×200).

beta-catenin, whereas nuclear staining is seldom found. DF has no beta-catenin gene mutations. Moreover, DF lacks expression of the IHC markers and gene fusions typical of BMETs.

The clinical and radiologic presentation of chondromyxoid fibroma (CMF) and BMETs may mimic each other. Microscopically distinctive features of CMF are lobules of which central zones contain eosinophilic spindle and stellate cells in a myxoid background, whereas peripheral zones tend to be more cellular and harbor osteoclasts. CMF is often S100 positive, but lacks expression of cytokeratins, EMA, or GFAP.

The preferential sites of leiomyoma of bone are mandible and tibia. Well-differentiated leiomyosarcoma may present in the long tubular bones of the lower extremity but also in craniofacial bones. With imaging, leiomyoma and well-differentiated leiomyosarcoma are lytic lesions that may show cortical expansion. Microscopically, smooth

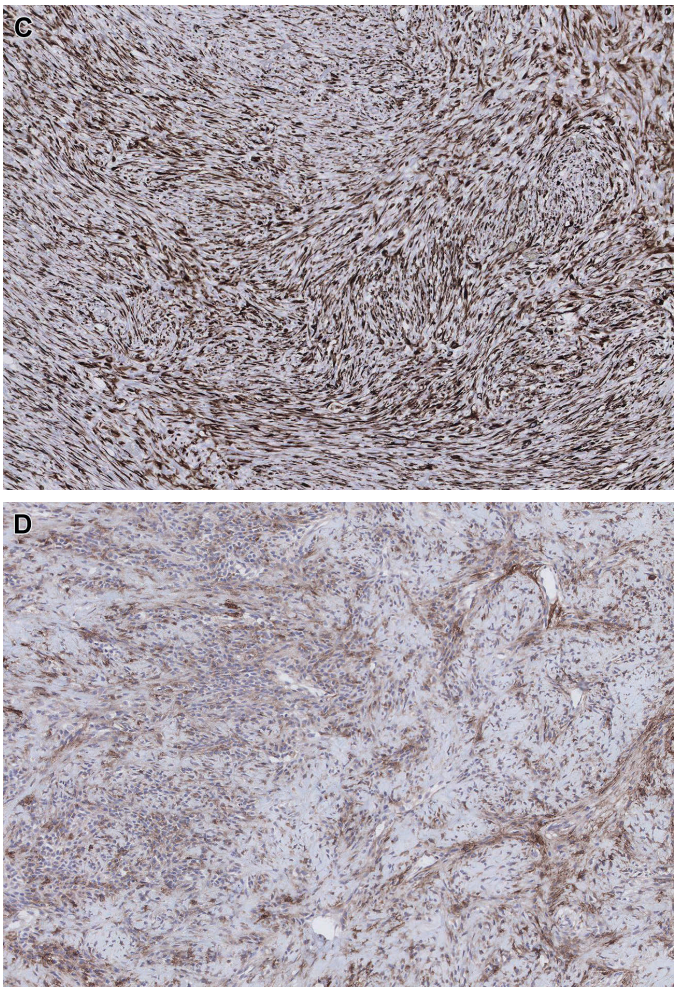

Fig. 14. (*continued*).

muscle tumors typically have interlacing bundles of eosinophilic spindle cells with elongated, hyperchromatic, cigar-shaped nuclei and well-defined eosinophilic cytoplasm. By IHC, smooth muscle tumors may express keratin, EMA, and calponin, but lack positivity for S100 or GFAP. Caldesmon and desmin are discriminatory markers of smooth muscle tumors. Given that primary smooth muscle tumors of bone are exceptionally rare, metastatic smooth muscle tumors should also be considered in the differential diagnosis. Metastatic gynecologic smooth muscle tumors show nuclear staining for hormone receptors.

Myxomas presenting in the mandible and maxilla, thought to be of odontogenic origin, are well-circumscribed lytic lesions and show a high T2-weighted signal by MRI. Histologically, myxomas of jawbones have abundant myxoid stroma containing bland stellate and spindle cells. BMETs may contain areas resembling myxoma, but

Fig. 14. (*continued*).

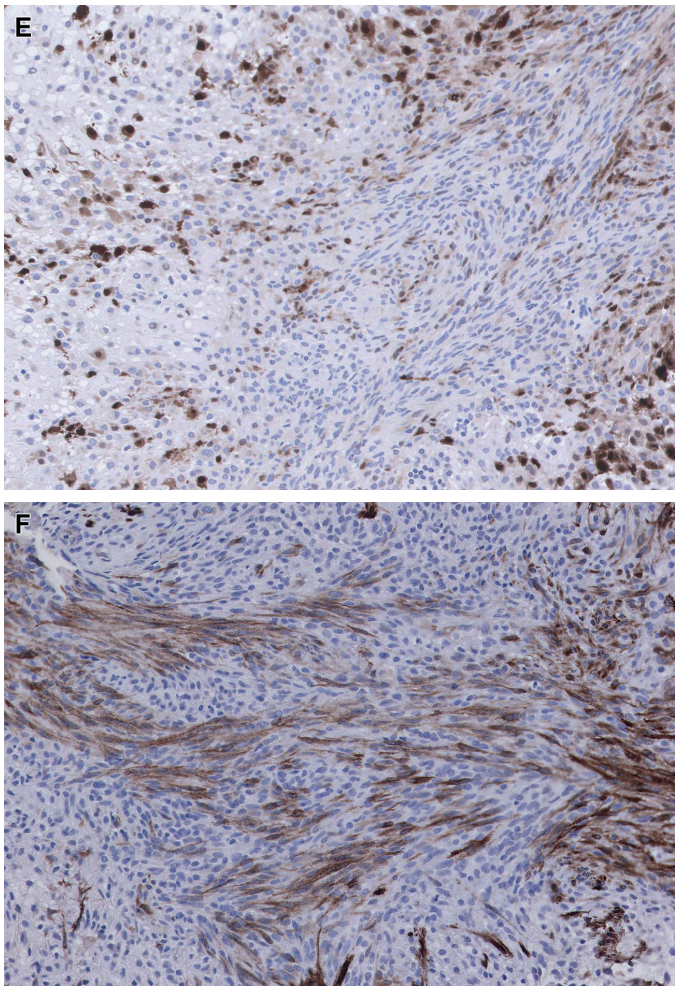

BMETs usually have a more variable histology and will stain for the IHC markers mentioned previously. Myxoma of jawbones does not have specific gene mutations or fusions (See Daniel Baumhoer's article, "Bone Related Lesions of the Jaws," in this issue).

Epithelioid tumors considered in the differential diagnosis of BMETs are chordoma, extraskeletal myxoid chondrosarcoma, sclerosing epithelioid fibrosarcoma, and epithelioid hemangioendothelioma.

Chordomas characteristically arise in the vertebral column, although rare extra-axial lesions also have been diagnosed.[17] Epithelioid areas in BMETs may show a striking resemblance to those seen in chordoma, hence the older term parachordoma for METs. However, usually, the tumor cells in chordomas are larger and more vacuolated than

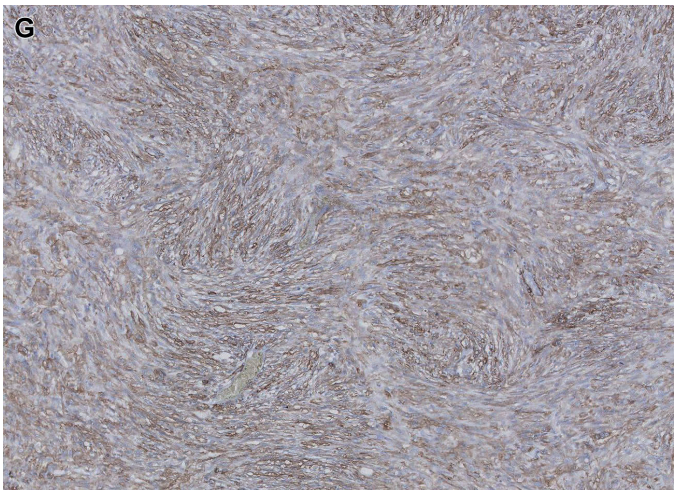

Fig. 14. (*continued*).

in BMETs. Both chordomas and BMETs express cytokeratins, EMA, and S100. Therefore, immunostaining for brachyury is required to diagnose chordoma (**Fig. 17**).[17]

Extraskeletal myxoid chondrosarcoma (EMC) is a distinct soft tissue sarcoma that may also show a striking resemblance to myoepithelioma. Although few cases have been described,[22] it is well appreciated that EMC also may present in bone. By IHC, EMC is often positive for S100 and EMA, but lacks cytokeratin expression. EMC often contains an NR4A3 fusion gene that allows a specific diagnosis. Importantly, EWSR1 is the most common fusion partner of NR4A3. Therefore, when using FISH, NR4A3 probes must be used instead of EWSR1 probes to distinguish between EMC and BMET.[23]

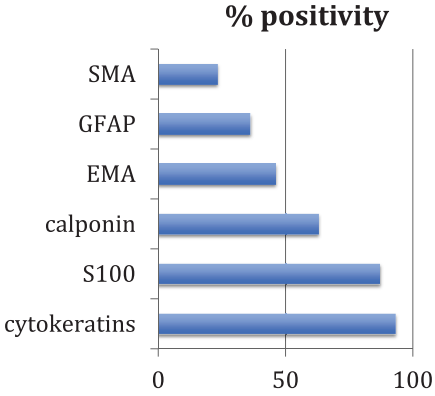

Fig. 15. IHC markers for myoepithelial tumors. (*Data from* Hornick JL, Fletcher CD. Myoepithelial tumors of soft tissue: a clinicopathologic and immunohistochemical study of 101 cases with evaluation of prognostic parameters. Am J Surg Pathol 2003;27:1183–96.)

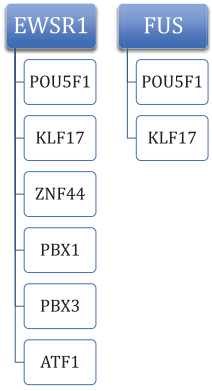

Fig. 16. Gene fusions in myoepithelial tumors.

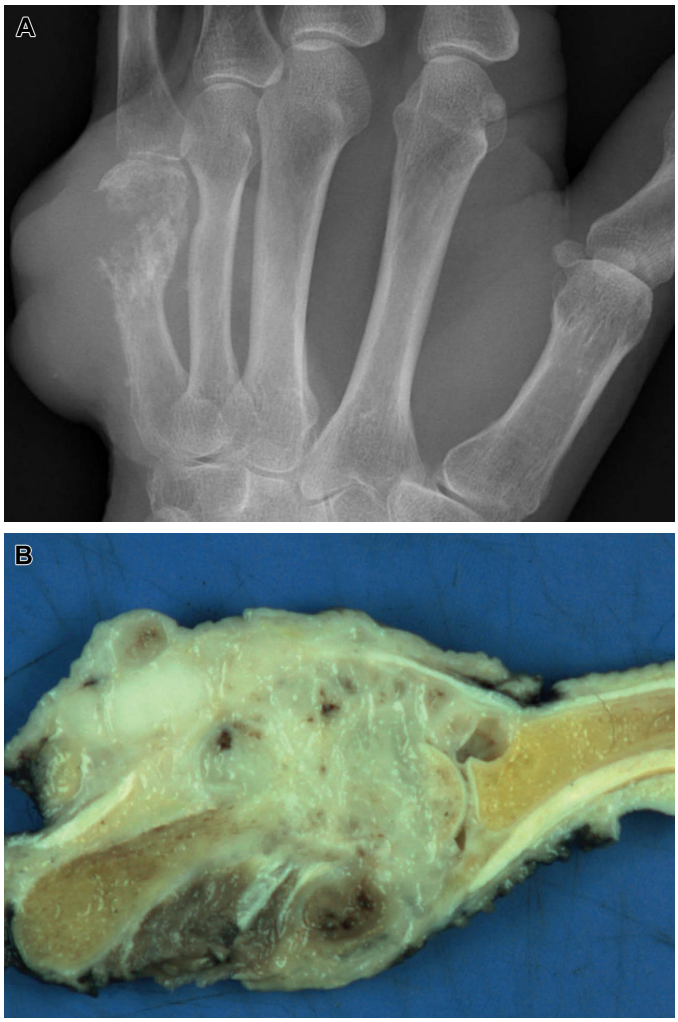

Fig. 17. Extra-axial chordoma of the fifth metacarpal bone, originally diagnosed as parachordoma. (*A*) Plain radiograph showing a lytic and destructive tumor of the fifth metacarpal bone that invades surrounding soft tissue. (*B*) Gross specimen showing a glistening myxoid bone tumor that invades surrounding soft tissue.

Sclerosing epithelioid fibrosarcoma (SEF) is a distinct soft tissue tumor that is related to low-grade fibromyxoid sarcoma (LGFMS). Rare cases of SEF have been described as primary bone tumors.[24] A case of SEF occurring in the distal femur is illustrated in **Fig. 18**. MUC4 immunostaining is very sensitive and specific for SEF and LGFMS. BMETs are negative for MUC4. SEF and LGFMS often have a gene fusion of either FUS or EWSR1 with CREBL1 or CREBL2. Thus, FISH for EWSR1 and FUS cannot be used to differentiate SEF from BMETs. RT-PCR or NGS can be applied for further confirmation of SEF by molecular pathology.

Epithelioid hemangioendothelioma (EHE) is an endothelial neoplasm composed of cords, nests, and strands of epithelioid endothelial cells arranged in myxohyaline stroma, by which it may

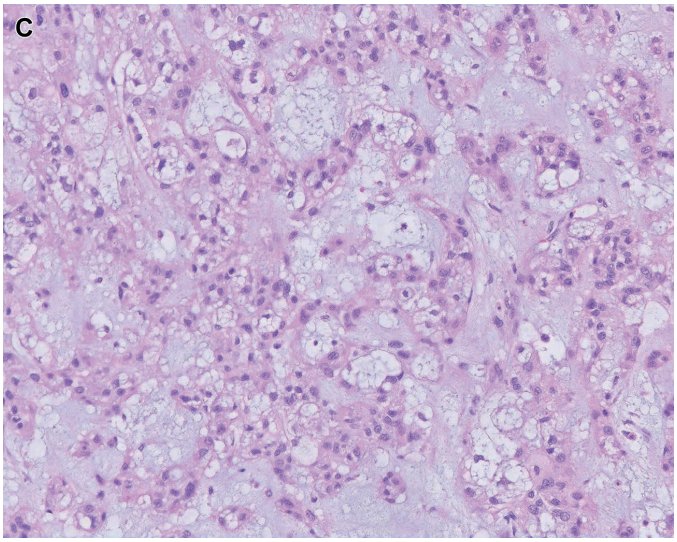

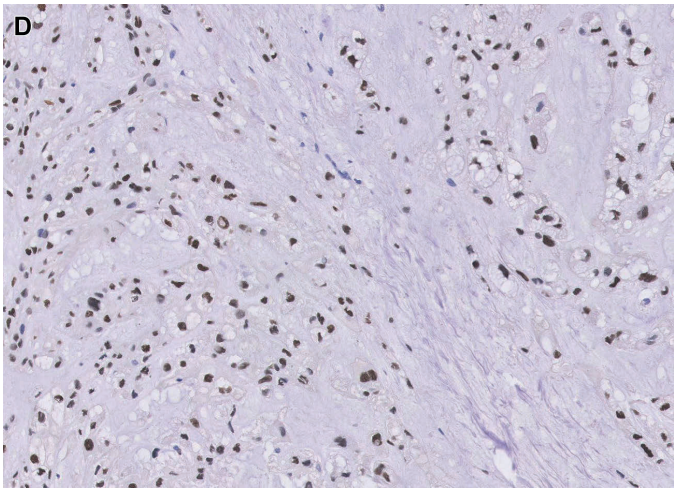

Fig. 17. (*continued*). (*C*) H and E microphotograph showing cords and nests with cohesive epithelioid tumor cells with strongly vacuolated (so-called physaliferous) cytoplasm. The tumor cells are embedded in myxohyaline stroma (H&E, original magnification, ×200). (*D*) IHC for brachyury showing nuclear staining of tumor cells (H&E, original magnification, ×200).

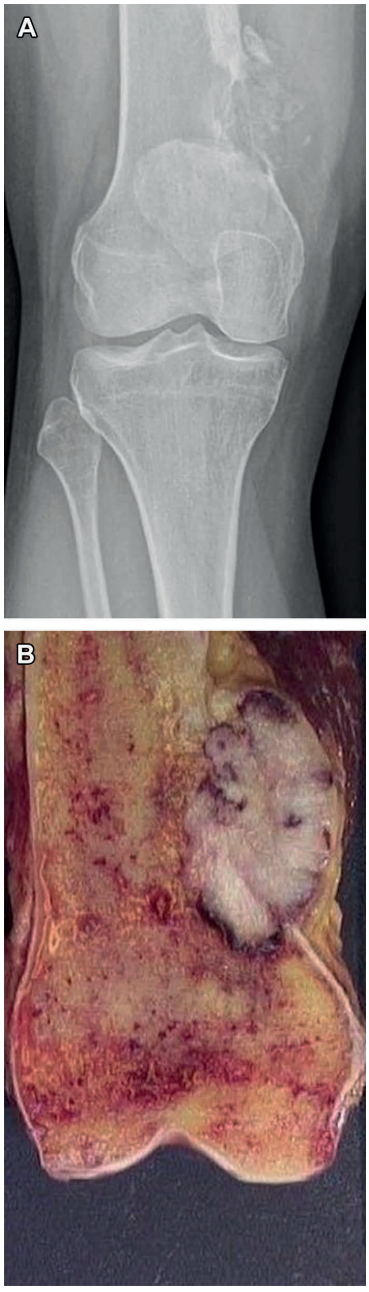

strongly resemble BMET. Bone locations of EHE include long and small tubular bones, vertebra, and jawbones.[25] The tumor cells of EHE often have vacuolated cytoplasm and may contain engulfed erythrocytes. EHE may express cytokeratins and EMA. However, IHC for endothelial markers (ERG, CD31, and CD34) will render a correct diagnosis. EHE has a consistent WWTR1-CAMTA1 fusion gene. An alternate YAP1-TFE3 fusion is present in a small subset of cases. For further details, see David G.P. van IJzendoorn and Judith V.M.G. Bovée's article, "Vascular Tumors of Bone: The Evolvement of a Classification Based on Molecular Developments," in this issue.

Understandably, myoepitheliomas with an epithelioid phenotype and cytoplasmic vacuolization or myoepithelial carcinomas showing clear-cut cytonuclear malignant features are easily confused with metastatic carcinoma. Hence, clinical evaluation and a panel of appropriate IHC markers for carcinomas that often metastasize to bone must be applied. Approximately 10% of myoepithelial carcinomas show loss of SMARCB1/INI1 in tumor cell nuclei by IHC.

Helpful distinguishing clinicopathological features of bone tumors mimicking BMETs are summarized in **Boxes 1** and **2**.

PROGNOSIS

Because of the rarity of METs in bone and limited follow-up of few published case series, it is as yet impossible to establish the prognostic value of cytologic features. It seems reasonable to adapt the criteria used for METs arising in soft tissue locations. Nuclear atypia and prominent nucleoli are currently considered to be the sole histologic features of (potential) malignant behavior. METs arising in soft tissue that show bland cytonuclear features usually have a good outcome, whereas METs with nuclear atypia and prominent nucleoli have metastatic potential.

Fig. 18. SEF of the distal femur. (*A*) Plain radiograph showing a lytic and destructive tumor of the distal femur that invades surrounding soft tissue. (*B*) Gross specimen showing a well-demarcated gray-white tumor that invades surrounding soft tissue. (*C*) H&E microphotograph showing cords of epithelioid tumor cells with clear cytoplasm surrounded by strands of hyalinized collagen (H&E, original magnification, ×100).

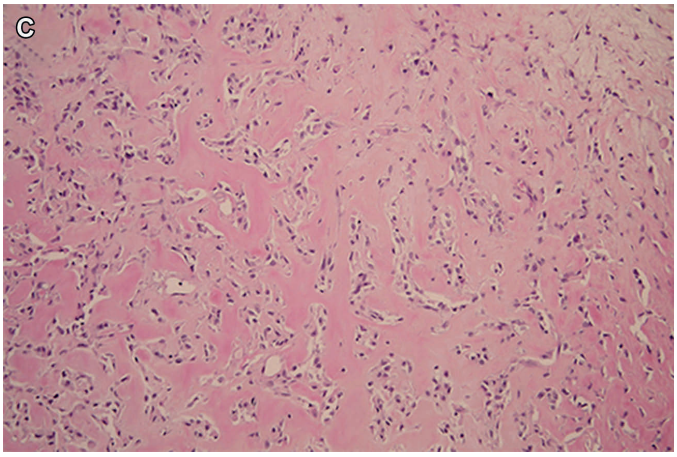

Fig. 18. (*continued*).

Box 1
Differential diagnosis of myoepithelioma

Helpful distinguishing features of spindle cell bone tumors resembling myoepithelioma

Fibrous dysplasia

- Imaging: nonaggressive, but often expansile lesion with ground glass appearance
- Histology: deposition of woven bone by spindle cells arranged in storiform pattern
- Immunohistochemistry (IHC): negative for keratins, epithelial membrane antigen (EMA), S100, glial fibrillary acidic protein (GFAP), and calponin
- Molecular pathology: 90% have GNAS1 mutations

Osteofibrous dysplasia (OFD) and OFD-like adamantinoma

- Epidemiology: predominantly presenting in children
- Imaging: cortical lesion in the diaphysis of the tibia
- Histology: deposition of woven bone by osteoblasts
- IHC: keratin/EMA-positive spindle cells are negative for S100, GFAP, and calponin

Desmoplastic fibroma

- Histology: collagen-rich bundles with fibroblasts, resembling desmoid fibromatosis
- IHC: negative for keratins, EMA, S100, and GFAP

Chondromyxoid fibroma

- Histology: lobular architecture with spindle and stellate cells in myxoid background
- IHC: S100 often positive, whereas keratins, EMA, and GFAP are negative

Leiomyoma and well-differentiated leiomyosarcoma

- Histology: interlacing bundles of smooth muscle cells with elongated nuclei
- IHC: caldesmon and desmin are positive in smooth muscle tumors, negative in bone myoepithelial tumors (BMETs)

Myxoma of jawbones

- Imaging: high T2-weighted signal on MRI
- Histology: abundant myxoid stroma with stellate tumor cells
- IHC: negative for keratins, EMA, S100, and GFAP

(*Continued*)

Box 1
Differential diagnosis of myoepithelioma (*continued*)

Helpful distinguishing features of epithelioid bone tumors resembling myoepithelioma

Chordoma

- Imaging: high T2-weighted signal on MRI
- Histology: large vacuolated (physaliferous) tumor cells
- IHC: chordoma is positive for the transcription factor brachyury

Extraskeletal myxoid chondrosarcoma

- IHC: EMC is keratin negative
- Molecular pathology: NR4A3 gene fusions (fluorescence in situ hybridization for EWSR1 does not help)

Sclerosing epithelioid fibrosarcoma

- IHC: MUC4 is a sensitive and specific marker
- Molecular pathology: FUS or EWSR1 gene fusions with CREBL1 or CREBL2

Epithelioid hemangioendothelioma

Histology: few vacuolated tumor cells have engulfed erythrocytes

IHC: tumor cells are positive for endothelial markers: ERG, CD31, and CD34

Molecular pathology: WWTR1-CAMTA1 fusion gene. A YAP1-TFE3 fusion is found in a small subset of epithelioid hemangioendothelioma cases

Box 2
Pathologic Key Features

Myoepithelioma of bone

- May arise in many different bones, including long and small tubular bones, the axial skeleton, and craniofacial bones
- Has a wide age range, but is rare in the elderly
- Has a variable histology, often with spindled and/or epithelioid cells in a variable amount of fibrous and myxohyaline stroma
- In addition to morphology, expression of cytokeratin/EMA with either S100 or GFAP, or calponin is required for an appropriate diagnosis
- Nearly half of the tumors harbor EWSR1 (or rare FUS) gene fusion with different partners
- Myoepithelial carcinoma shows cytonuclear atypia and prominent nucleoli and sometimes consists of sheets of undifferentiated round epithelioid cells

Key Features

- Myoepithelial tumors (METs) of bone (BMETs) are a rare but distinct tumor entity.
- METs that are cytologically benign are termed myoepitheliomas, whereas METs with malignant histologic features are called myoepithelial carcinomas.
- BMETs have a wide age range, may involve any part of the skeleton, and have a variable spindle cell and epithelioid morphology.

REFERENCES

1. Alberghini M, Pasquinelli G, Zanella L, et al. Primary malignant myoepithelioma of the distal femur. APMIS 2007;115:376–80.
2. Biradar P, Menon S, Patil A, et al. Primary myoepithelial carcinoma of rib bone: morphology, immunohistochemical evaluation and diagnostic dilemma in an unusual case. J Cancer Res Ther 2015;11:647.
3. Cuesta Gil M, Bucci T, Navarro Cuellar C, et al. Intraosseous myoepithelioma of the maxilla: clinicopathologic features and therapeutic considerations. J Oral Maxillofac Surg 2008;66:800–3.
4. Antonescu CR, Zhang L, Chang NE, et al. EWSR1-POU5F1 fusion in soft tissue myoepithelial tumours. A molecular analysis of sixty-six cases, including soft tissue, bone, and visceral lesions, showing common involvement of the EWSR1 gene. Genes Chromosomes Cancer 2010;49:1114–24.
5. Park JS, Ryu KN, Han CS, et al. Malignant myoepithelioma of the humerus with satellite lesion: a case report and literature review. Br J Radiol 2010; 83:161–4.
6. Rekhi B, Amare P, Gulia A, et al. Primary intraosseous myoepithelioma arising in the iliac bone and displaying trisomies of 11, 15, 17 with del (16q) and del (22q11)–a rare case report with review of literature. Pathol Res Pract 2011;207:780–5.
7. Kurzawa P, Kattapuram S, Hornicek FJ, et al. Primary myoepithelioma of bone: a report of 8 cases. Am J Surg Pathol 2013;37:960–8.
8. Franchi A, Palomba A, Roselli G, et al. Primary juxtacortical myoepithelioma/mixed tumour of the bone: a report of 3 cases with clinicopathologic, immunohistochemical, ultrastructural, and molecular characterization. Hum Pathol 2013;44:566–77.
9. Puls F, Arbajian E, Magnusson L, et al. Myoepithelioma of bone with a novel FUS-POU5F1 fusion gene. Histopathology 2014;65:917–22.
10. Huang SC, Chen HW, Zhang L, et al. Novel FUS-KLF17 and EWSR1-KLF17 fusions in myoepithelial tumors. Genes Chromosomes Cancer 2015;54:267–75.
11. Nambirajan A, Mridha AR, Sharma MC, et al. Primary intra-osseous myoepithelioma of phalanx mimicking an enchondroma. Skeletal Radiol 2016;4:1453–8.
12. Rekhi B, Joshi S, Panchwagh Y, et al. Clinicopathological features of five unusual cases of intraosseous myoepithelial carcinomas, mimicking conventional primary bone tumours, including EWSR1 rearrangement in one case. APMIS 2016;124:278–90.
13. Kilpatrick SE, Hitchcock MG, Kraus MD, et al. Mixed tumors and myoepitheliomas of soft tissue: a clinicopathologic study of 19 cases with a unifying concept. Am J Surg Pathol 1997;21:13–22.
14. Hornick JL, Fletcher CD. Myoepithelial tumours of soft tissue: a clinicopathologic and immunohistochemical study of 101 cases with evaluation of prognostic parameters. Am J Surg Pathol 2003;27:1183–96.
15. Gleason BC, Fletcher CD. Myoepithelial carcinoma of soft tissue in children: an aggressive neoplasm analyzed in a series of 29 cases. Am J Surg Pathol 2007;31:1813–24.
16. Kilpatrick SE, Limon J. Mixed tumor/myoepithelioma/parachordoma. In: Fletcher CDM, Unni K, Mertens F, editors. World Health Organization classification of tumours. Tumours of soft tissue and bone. Lyon (France): IARC; 2002. p. 198–9.
17. Tirabosco R, Mangham DC, Rosenberg AE, et al. Brachyury expression in extra-axial skeletal and soft tissue chordomas: a marker that distinguishes chordoma from mixed tumor/myoepithelioma/parachordoma in soft tissue. Am J Surg Pathol 2008;32:572–80.
18. Chitturi RT, Veeravarmal V, Nirmal RM, et al. Myoepithelial cells (MEC) of the salivary glands in health and tumours. J Clin Diagn Res 2015;9:14–8.
19. Miettinen M, McCue PA, Sarlomo-Rikala M, et al. Sox10-a marker for not only schwannian and melanocytic neoplasms but also myoepithelial cell tumors of soft tissue: a systematic analysis of 5134 tumors. Am J Surg Pathol 2015;39:826–35.
20. Agaram NP, Chen HW, Zhang L, et al. EWSR1-PBX3: a novel gene fusion in myoepithelial tumors. Genes Chromosomes Cancer 2015;54:63–71.
21. Flucke U, Mentzel T, Verdijk MA, et al. EWSR1-ATF1 chimeric transcript in a myoepithelial tumor of soft tissue: a case report. Hum Pathol 2012;43:764–8.
22. Demicco EG, Wang WL, Madewell JE, et al. Osseous myxochondroid sarcoma: a detailed study of 5 cases of extraskeletal myxoid chondrosarcoma of the bone. Am J Surg Pathol 2013;37: 752–62.
23. Flucke U, Tops BB, Verdijk MA, et al. NR4A3 rearrangement reliably distinguishes between the clinicopathologically overlapping entities myoepithelial carcinoma of soft tissue and cellular extraskeletal myxoid chondrosarcoma. Virchows Arch 2012;460: 621–8.
24. Wojcik JB, Bellizzi AM, Dal Cin P, et al. Primary sclerosing epithelioid fibrosarcoma of bone: analysis of a series. Am J Surg Pathol 2014;38:1538–44.
25. Flucke U, Vogels RJ, de Saint Aubain Somerhausen N, et al. Epithelioid hemangioendothelioma: clinicopathologic, immunohistochemical, and molecular genetic analysis of 39 cases. Diagn Pathol 2014;9:131.

Chapter 5

Novel recurrent *PHF1-TFE3* fusions in ossifying fibromyxoid tumors

This chapter is based on the publication: Suurmeijer AJH, **Song W**, Sung YS, et.al. Novel recurrent *PHF1-TFE3* fusions in ossifying fibromyxoid tumors. Genes Chromosomes Cancer. 2019 Sep;58(9):643-649

Novel recurrent *PHF1-TFE3* fusions in ossifying fibromyxoid tumors

Albert J. H. Suurmeijer[1] | Wangzhao Song[1] | Yun-Shao Sung[2] | Lei Zhang[2] | David Swanson[3] | Christopher D. M. Fletcher[4] | Brendan C. Dickson[3] | Cristina R. Antonescu[2]

[1]Department of Pathology, University Medical Center Groningen, University of Groningen, Groningen, The Netherlands

[2]Department of Pathology, Memorial Sloan Kettering Cancer Center, New York, New York

[3]Department of Pathology and Laboratory Medicine, Mount Sinai Hospital, Toronto, Ontario, Canada

[4]Department of Pathology, Brigham and Women's Hospital, Harvard Medical School, Boston, Massachusetts

Correspondence
Albert J. H. Suurmeijer, Department of Pathology and Medical Biology, University Medical Center Groningen, Hanzeplein 1, 9713 GZ Groningen, The Netherlands.
Email: a.j.h.suurmeijer@umcg.nl

Cristina R. Antonescu, Department of Pathology, Memorial Sloan Kettering Cancer Center, 10021 New York, NY.
Email: antonesc@mskcc.org

Funding information
National Cancer Institute, Grant/Award Number: P30 CA008748; National Institue of Health, Grant/Award Number: P50 CA217694; National Institute of Health, Grant/Award Number: P50 CA 140146-01; Cycle for Survival, Slifka Foundation; St Baldrick Foundation

Abstract

Ossifying fibromyxoid tumor (OFMT) is an uncommon mesenchymal neoplasm of uncertain differentiation and intermediate malignant potential. Recurrent *PHF1* gene rearrangements are detected in up to 80% of OFMTs. We describe the clinicopathologic features of five OFMTs harboring a novel *PHF1-TFE3* fusion. In two cases, RNA sequencing identified a fusion transcript composed of *PHF1* exon 11 fused to *TFE3* exon 3, whereas in a third case *PHF1* exon 12 was fused to *TFE3* exon 7. A FISH break-apart assay revealed rearrangements in both *PHF1* and *TFE3* genes in all cases. The cohort included three males and two females with a median age of 64 years. One OFMT originated in the scapula, while four occurred in the deep soft tissues. Two OFMTs had typical features, whereas three were classified as malignant. Despite uniform cytologic features and fibromyxoid stroma compatible with an OFMT diagnosis, none showed a peripheral shell of lamellar bone. S100 expression was focally present in only one case, while desmin was positive in three cases. All tumors showed strong nuclear immunopositivity for TFE3. All three malignant OFMTs developed metastases, either regionally or to the lung. One patient died of disease 1 year after diagnosis, while the remaining two are alive with disease. In summary, we report novel recurrent *PHF1-TFE3* fusions in a subset of OFMTs with aggressive clinical behavior. The *PHF1-TFE3* fusions resulted in consistent protein TFE3 overexpression which can be used as a reliable screening tool, adding OFMT as another tumor driven by TFE3 oncogenic activation pathway.

KEYWORDS
fusion, ossifying fibromyxoid tumor, PHF1, TFE3

1 | INTRODUCTION

Ossifying fibromyxoid tumor (OFMT) is a rare soft tissue neoplasm, affecting middle-aged and older adults with a slight male predominance and presenting as slow growing, superficial or deep-seated masses in the extremities, head and neck area or trunk. The tumors have a local recurrence rate of 10%-20% and a very low risk of metastatic disease. Grossly, OFMT is a multinodular neoplasm surrounded by a thick fibrous capsule, often containing a thin shell of trabecular bone. Like most other translocation-positive soft tissue tumors, OFMT has a uniform cytomorphology and is composed of epithelioid, ovoid, short spindled, and sometimes rhabdoid cells arranged in nests, cords or lace-like architectural patterns, typically in a fibromyxoid or myxohyaline stroma. In typical OFMT mitoses are

scarce. The appropriate terminology of lesions with worrisome histologic features, such as high cellularity and increased mitotic activity, is still debatable, in particular if such cases should be designated as atypical or malignant OFMT.[1,2] Most OFMTs are positive for S100, while the remaining 10%-20% of negative cases may show only desmin reactivity or a nonspecific immunoprofile. The genetic hallmark of OFMTs are recurrent *PHF1* gene rearrangements, detected in up to 80%, spanning both typical and diagnostically challenging tumors at the atypical or malignant end of the morphologic spectrum.[3–5] The most common *PHF1* fusion partner is *EP400*, reported in almost half of cases,[5] with occasional cases showing variant fusions with *MEAF6* and *EPC1* genes.[5] Other less common gene fusions include *ZC3H7B-BCOR*, *CREBBP-BCORL1*, and *KDM2A-WWTR1* reported in a handful of cases.[5,6] Prompted by an index case of malignant OFMT with an unusual immunoprofile and a novel *PHF1-TFE3* fusion detected by RNA sequencing (RNA Seq), we sought to investigate this abnormality in a group of OFMTs lacking defined genetic alterations.

2 | MATERIALS AND METHODS

2.1 | Index case and patient selection

A 70-year-old male patient presented with a large, deep-seated soft tissue mass within the gluteal muscle. Grossly, the tumor measured 10 cm in largest diameter and showed an infiltrative growth within the surrounding soft tissues, with multiple satellite nodules extending along the fascia (Figure 1). Microscopically, the tumor was composed of encapsulated nodules of myxohyaline stroma with radiating cords of uniform epithelioid and ovoid spindle cells with atypical hyperchromatic nuclei, indistinct nucleoli and granular eosinophilic cytoplasm. The tumor showed overtly malignant features, including infiltrative growth within skeletal muscle, increased mitotic activity of up to 16 mitoses in 25 HPF corresponding to 5 mm^2, areas of necrosis, and lymphovascular invasion (Figure 2). Immunohistochemically, the tumor diffusely expressed cytokeratins (including CK19), E-cadherin, CD56, and synaptophysin, in addition to focal EMA and S100. Desmin stain was negative. Given the immunophenotype of the tumor, the differential diagnosis included neuroendocrine carcinoma and myoepithelial carcinoma. Staging work-up at diagnosis detected two small lung metastases, measuring 6 and 13 mm. Subsequently, two inguinal lymph node metastases of 12 mm were identified 2 months after initial presentation, which were treated with local radiotherapy. The patient died of progressive disease (lung metastases) 1 year after diagnosis. By RNA sequencing a novel *PHF1-TFE3* fusion gene was identified in keeping with a malignant OFMT.

In order to establish its recurrent potential as well as estimate the frequency of this novel *PHF1-TFE3* fusion, we searched our files for OFMT cases with either unknown genetic abnormalities or tumors with *PHF1* rearrangements, but lacking a known gene partner. A combined molecular approach, including targeted RNA Seq and fluorescence in situ hybridization (FISH) was used to identify fusion candidates. Tumors were re-reviewed and morphologic findings were recorded, especially ones related to worrisome or atypical histologic features. Previously described diagnostic criteria for malignancy were applied.[2,5] Briefly, malignant OFMT was defined as showing high nuclear grade or high cellularity and mitotic activity > 2/50 HPF. Atypical OFMT has been defined as a tumor with histologic findings deviating from typical OFMT, but fall short meeting the above criteria for malignancy. All cases were tested by IHC for S100, desmin, and TFE3; however, most cases had a more extensive immunopanel available, as described in the index case. Clinical follow-up was retrieved where available. The study was approved by the Institutional Review Board.

FIGURE 1 Gross examination of a resected malignant OFMT specimen (index case OFMT#1) arising in the deep gluteal muscle of a 70-year-old-male. The tumor had a nodular fibromyxoid cut-surface, being partly well-circumscribed and partly infiltrative, showing multiple small satellite lesions extending along the fascia [Color figure can be viewed at wileyonlinelibrary.com]

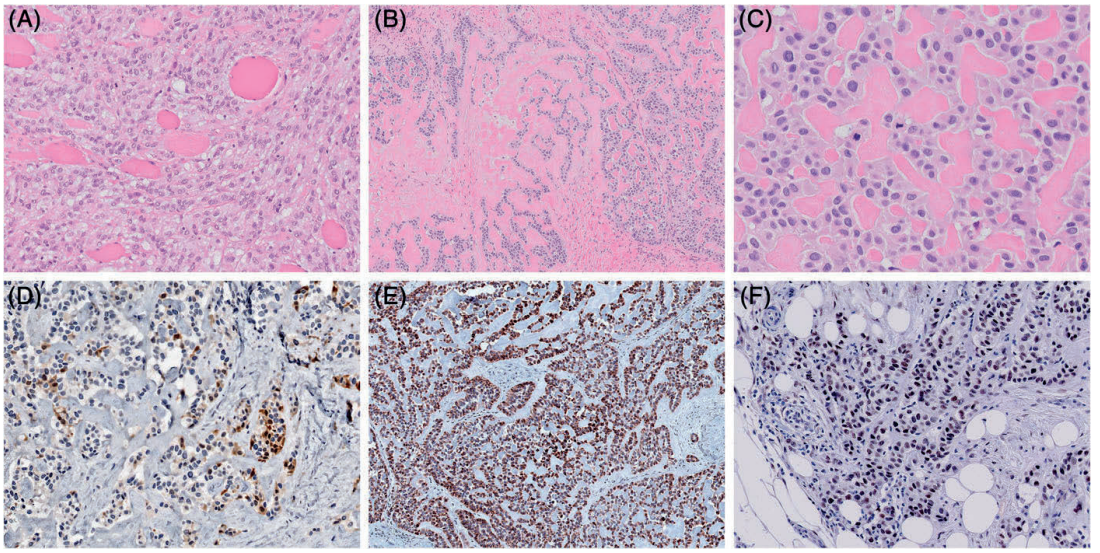

FIGURE 2 Microscopic appearance of the index malignant OFMT case (OFMT#1) showing monomorphic ovoid spindle cells with an infiltrative growth within the muscle (A, 200×), arranged in solid sheets (A, 200×) and cords within a hyalinized stroma (B, 100×). Higher power shows cohesive epithelioid tumor cells with nuclear atypia and increased mitotic activity (C, 400×). Immunohistochemistry shows focal expression of S100 (D, 100×) and diffuse staining for cytokeratin (E, AE1:AE3, 100×) and TFE3 (F, 200×)

2.2 | Targeted RNA sequencing

In three cases, targeted RNA sequencing was performed on samples of primary tumors. Total RNA was extracted from formalin-fixed paraffin-embedded tissue scrolls (3-4 per case) using the ExpressArt FFPE Clear RNA Ready kit (Amsbio, Cambridge, MA); it was assessed using the RNA 6000 Nano Bioanalyzer Kit (Agilent, Mississauga, ON) and quantitated using the Qubit RNA HS Assay Kit (ThermoFisher Scientific, Mississauga, ON). An input of 20-100 ng total RNA and the TruSight RNA Fusion Panel were used to prepare the RNA-seq libraries (Illumina, San Diego, CA), following manufacturer's instructions and as previously described.[7,8] Sequencing of each sample was performed with 76 base-pair paired-end reads on an Illumina MiSeq at eight samples per flow cell (~3 million reads per sample). The results were then analyzed using the STAR and BOWTIE2 aligners, and Manta and JAFFA fusion callers, respectively.[9,10]

2.3 | Fluorescence in situ hybridization (FISH)

In all five primary tumors, FISH was performed on interphase nuclei from paraffin-embedded 4-μm sections using bacterial artificial chromosomes (BAC) custom probes, flanking genes of interest. The BAC clones were obtained from BACPAC sources of Children's Hospital of Oakland Research Institute (Oakland, CA; http://bacpac.chori.org). DNA from individual BACs was isolated according to the manufacturer's instructions, labeled with different fluorochromes in a nick translation reaction, denatured, and hybridized to pretreated slides. Slides were then incubated, washed, and mounted with DAPI (4′,6-diamidino-2-phenylindole) in an antifade solution, as previously described.[5,11] The genomic location of each BAC set was verified by hybridizing them to normal metaphase chromosomes. Two hundred successive nuclei were examined using a Zeiss fluorescence microscope (Zeiss Axioplan, Oberkochen, Germany), controlled by Isis 5 software (Metasystems, Newton, MA). A positive score was interpreted when at least 20% of the nuclei showed a break-apart signal. Nuclei with incomplete set of signals were omitted from the score. All cases were tested for ALK gene rearrangements.

3 | RESULTS

A total of five OFMT cases, including the index case, displayed *PHF1-TFE3* fusions, presenting in three males and two females, with a median age of 64 years (range 62-70) (Table 1). None of these cases were previously reported. All except one OFMT originated in the deep soft tissues, spanning a wide range of locations (gluteal muscle, thigh, abdominal wall and cervical, paraspinal), while one tumor appeared to be centered in the scapula. Median tumor size was 10 cm (range 5.2-19 cm). Follow-up was available in all but one recent case. Three patients diagnosed with malignant OFMT developed lung metastases or locoregional metastases (two at presentation, one after 4 years). One patient developed bone metastases 10 years after diagnosis. Of the four patients with available follow-up, one died of disease 1 year after diagnosis, while the remaining three are alive with disease 6 months, 2 years, and 10 years after diagnosis.

TABLE 1 Clinical, pathologic, and molecular findings of the *PHF1-TFE3* fusion-positive OFMTs

OFMT	Age/sex	Location	Size (cm)	Histology	IHC pos	IHC neg	RNAseq	FU
1	70/M	Gluteal	10	Epithelioid and spindle	TFE3, S100 (focal)	Desmin	*PHF1-TFE3*	DOD, 12 months
2	62/M	Thigh	19	Epithelioid	TFE3, desmin	S100	NP	AWD, 6 months
3	69/F	Abdominal wall	5.2	Spindle	TFE3, desmin	S100	*PHF1-TFE3*	NED, 24 months
4	59/F	Cervical paraspinal	8.9	Epithelioid	TFE3, desmin	S100	NP	Recent case
5	64/M	Scapula	13.5	Epithelioid and spindle	TFE3	S100, desmin	*PHF1-TFE3*	AWD, 10 years

AWD, alive with disease; DOD, died of disease; FU, follow up; NED, no evidence of disease.

3.1 | The histologic spectrum of OFMTs with *PHF1-TFE3* fusions resembles that of other OFMTs, yet tumors with malignant features are overrepresented

All tumors had morphologic features compatible with OFMT, as illustrated in Figures 2 and 3. In two cases (OFMT #2&4) only needle biopsies were available, while the remaining three underwent surgical resection of the mass, allowing full assessment of histologic features. The tumors showed a multinodular growth surrounded by thin, fibrous capsules. Peripheral ossification was not found in any of the cases. The tumors were composed of uniform epithelioid to ovoid cells with scant light eosinophilic cytoplasm and round-ovoid nuclei with fine chromatin, embedded in a loose fibromyxoid stroma (Figures 2–4). By histologic criteria, two OFMTs had typical features, whereas three tumors (OFMT #3&5 and the index case OFMT #1, as described above) were overtly malignant, harboring areas with increased cellularity, nuclear atypia and mitotic activity (range 5-16 mitoses in 25 HPF equaling to 5 mm^2). Malignant OFMTs with a *PHF1-TFE3* fusion were morphologically similar to other *PHF1*-rearranged genetic subsets (Figure 3). One of the three malignant OFMTs (OFMT #5) presented in a 62-year-old male as a 13.5 cm bone tumor that was centered in the scapula and invaded surrounding soft tissue. The patient developed lung metastases 2 years after initial diagnosis, local tumor recurrences in the thoracic wall 4 years after diagnosis, and bone metastases in the femur 10 years after diagnosis and is alive with disease 10 years after initial diagnosis. Notably, the lung and bone metastases were composed of epithelioid cells arranged in trabeculae and pseudoglandular formations that expressed cytokeratins, CD56 and synaptophysin (Figure 4), suggestive of neuroendocrine differentiation, as also found in the malignant OFMT (index case OFMT #1, see Section 2). Focal areas of more conventional OFMT were detected in one of the recurrence.

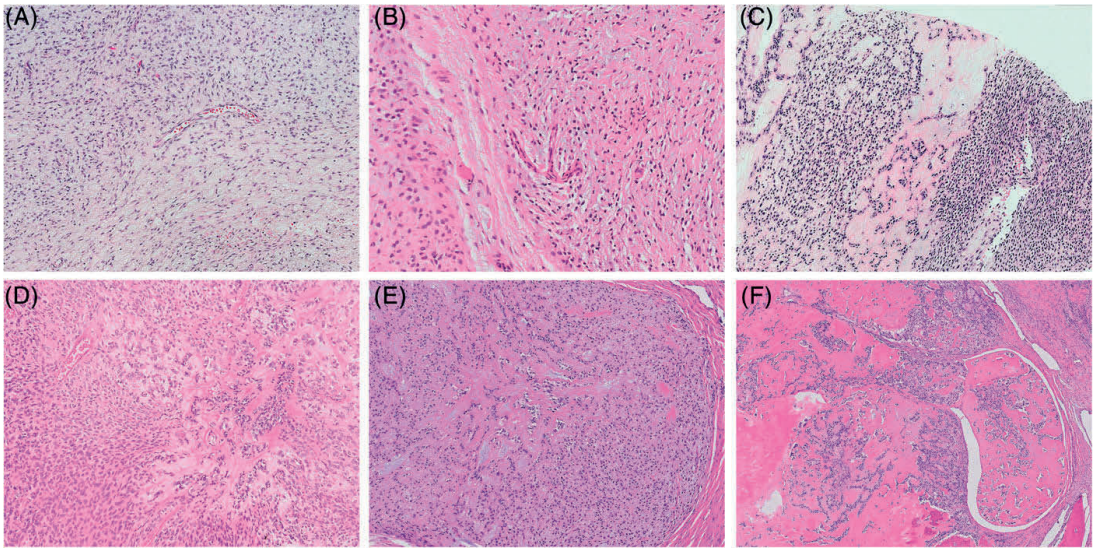

FIGURE 3 Microscopic findings of four additional OFMTs with *PHF1-TFE3* fusions. Tumors displayed a typical morphology, such as OFMT#3 arising in the abdominal wall of a 69-year old female (A); OFMT#4 arising in the deep soft tissue of the posterior neck in a 59-year-old-female (B), a malignant OFMT, OFMT#2, arising in the deep soft tissue of the thigh in a 62-year-old male (C); and a malignant OFMT, OFMT#5 arising in the scapula of a 64-year-old male (D). These tumors were composed of ovoid to epithelioid tumor cells, arranged in reticular, fascicular, and trabecular patterns, with the malignant tumors showing increased cellularity. The microscopic features of these four OFMTs with *PHF1-TFE3* fusions match that of a malignant OFMT with a *PHF1-MEAF6* fusion as shown in Figures 3E-F for comparison

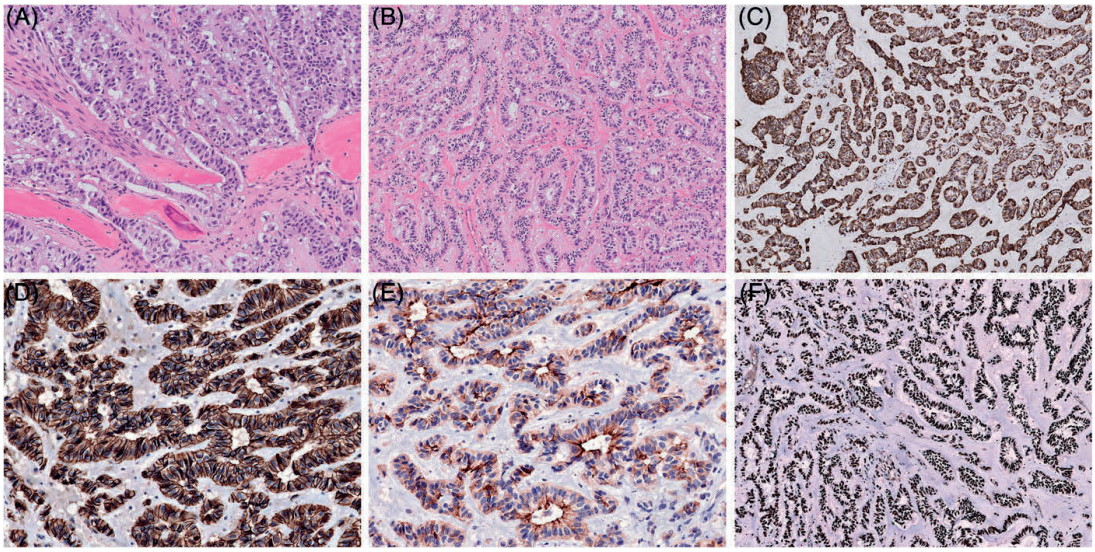

FIGURE 4 Pathologic findings of a malignant OFMT arising in the scapula of a 64-year-old male (OFMT#5). Metastases in bone (A, 100×) and lung (B, 100×) have a trabecular and pseudoglandular morphology (B, 100×) with tumor cells expressing cytokeratins (C, 100×), CD56 (D, 200×), synaptophysin (E, 200×), and TFE3 (F, 100×)

By immunohistochemistry, all but one of the cases were negative for S100 protein. Desmin was focally expressed in three cases. After the molecular findings became available, all tumors were tested in retrospect for TFE3 and showed diffuse nuclear staining (Figures 2 and 4).

3.2 | RNA sequencing and fluorescence in situ hybridization

RNA sequencing was performed in the three cases with overtly malignant features (OFMT #1&3&5) (Figure 5). OFMT1 had exonic breakpoints resulting in a fusion between middle of *PHF1* exon 11 and middle of *TFE3* exon 3. OFMT3 showed intronic breakpoints resulting in a fusion between *PHF1* exon 11 and *TFE3* exon 3. OFMT5 showed a fusion between *PHF1* exon 12 and *TFE3* exon 7. These results were further validated by FISH in each case, showing a break-apart signal in both genes. In the remaining two cases with typical morphology (OFMT #2&4) (Figure 6), FISH revealed rearrangements in both *PHF1* and *TFE3* genes (6). Additionally, FISH was also performed confirming the TFE3 gene rearrangements in the lung metastasis and one local recurrence of case#5, which showed unusual neuroendocrine features.

4 | DISCUSSION

OFMT is a rare soft tissue neoplasm of uncertain histogenesis and intermediate malignant potential.[1,2] Established diagnostic criteria in separating typical OFMT from atypical or malignant variants remain elusive. However, most studies define a malignant phenotype based on high cellularity and mitotic activity, which often correlates with lack of S100 reactivity.[2,5] In contrast, atypical OFMT has been defined more loosely, as lesions which deviate from conventional OFMT morphology, typically lacking the peripheral shell of bone and S100 expression, but not meeting the criteria for malignancy.[2] In the context of these challenging cases, molecular studies are quite helpful to confirm the diagnosis of OFMT.

The genetic hallmarks of OFMTs are recurrent gene fusions that involve *PHF1* gene rearrangement in approximately 80% of cases, regardless of risk of malignancy. The most common gene fusion variant is *EP400-PHF1* accounting for 44% of cases, with more than half displaying typical histology and co-expression of S100 and desmin. Other less common partners include *EPC1* and *MEAF6*.[5] In about 30% of tumors with *PHF1* gene rearrangements no gene partner is identified, suggesting additional undetected fusion variants yet to be determined. Triggered by the RNA-Seq result of a novel *PHF1-TFE3* fusion in an index case with unusual pathologic findings and overt features of malignancy, we investigated this genetic abnormality in a cohort of OFMTs lacking a known *PHF1* gene partner. A total of 5 (10%) cases were identified of the 51 cases studied carrying *PHF1* gene abnormalities. This small cohort was enriched by patients who followed a clinically aggressive course. By histologic criteria this genetic abnormality spanned two typical and three overtly malignant OFMT cases. Despite a uniform epithelioid to ovoid cytomorphology and fibromyxoid stroma compatible with an OFMT diagnosis, none of the cases showed evidence of a peripheral shell of lamellar bone and S100 expression was only focally present in one malignant OFMT. Desmin was positive in three of the cases and was negative in two malignant OFMTs. Malignant OFMTs with a *PHF1-TFE3* fusions were morphologically similar to other *PHF1*-rearranged genetic subsets. As expected from its genetic abnormality resulting in TFE3 oncogenic activation through gene fusions, all tumors showed strong nuclear positivity for TFE3 immunohistochemically.

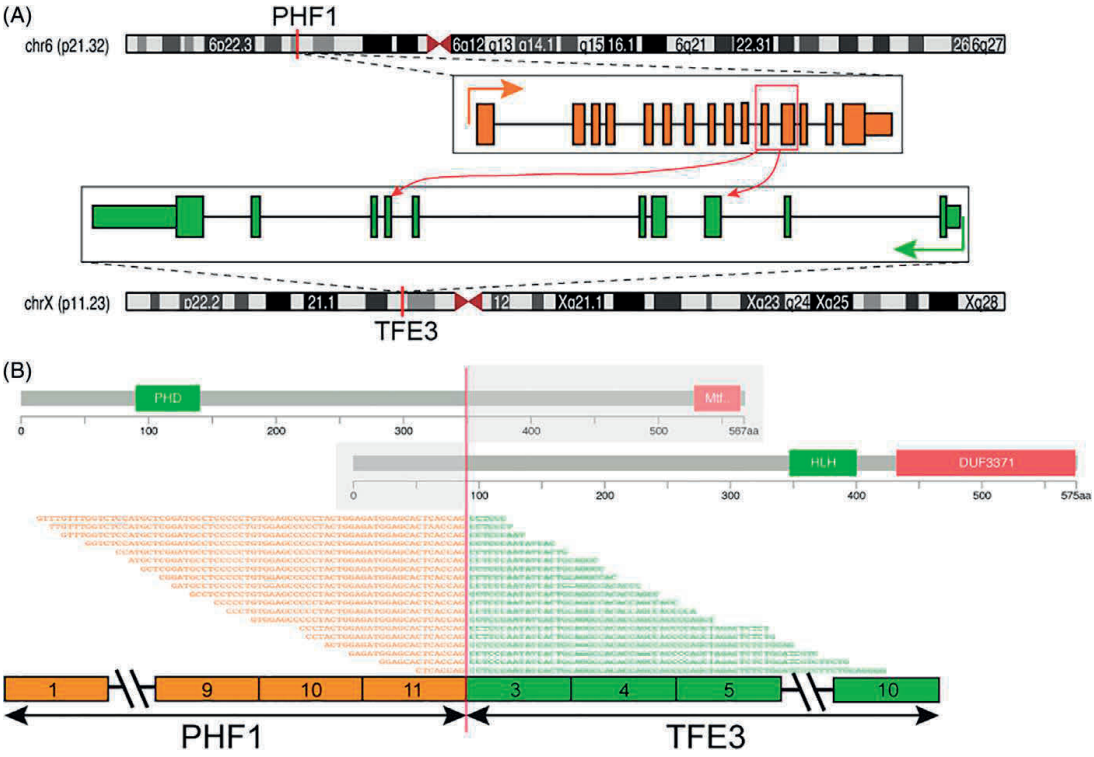

FIGURE 5 Diagrammatic representation of the *PHF1-TFE3* fusion showing (A) PHF1 gene on 6p21.32 is fused to TFE3 on xp11.23 (thick arrows show the direction of transcription of each gene; delicate red arrows show the two fusion variants encountered. (B) RNAseq reads show the dominant transcript resulting in the fusion of *PHF1* exon 11 to *TFE3* exon 3. Protein domains for both PHF1 and TFE3 are also illustrated above [Color figure can be viewed at wileyonlinelibrary.com]

By RNA-Seq, the three *PHF1-TFE3* fusion positive cases showed upregulation of *TFE3* mRNA. The transcription factor E3 (TFE3) is a member of the microphthalmia (MiT) family, together with MITF, TFEB and TFEC, sharing a helix-loop-helix leucine zipper (bHLH-LZ) dimerization domain motif, a transactivation domain and basic region involved in DNA contact and binding.[13] Because of their sequence homology, all MiT family members bind to identical DNA recognition sequences (CA [T/C]GTG) termed E-boxes. Similar to other Xp11 translocation associated tumors, the *TFE3*-fusion positive OFMTs retain the bHLH-LZ and transcriptional activation domains of TFE3.[14] Chromosomal translocations involving *TFE3* gene have been described in a number of neoplasms, including mesenchymal and epithelial malignancies. In alveolar soft part sarcoma, an unbalanced translocation, der(17)t(X;17)(p11;q25) results in the formation of an *ASPSCR1-TFE3* fusion gene.[13] *TFE3*

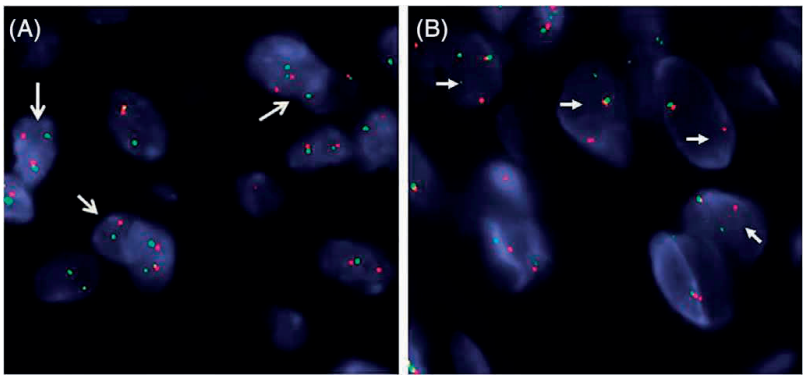

FIGURE 6 FISH analysis showed the presence of break-apart signals (arrows) in both *PHF1* (A) and *TFE3* genes (B) (OFMT #2; red, centromeric; green, telomeric) [Color figure can be viewed at wileyonlinelibrary.com]

related fusions with various gene partners have also been described in the so-called Xp11 renal cell carcinoma as well as in a small subset of perivascular epithelioid cell tumors (PEComa), including *SFPQ* (*PSF*), *PRCC*, *ASPSCR1*, *NONO*, *RBM10*, and *DVL2*.[11,15,16] In most of these various fusion variants, the *TFE3* breakpoint resides in exons 3-5.[15,17] More recently, recurrent *YAP1-TFE3* fusions have been reported in a distinct subset of epithelioid hemangioendothelioma, showing vasoformative features and abundant eosinophilic cytoplasm.[14] The fusion transcript in that study was defined as *YAP1* exon 1 to *TFE3* exon 4. In our three malignant OFMT cases, the RNA-seq showed that *PHF1* exon 11 was fused to *TFE3* exon 3 in two cases, whereas in the third case *PHF1* exon 12 was fused to *TFE3* exon 7 (Figure 4 Figure 5).

In about 5%-10% of cases, OFMTs are characterized by non-*PHF1* type fusions, including *ZC3H7B-BCOR*, *CREBBP-BCORL1*, and *KDM2A-WWTR1*.[5,6] Some of these rare alternative fusions have been associated with a malignant phenotype and aggressive clinical outcome. Moreover, in this current series, the index patient with malignant OFMT followed a fulminant course with lung and locoregional metastases, succumbing to disease 1 year after diagnosis. Two additional patients with malignant OFMT remain alive with disease after developing a similar pattern of local and distant metastases. It remains to be determined in larger series of patients if oncogenic TFE3 activation as the driver of OFMT pathogenesis is associated with a more unfavorable outcome compared to other *PHF1* fusion variants.

In summary, we report novel recurrent *PHF1-TFE3* fusions in a subset of OFMTs with aggressive clinical behavior, including local recurrences and distant lung metastases. Although morphologically the tumors had features in keeping with OFMT, none showed areas of peripheral ossification and all but one was negative for S100 protein. The *PHF1-TFE3* fusions resulted in protein TFE3 overexpression, adding OFMT as an additional tumor driven by oncogenic activation of TFE3 pathway. Thus, in the setting of tumors with malignant phenotype and a nonspecific immunoprofile (S100/desmin negativity), TFE3 immunoreactivity might serve as a useful ancillary test in these challenging cases. Our results add OFMT to the list of tumors driven by TFE3 oncogenic activation through recurrent gene fusions, suggesting that TFE3 immunoreactivity can be thus used as a screening tool for this genetic abnormality.

ORCID

Albert J. H. Suurmeijer https://orcid.org/0000-0003-1361-9454
Brendan C. Dickson https://orcid.org/0000-0003-2269-6216
Cristina R. Antonescu https://orcid.org/0000-0002-9717-8205

REFERENCES

1. Miettinen M, Finnell V, Fetsch JF. Ossifying fibromyxoid tumor of soft parts—a clinicopathologic and immunohistochemical study of 104 cases with long-term follow-up and a critical review of the literature. *Am J Surg Pathol*. 2008;32:996-1005.
2. Folpe AL, Weiss SW. Ossifying fibromyxoid tumor of soft parts: a clinicopathologic study of 70 cases with emphasis on atypical and malignant variants. *Am J Surg Pathol*. 2003;27:421-431.
3. Gebre-Medhin S, Nord KH, Moller E, et al. Recurrent rearrangement of the PHF1 gene in ossifying fibromyxoid tumors. *Am J Pathol*. 2012; 181:1069-1077.
4. Graham RP, Weiss SW, Sukov WR, et al. PHF1 rearrangements in ossifying fibromyxoid tumors of soft parts: a fluorescence in situ hybridization study of 41 cases with emphasis on the malignant variant. *Am J Surg Pathol*. 2013;37:1751-1755.
5. Antonescu CR, Sung YS, Chen CL, et al. Novel ZC3H7B-BCOR, MEAF6-PHF1, and EPC1-PHF1 fusions in ossifying fibromyxoid tumors—molecular characterization shows genetic overlap with endometrial stromal sarcoma. *Genes Chromosomes Cancer*. 2014;53:183-193.
6. Kao YC, Sung YS, Zhang L, Chen CL, Huang SC, Antonescu CR. Expanding the molecular signature of ossifying fibromyxoid tumors with two novel gene fusions: CREBBP-BCORL1 and KDM2A-WWTR1. *Genes Chromosomes Cancer*. 2017;56:42-50.
7. Dickson BC, Hornick JL, Fletcher CDM, et al. Dermatofibrosarcoma protuberans with a novel COL6A3-PDGFD fusion gene and apparent predilection for breast. *Genes Chromosomes Cancer*. 2018;57:437-445.
8. Dickson BC, Sung YS, Rosenblum MK, et al. NUTM1 gene fusions characterize a subset of undifferentiated soft tissue and visceral tumors. *Am J Surg Pathol*. 2018;42:636-645.
9. Liu S, Tsai WH, Ding Y, et al. Comprehensive evaluation of fusion transcript detection algorithms and a meta-caller to combine top performing methods in paired-end RNA-seq data. *Nucleic Acids Res*. 2016;44:e47.
10. Chen X, Schulz-Trieglaff O, Shaw R, et al. Manta: rapid detection of structural variants and indels for germline and cancer sequencing applications. *Bioinformatics*. 2016;32:1220-1222.
11. Argani P, Zhong M, Reuter VE, et al. TFE3-fusion variant analysis defines specific clinicopathologic associations among Xp11 translocation cancers. *Am J Surg Pathol*. 2016;40:723-737.
12. Fletcher C, Bridge JA, Hogendoorn PC, et al. *WHO Classification of Tumours of Soft Tissue and Bone*. 4th ed. Lyon: IARC; 2013:281-295.
13. Ladanyi M, Lui MY, Antonescu CR, et al. The der(17)t(X;17)(p11;q25) of human alveolar soft part sarcoma fuses the TFE3 transcription factor gene to ASPL, a novel gene at 17q25. *Oncogene*. 2001;20:48-57.
14. Antonescu CR, Le Loarer F, Mosquera JM, et al. Novel YAP1-TFE3 fusion defines a distinct subset of epithelioid hemangioendothelioma. *Genes Chromosomes Cancer*. 2013;52:775-784.
15. Agaram NP, Sung YS, Zhang L, et al. Dichotomy of genetic abnormalities in PEComas with therapeutic implications. *Am J Surg Pathol*. 2015;39:813-825.
16. Argani P, Zhang L, Reuter VE, Tickoo SK, Antonescu CR. RBM10-TFE3 renal cell carcinoma: a potential diagnostic pitfall due to cryptic Intrachromosomal Xp11.2 inversion resulting in false-negative TFE3 FISH. *Am J Surg Pathol*. 2017;41:655-662.
17. Wang XT, Xia QY, Ni H, et al. Xp11 neoplasm with melanocytic differentiation of the prostate harbouring the novel NONO-TFE3 gene fusion: report of a unique case expanding the gene fusion spectrum. *Histopathology*. 2016;69:450-458.

How to cite this article: Suurmeijer AJH, Song W, Sung Y-S, et al. Novel recurrent *PHF1-TFE3* fusions in ossifying fibromyxoid tumors. *Genes Chromosomes Cancer*. 2019;1–7. https://doi.org/10.1002/gcc.22755

Chapter 6

Soft tissue aneurysmal bone cyst: six new cases with imaging details, molecular pathology, and review of the literature

This chapter is based on the publication: **Song W**, Suurmeijer AJH, Bollen SM, et.al. Soft tissue aneurysmal bone cyst: six new cases with imaging details, molecular pathology, and review of the literature. Skeletal Radiol. 2019 Jul;48(7):1059-1067.

Soft tissue aneurysmal bone cyst: six new cases with imaging details, molecular pathology, and review of the literature

Wangzhao Song[1] · Albert J. H. Suurmeijer[1] · Stijn M. Bollen[2] · Anne-Marie Cleton-Jansen[3] · Judith V. M. G. Bovée[3] · Herman M. Kroon[2]

Received: 1 October 2018 / Revised: 28 November 2018 / Accepted: 10 December 2018

Abstract

Objective Aneurysmal bone cysts (ABC) rarely present in soft tissue locations (STABC). The 30 cases of STABC reported in the English literature were reviewed. Six new cases retrieved from the files of the Netherlands Committee on Bone Tumors were compared to the six cases described in the radiological literature.

Materials and methods Imaging studies and histopathology of six new STABC cases were reviewed. Follow-up was recorded with respect to local recurrence. FISH for *USP6* rearrangement and/or anchored multiplex PCR-based targeted NGS using Archer FusionPlex Sarcoma Panel were attempted.

Results On imaging, the six STABC cases presented as a solid or multicystic intramuscular soft tissue mass, usually with thin peripheral mineralized bone shell. On MRI, perilesional edema was visualized in nearly all cases. Fluid-fluid levels were observed in one case. All lesions had the distinct histologic features of STABC. In three cases suitable for NGS, the diagnosis of STABC was confirmed by a *COL1A1–USP6* fusion gene. In one additional case, *USP6* gene rearrangement was detected by FISH. After marginal excision, none of the six STABC recurred after a mean follow-up period of 50 months (range, 39–187 months).

Conclusions On imaging, it can be difficult to discriminate between STABC and myositis ossificans. The presence of a thin bony shell and fluid-fluid levels can be helpful in discriminating these two entities. STABC is readily diagnosed after histopathologic examination of the resection specimen. STABC belongs to the spectrum of tumors with *USP6* rearrangements, which includes ABC, myositis ossificans, and nodular fasciitis.

Keywords Soft tissue · Aneurysmal bone cyst · USP6 · Radiography · CT · MRI · Ultrasound · Radionuclide imaging

Introduction

Aneurysmal bone cyst (ABC) is a distinct bone tumor, which is either primary or secondary to another tumor or tumor-like lesion of bone. Primary ABC usually occurs in children and adolescents. The most common sites are the metaphysis of the long tubular bones and the posterior elements of the vertebrae, where it usually presents as a relatively well-defined osteolytic lesion, often with expansion of the bone and fluid-fluid levels on MR imaging [1]. Aneurysmal bone cyst rarely occurs as a primary soft tissue tumor (STABC). Salm and Sissons (1972) [2] were the first to describe two cases of extraskeletal giant-cell-containing lesions with histological features identical to ABC of bone. To our knowledge, only up to 30 cases of STABC were reported in the English literature to date. Thus far, only six have been reported in the radiological literature [3–8]. In this article, we describe imaging and histopathologic features of six new cases of primary STABC. Moreover, molecular studies (FISH and anchored multiplex PCR-based targeted NGS, using the Archer FusionPlex Sarcoma kit) were done in an attempt to demonstrate specific gene fusions of ABC. We compared our findings to those reported in the literature.

✉ Herman M. Kroon
h.m.j.a.kroon@lumc.nl

[1] Department of Pathology and Medical Biology, University Medical Center Groningen, University of Groningen, Groningen, The Netherlands

[2] Department of Radiology, C-2-S, Leiden University Medical Center, PO Box 9600, 2300RC Leiden, The Netherlands

[3] Department of Pathology, Leiden University Medical Center, Leiden, The Netherlands

Materials and methods

Patient data

The six STABC cases were retrieved from the files of the Netherlands Committee on Bone Tumors. Imaging studies and histopathologic features of the cases were reviewed by experienced radiologists and pathologists, respectively. Follow-up was recorded with respect to local recurrence.

Conventional radiography was available in all six cases, MR imaging in five cases (except case 5), MR + contrast-enhanced MR were performed in three cases (cases 1, 2, 3). CT + radionuclide imaging was available in three patients (case 4: CT + SPECT; case 5: CT + conventional radionuclide imaging; case 6: CT + PET-CT), whereas ultrasonography was done in two cases (cases 1, 3).

In each case, formalin-fixed, paraffin-embedded material was available for review. The study was performed in accordance with the code of conduct for responsible use of human tissue that is used in the Netherlands (Dutch Federation of Biomedical Scientific Societies; http://www.federa.org).

FISH

A commercial fusion probe (Kreatech, Amsterdam, the Netherlands) that detects USP6 rearrangements was used to do fluorescence in situ hybridization (FISH). Three-μm-thick FFPE slides were deparaffinized and ethanol dehydrated, and FISH was performed using the Histology Fish Accessory Kit (Dako, Glostrup, Denmark), as per the manufacturer's description. Slides were counterstained with 10 μl of 4′,6-diamidino-2-phenylindole (DAPI) before visualization and quantification (200 nuclei) by fluorescence microscopy. Two hundred nuclei of the spindle cells were counted for the presence of break-apart signals. When at least ten nuclei with a break apart signal are observed, this is considered as an USP6 translocation. This is a lower threshold than for other translocations, because in STABC it is difficult to distinguish lesional cells from non-lesional cells.

Targeted next-generation sequencing (NGS) based on anchored multiplex PCR (AMP)

Total nucleic acid (DNA and RNA) was isolated from 50-μm FFPE slides using the TPS (tissue preparation system) (Siemens), as described previously [9]. A target-enriched cDNA library was prepared with the Archer® FusionPlex® Sarcoma kit as described by the manufacturer (http://archerdx.com/fusionplex-assays/sarcoma). In short, reverse transcription of RNA was followed by end repair, adenylation, and universal half-functional adapter ligation of double-stranded cDNA fragments. This was followed by two rounds of low-cycle PCR with universal primers and gene-specific primers, covering 26 target genes that rendered the library fully functional for clonal amplification and sequencing using the Ion Proton™ system. With the Archer-DX analysis software, the libraries were analyzed for presence of relevant fusions and in their absence sequence quality was assessed by the manufacturer's criteria.

Results

Clinicopathologic features

Four female and two male patients were included in this study (Table 1). Their age ranged from 15 to 49 years (mean age, 27 years, median age, 25.5 years). All patients presented with a painful mass without a history of previous trauma in any of them. Four lesions were located in the upper leg; the remaining two were located in the lower abdominal wall and anterior pelvic region. All tumors were excised with narrow margins. On gross examination, tumor size ranged from 2.5 to 8.0 cm (mean size, 4.5 cm). In all but one case, STABC was a multilocular cystic tumor. One case was predominantly solid and had one small cyst. Microscopically, the distinctive appearance of STABC included areas with blood-filled cysts and septa (Fig. 1a, f) or more solid areas (Fig. 1b) with bland spindle cells and osteoclastic giant cells. In case 3, the

Table 1 Distinct histologic features of our six STABC cases

Case	Age/ sex	Location, muscle	Size	Solid/cystic	Blue bone	USP6 FISH	NGS	FU/ NED
1	49/F	Biceps femoris	4.5 cm	Cystic	No	Yes	COL1A1-USP6	42 mo
2	34/F	Vastus lateralis	4.0 cm	Cystic	Yes	NP	COL1A1-USP6	57 mo
3	15/M	Vastus medialis	2.5 cm	Cystic	Yes	Failure	Failure	39 mo
4	19/F	Vastus medialis	4.0 cm	1 small cyst	Yes	NP	COL1A1-USP6	50 mo
5	16/F	Oblique transverse abdominal	8.0 cm	Cystic	No	Yes	NP	187 mo
6	32/M	Gluteus minimus	4.0 cm	Cystic	Yes	Failure	Failure	45 mo

NP not performed, *FU* follow-up, *NED* no evidence of disease, *mo* month

multilocular cysts were filled with proteinaceous fluid (Fig. 1c). Mitotic activity or nuclear atypia were absent. In the tumor border zone, a shell of mature lamellar bone was formed via differentiating areas of woven bone surrounded by osteoblasts (Fig. 1f). Blue osteoid bone matrix was found in four cases (Fig. 1b, c, and f). Notably, case 4 showed a distinct histological feature compared with other cases. Grossly, this tumor was located in skeletal muscle had a 1-cm-thick peripheral bone shell (Fig. 2). In the center, only glistening myxoid tissue was discerned and cystic cavities were absent. By histology, this central area was composed of loose myxoid stroma with focal cellular areas with myofibroblasts, hemosiderin, and osteoclast-like giant cells (Fig. 1d). There was an extensive formation of woven trabecular bone with peripheral maturation and formation of lamellar bone surrounded by osteoblasts, a morphology reminiscent of myositis ossificans. However, the previous needle biopsy material contained a small cystic area with distinct histological features of STABC. On clinical follow-up, none of the tumors recurred.

Imaging

Imaging findings of six STABCs are summarized in Table 2. Ultrasound examination was performed in two cases, which showed a calcified cystic lesion with acoustic shadowing (case 1 and 3, Fig. 3). Conventional radiography revealed a relatively well-demarcated soft tissue mass surrounded by a bone shell (Fig. 4a, b). None of the tumors originated from or was connected to the underlying bone.

On MRI, STABC presented as a lobulated soft tissue mass with a predominantly intermediate signal intensity on T1-weighted images (Fig. 5a, b). In one case, the signal intensity on the T1-weighted sequences was predominantly high with fluid-fluid levels consistent with blood-filled cystic spaces (Fig. 5a). On T2-weighted images with fat suppression, there was heterogeneous, predominantly high signal intensity (Fig. 5c, d). After intravenous contrast administration, there was a heterogeneous diffuse enhancement of the mass in two patients (cases 2 and 3) and septal enhancement in one (case 1,

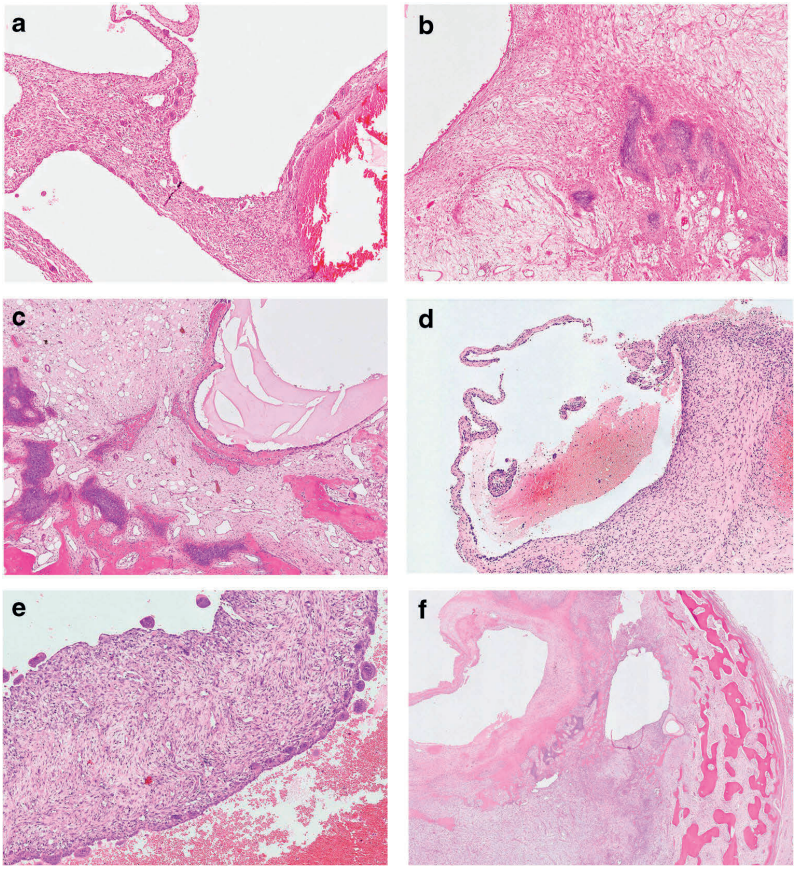

Fig. 1 Microphotographs of the six STABC cases (**a**–**f** corresponding to case 1–6) described (H&E stain). STABC has blood-filled cysts and septa (**a**, **f**) or more solid areas (**b**) with bland spindle cells and osteoclast-type giant cells. Woven bone deposited along the cyst cavity (**c**, **d**) is a typical feature and blue bone (**b**, **c**, **f**) is considered to be a hallmark of STABC. At the border area, the peripheral bone shell consisted of mature trabecular bone (**f**)

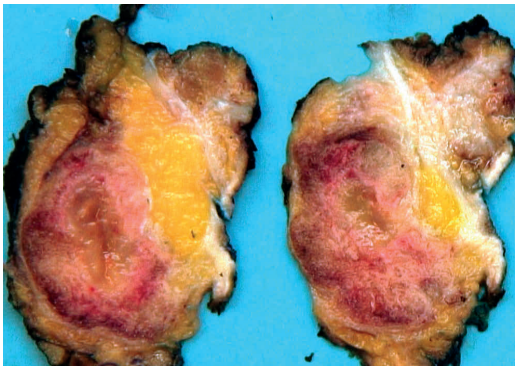

Fig. 2 Gross features of case 4, the tumor with thick peripheral bone shell, glistening myxoid tissue in the center and absent cystic cavities

Fig. 5e). Perilesional edema was observed in all five patients with MR imaging, with extensive ill-defined high signal intensity in the adjacent muscle beyond the periphery of the mass (Fig. 5c–e). Fluid-fluid levels were evident in one case. In all five patients with MR, on all sequences, a peripheral hypo-intense rim, corresponding with the peripheral mineralization, was visualized. On CT, a shell of peripheral mineralization was demonstrated in cases 4, 5, and 6 (Fig. 6). A technetium-99 m-MDP bone study in case 5 demonstrated increased uptake of the radiotracer, predominantly in the periphery, whereas a SPECT study showed intense uptake of the radiopharmacon throughout the lesion (Fig. 7). A PET-CT performed in case 6 showed a soft tissue mass surrounded by a bony shell with variable thickness from thin to intermediate, but predominantly thin. There was markedly increased uptake of the radiopharmacon at the periphery of the lesion (Fig. 8).

Molecular analysis

In two cases, *USP6* gene rearrangement was detected by *USP6* break-apart FISH assay (cases 1 and 5). In three cases (cases 1, 2, and 4) suitable for analysis, a fusion of exon1 of *COL1A1* with exon 1 of *USP6* was found with anchored multiplex PCR-based targeted NGS. Due to acid decalcification and subsequent DNA denaturation, it was not possible to perform FISH and NGS in cases 3 and 6. However, as shown in Fig. 1c and f, the histology was typical of STABC.

Discussion

Jaffe and Lichtenstein (1942) [1] were the first to describe aneurysmal bone cyst (ABC), a benign, locally aggressive, and expansile lesion that typically occurs in the long tubular bones or vertebrae of children and young adults, both male and female [1, 10, 11]. ABC of bone can occur as a primary lesion or be associated with a pre-existing bone condition such as chondroblastoma, giant cell tumor, fibrous dysplasia, and even osteosarcoma [12]. In these cases, ABC is considered to be secondary. Radiographically, the characteristics of a primary ABC of bone are an osteolytic lesion, usually eccentrically, expansile with well-defined margins, and predominantly located in the metaphysis of long tubular bones or the posterior elements of vertebrae.

Aneurysmal bone cyst has a soft tissue counterpart. Soft tissue ABC (STABC) was first reported by Salm and Sissons in 1972 [2]. Since then, only up to 30 cases have been reported in the English literature, with only six cases published in the radiological literature [3–8]. We add six more cases and reviewed the literature with regard to clinical presentation,

Table 2 Imaging features of 12 cases of STABC, including the six cases described herein

Case	Author	Bone shell on radiograph and/or CT	Multicystic/ solid (CT, MR)	Fluid-fluid levels (MR)	Septal enhancement (MR)	Perilesional edema on MR	Gross pathology
1	Amir	Yes, thick	Solid	NP	NP	NP	Multicystic
2	Samura	No	Multicystic	No	NP	Yes	Multicystic
3	Wang	Yes, thin	Multicystic	Yes	Yes	Yes	Multicystic
4	Ajilogba	No	Solid	No	No	Yes	Multicystic
5	Jacquot	Yes, thin	Multicystic	Yes	NP	No	Multicystic
6	Baker	Yes, thin	Multicystic	Yes	Yes	Yes	Multicystic
7	Case 1	Yes, thin	Multicystic	Yes	Yes	Yes	Multicystic
8	Case 2	Yes, thin	Solid	No	No	Yes	Multicystic
9	Case 3	Yes, thin	Solid	No	No	Yes	Multicystic
10	Case 4	Yes, thick	Solid	No	NP	Yes	1 small cyst
11	Case 5	Yes, thin	Probably cystic	NP	NP	NP	Multicystic
12	Case 6	Yes, thin	Multicystic	No	NP	Yes	Multicystic

NP not performed

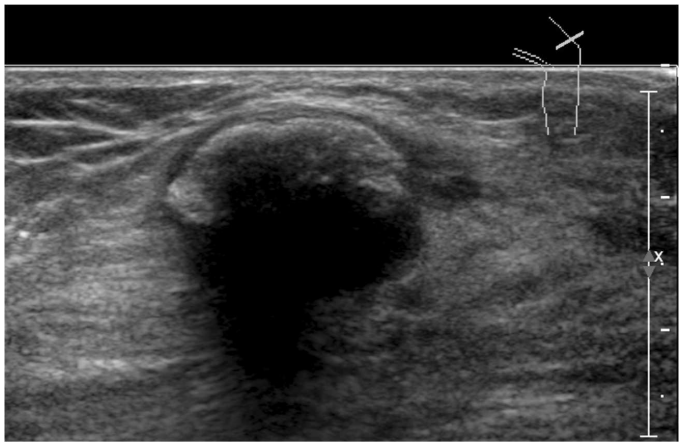

Fig. 3 Ultrasound image with highly reflective shell and acoustic shadowing caused by the peripheral calcification (case 3)

tumor localization, radiological features, as far as these could be derived from the text and/or available illustrations, and follow-up.

Clinical features of STABC

Reviewing the literature [1–8, 13–29], patients with STABC presented with a painless or tender, slow-growing mass, with a mean size of 5.5 cm (range, 2–12 cm). The vast majority of patients indicated no previous trauma (30/36; 83.3%). Remarkably, in two patients, STABC occurred in an area of previous surgery [2, 16]. There was a female predominance; 22/36 (61.1%). Mean age and median age at presentation were 28.7 and 27 years, respectively, which is higher than that of patients with ABC of bone (75% of the patients with primary ABC of bone are younger than 20). The lesions were mainly located in the upper leg, groin, or buttock region (15/36, 41.7%), followed by upper arm and shoulder region (9/36, 25.0%). Other locations reported are the retroclavicular region, breast, common carotid artery, pelvic cavity, cerebro-pontine angle, lower leg, hand, abdominal wall, and larynx [2–4, 7, 8, 13–23, 25, 26, 28, 29]. By definition, STABC has no connection to the adjacent or underlying bone [16]. Twenty-seven cases (75%) were deep seated, either intramuscular or intermuscular, whereas others were superficial subcutaneous lesions [7]. None of our six STABC cases had a history of previous trauma. All were intramuscular tumors of the extremities (four cases), pelvis (one case), or abdominal wall (one case).

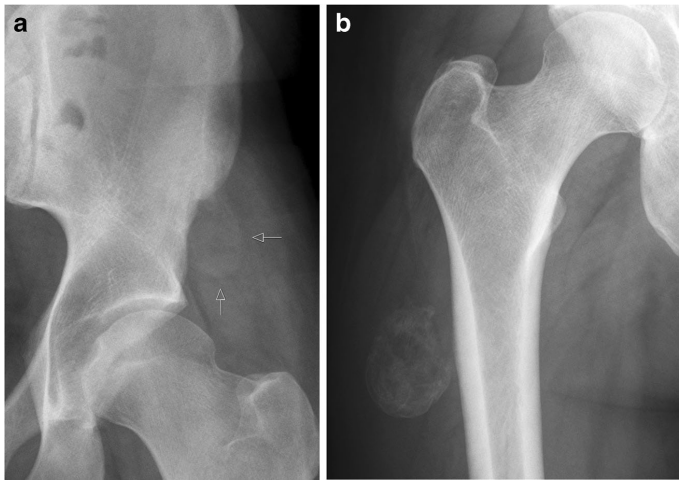

Fig. 4 Conventional radiograph of STABC. Antero-posterior radiograph of the left side of the pelvis (case 6). Mass projecting under the anterior iliac spine with discrete egg-shell mineralization along the periphery (*arrows*) (**a**). Antero-posterior radiograph of the upper leg (case 2) demonstrates a mass in the soft tissues surrounded by an ossified shell (**b**)

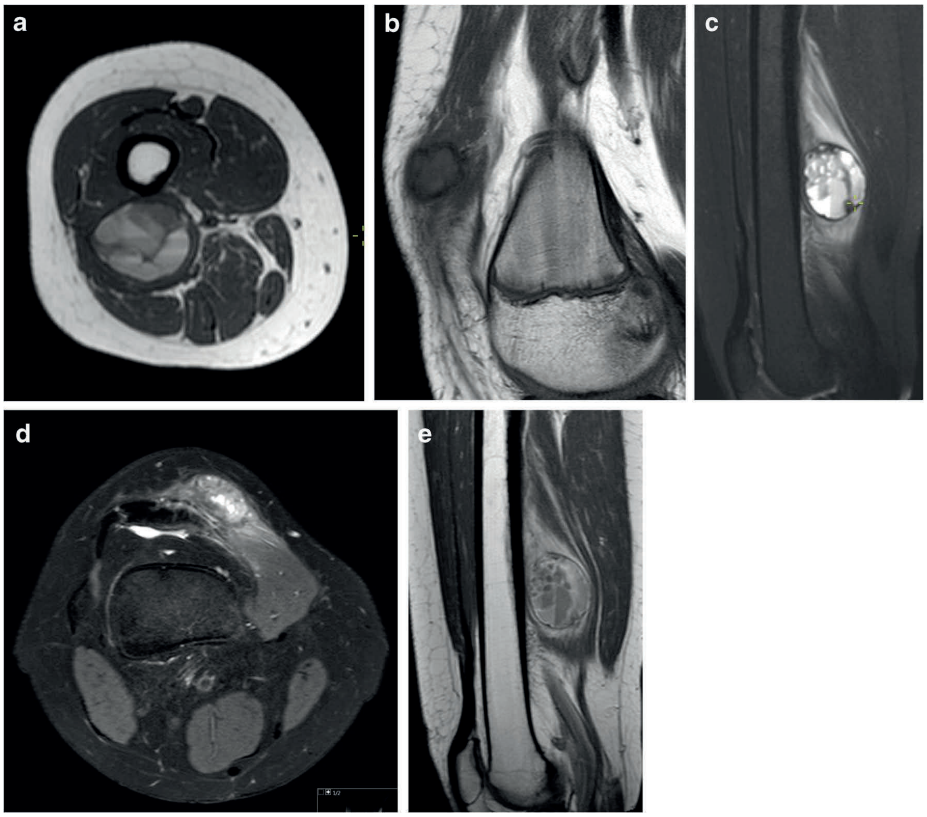

Fig. 5 MRI features of STABC. Axial T1-weighted image (case 1). Intramuscular mass in the short head of the biceps femoral muscle. Predominantly high signal intensity and multiple fluid-fluid levels (**a**). Sagittal T1-weighted MR image (case 3). Intramuscular lesion of intermediate signal intensity surrounded by a rim of low signal intensity caused by the peripheral calcification. Ill-defined stranding beyond this rim is caused by edema (**b**). Sagittal T2-weighted image with fat suppression (case 1). Intramuscular mass with predominantly high signal intensity and multiple fluid-fluid levels. Surrounding rim of low signal intensity represents the egg-shell mineralization. Extensive ill-defined perilesional edema in the adjacent muscle tissue (**c**). Axial T2-weighted image with fat suppression (case 3). Intramuscular mass with predominantly high signal intensity surrounded by the low signal intensity rim from the peripheral calcification. Edema in the adjacent muscular tissue (**d**). Sagittal T1-weighted image after intravenous contrast administration (case 1). Septal enhancement within the lesion. Low signal intensity rim similar to the T2-weighted image. Enhancement of the edema (**e**)

Imaging features of STABC

Imaging features of our six STABC cases and the six cases reported in the radiological literature are summarized in Table 2. Peripheral mineralization was present in ten out of 12 cases (80%), either continuous or as an interrupted calcification [3, 8, 16–18, 25, 28]. In the majority of cases, the peripheral mineralization was eggshell-like. However, coarse peripheral ossification, similar to that encountered in myositis ossificans, may also occur [4, 13, 21, 29], as was seen in our case 4. Five STABC cases had a solid appearance, whereas seven STABC were multicystic with fluid-fluid levels found on MR in four cases (40%, see Table 2). On MR, the lesion usually has an intermediate signal intensity on T1-weighted sequences and intermediate to high signal intensity on T2-weighted sequences, surrounded by a rim of low signal intensity on all sequences caused by the peripheral bone shell. In case of blood-filled spaces, the signal intensity was high on T1 with fluid-fluid levels, as was seen in our case 1. Septal enhancement was present in all three patients with a multicystic appearance on T2-weighted images that had post-contrast imaging. On MRI, nine lesions showed perilesional edema in adjacent soft tissues, which can lead to the impression of an aggressive or even malignant lesion. Some authors speculated that perilesional edema is only present in the active phase of STABC and disappears in a later, more quiescent stage. That

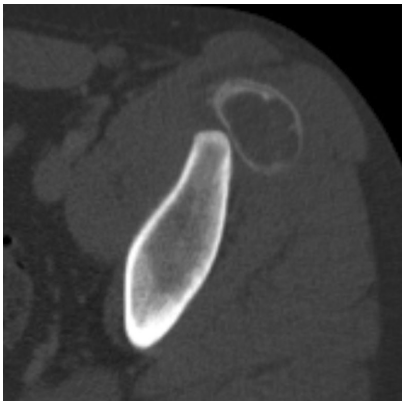

Fig. 6 CT image (case 6) with thin peripheral bone shell in the soft tissues anterior of the left iliac spine

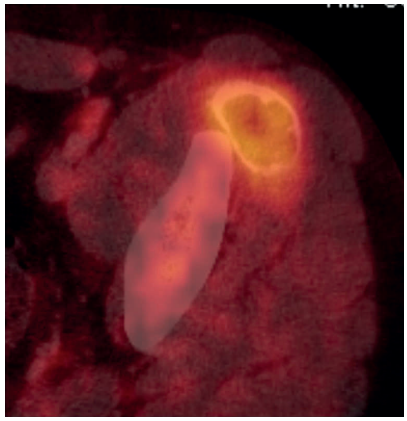

Fig. 8 The fused image of the PET-CT shows predominantly peripheral increased uptake of the radionuclide tracer (case 6)

may be deduced from the case described by Jacquot et al. [6] where MR was only performed late in the course of the disease and edema was absent. On CT, the shell of peripheral mineralization can easily be appreciated and usually is thin, but can be thicker and more coarse. On ultrasonography, the mass may demonstrate a cystic lesion with acoustic shadowing, depending on the presence of peripheral mineralization. Radionuclide imaging shows increased uptake of the radiotracer, as was present in three of our cases and the one reported by Jacquot et al. [6]. In two of our cases, the increased uptake was predominantly peripheral.

The radiological differential diagnosis of STABC mainly includes myositis ossificans. In STABC, however, the shell with peripheral mineralization is usually thin in contrast to the usually thicker and coarser peripheral mineralization in myositis ossificans. Importantly, on MRI scans, the presence of cavities, separated by septations, and fluid-fluid levels are very helpful to differentiate STABC from myositis ossificans [18, 21, 28]. Nevertheless, it can still be difficult to distinguish myositis ossificans from STABC on the basis of radiographic features only [18]. In some cases, such as in our cases 2–4, the cystic cavities, while apparent by gross and/or histological examination, were not visualized by MR imaging. By histology, the cysts of the three STABC cases had a diameter of 11 mm (case 2), 13 mm (case 3), and 1.7 mm (case 4). Given the spatial resolution of MRI, it may seem surprising that cysts larger than 1 cm were not visible with this imaging technique. We cannot exclude, however, that the cysts in these two STABC cases developed or increased in size in the period between imaging and surgery (4 and 7 months). Notably, our STABC case 4 appeared to be solid and a 1.7-mm ABC-like cyst was only discerned by microscopy of the previous needle biopsy, as shown in Fig. 1d. Thus, histology seems indispensable for a morphologic diagnosis of STABC as a distinct entity. Another tumor entering the radiological differential diagnosis because of the presence of a peripheral bone shell is ossifying fibromyxoid tumor (OFMT) [28]. However, OFMT is a solid tumor with a different histology and the majority of OFMT has *PHF1* gene rearrangements [30]. STABC should also be distinguished from liquefied hematoma and cavernous hemangioma, two lesions with cystic areas of high signal intensity on T1- and T2-weighted MR sequences. In addition, extraskeletal telangiectatic osteosarcoma may have fluid-fluid levels similar to those of soft tissue aneurysmal bone cyst [28]. Giant cell tumor of soft tissue should be included in the differential diagnosis, because this tumor may show secondary ABC formation. Notably, in one report, giant cell tumor of soft tissue with hemorrhage and large cystic degeneration was thought to represent STABC [27].

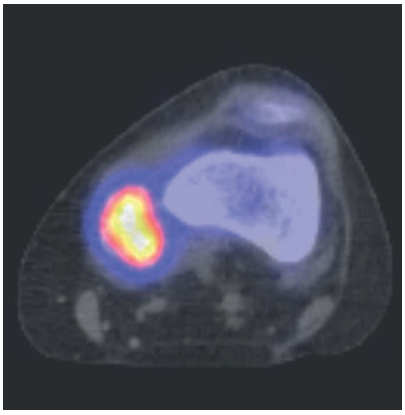

Fig. 7 SPECT fusion image (case 4) with diffuse increased uptake of the radiopharmacon within the lesion

Histopathology and molecular pathology of STABC

The histological features of STABC are indistinguishable from those of ABC arising within bone [1, 18]. Histologically, STABC presents as a well-defined soft tissue mass consisting of cavernous spaces filled with blood and separated by fibrous septa, which lack smooth muscle or an endothelial lining, but contain osteoclast-type multinucleated giant cells, flattened spindle-shaped fibroblasts, and delicate reactive woven bone, often including so-called blue bone. STABC has a thin shell of bone [10, 16, 18, 20, 21]. The six STABC cases presented herein all had the distinct histologic features of STABC, as summarized in Table 1 and illustrated in Fig. 1a–f. Interestingly, after a diagnosis of STABC had been made on needle biopsy material available in case 4, the gross and microscopical features of the excised residual tumor were more reminiscent of myositis ossificans, and a *COL1A1-USP6* fusion gene was detected with NGS. Although ABC of bone and STABC have long been regarded as a reactive process, cytogenetic and molecular studies have provided evidence that (ST)ABC is a true neoplastic process [8, 16, 18, 28, 31, 32]. FISH can be used to demonstrate *USP6* rearrangements, whereas RT-PCR or anchored multiplex PCR-based targeted NGS may be used to detect the fusion partner. Importantly, using FISH, *USP6* rearrangement has also been found in myositis ossificans [33]. Some authors have questioned the specificity of *USP6* rearrangements in myositis ossificans and considered the possibility that these cases actually represent the early stage of soft tissue ABCs [31]. On the other hand, it was recently described that soft tissue lesions histologically diagnosed as myositis ossificans also have USP6 rearrangements [33] and the fusion partner was *COL1A1* in 4/6 cases [34]. Thus, it appears that soft tissue lesions with *USP6* rearrangements, which include nodular fasciitis, myositis ossificans, and STABC may be part of a morphologic spectrum of the same biological entity. In fact, these lesions have overlapping morphologic features. Nodular fasciitis is a solid myofibroblastic neoplasm, with rare cases showing osteoclast-type giant cells and metaplastic bone formation. Myositis ossificans is a solid myofibroblastic tumor with extensive formation of lamellar trabecular bone via woven bone, whereas in STABC clear-cut cystic ABC areas are present, sometimes with areas of woven blue bone. Interestingly, our case 4 had overlapping features of STABC and myositis ossificans. With respect to *USP6* fusion genes, in nodular fasciitis the fusion partner is *MYH7*. In skeletal ABC, other fusion partners of *USP6* have been found, *CDH11* being the most frequent one (found in 30% of cases). Remarkably, in STABC only *COLA1A-USP6* fusions have been found so far (the three cases reported here and those described by Jacquot et al.). Moreover, Flucke et al. found co-existing *USP6* and *COL1A1* rearrangements in 4/6 tumors with features of myositis ossificans. More cases of myositis ossificans have to be studied to evaluate the significance of this observation.

In contrast to myositis ossificans, in which currently the therapy of first choice is non-surgical, the therapy of choice for STABC is wide local excision, given the growth potential of this lesion. Local recurrence is rare. In the literature, only two out of 36 tumors recurred after incomplete excision (5%) [2, 15]. Four patients were lost to follow-up [2, 3, 18, 19].

In conclusion, STABC is a rare soft tissue tumor, predominantly occurring in the upper leg and hip or upper arm and shoulder region and in a somewhat older age group than ABC of bone. Radiologically, STABC may present as a solid or cystic mass. Most often, an eggshell-thin mineralized layer surrounds STABC, but sometimes a coarser calcified layer similar to myositis ossificans is found. Perilesional edema is a prominent radiological feature on MR, which may erroneously suggest an aggressive or even malignant nature. Fluid-fluid levels were present in 40% of cases. Recently, it became apparent that STABC may belong to a spectrum of tumors with *USP6* gene rearrangement and *COL1A1-USP6* fusions, including myositis ossificans and nodular fasciitis. Clinically, the local recurrence rate of STABC is very low. It appears that only lesions that are excised incompletely may sometimes recur.

Authors' contributions Wangzhao Song studied the pathology specimens and drafted the manuscript with Stijn M. Bollen. Albert J. H. Suurmeijer conceived the study, participated in its design, and supervised this article. Anne-Marie Cleton-Jansen performed FISH and next-generation sequencing. Judith V.M.G. Bovée studied the pathology specimens and participated in the study design. Herman M. Kroon conceived the study, interpreted imaging features, designed, supervised, and finally approved this article. All authors read and approved the final manuscript.

Compliance with ethical standards

Conflict of interest No funds were received in support of this work. The authors declare that they have no conflicts of interest.

Sources of support W. Song receives funding from the China Scholarship Council (CSC) program (grant no: 201606940023).

Ethical approval All procedures performed in studies involving human participants were in accordance with the ethical standards of the institutional and/or national research committee and with the 1964 Helsinki Declaration and its later amendments or comparable ethical standards.

Informed consent Informed consent was obtained from all individual participants included in the study.

References

1. Jaffe HL, Lichtenstein L. Solitary unicameral bone cyst with emphasis on the roentgen picture, the pathologic picture and the pathogenesis. Arch Surg. 1942;46:1004–25.
2. Salm R, Sissons HA. Giant-cell tumours of soft tissues. J Pathol. 1972;107:27–39.
3. Ajilogba KA, Kaur H, Duncan R, McFarlane JH, Watt AJ. Extraosseous aneurysmal bone cyst in a 12-year-old girl. Pediatr Radiol. 2005;35:1240–2.

4. Amir G, Mogle P, Sucher E. Case report 729. Myositis ossificans and aneurysmal bone cyst. Skelet Radiol. 1992;21:257–9.
5. Baker KS, Gould ES, Patel HB, Hwang SJ. Soft tissue aneurysmal bone cyst: a rare case in a middle aged patient. J Radiol Case Rep. 2015;9:26–35.
6. Jacquot C, Szymanska J, Nemana LJ, Steinbach LS, Horvai AE. Soft-tissue aneurysmal bone cyst with translocation t(17;17)(p13;q21) corresponding to COL1A1 and USP6 loci. Skelet Radiol. 2015;44:1695–9.
7. Samura H, Shiraishi M, Tokashiki H, Nosato E, Miyazato H, Muto Y. An extraosseous aneurysmal cyst in the pelvic cavity: report of a case. Clin Imaging. 2000;24:68–71.
8. Wang XL, Gielen JL, Salgado R, Delrue F, De Schepper AM. Soft tissue aneurysmal bone cyst. Skelet Radiol. 2004;33:477–80.
9. Van Eijk R, Stevens L, Morreau H, van Wezel T. Assessment of a fully automated high-throughput DNA extraction method from formalin-fixed, paraffin-embedded tissue for KRAS, and BRAF somatic mutation analysis. Exp Mol Pathol. 2013;94:121–5.
10. Meyers SP. MRI of bone and soft tissue tumors and tumorlike lesions—differential diagnosis and atlas. Stuttgart: Thieme Medical Publishers; 2008. p. 814.
11. Kransdorf MJ, Sweet DE. Aneurysmal bone cyst: concept, controversy, clinical presentation, and imaging. AJR Am J Roentgenol. 1995;164:573–80.
12. Martinez V, Sissons HA. Aneurysmal bone cyst. A review of 123 cases including primary lesions and those secondary to other bone pathology. Cancer. 1988;61:2291–304.
13. Hao Y, Wang L, Yan M, Jin F, Ge S, Dai K. Soft tissue aneurysmal bone cyst in a 10-year-old girl. Oncol Lett. 2012;3:545–8.
14. McCann KM, Clifford CE, Salton HL. Soft tissue aneurysmal bone cyst: a case report. FAOJ. 2011;4(6):No. 1.
15. Dal Cin P, Kozakewich HP, Goumnerova L, Mankin HJ, Rosenberg AE, Fletcher JA. Variant translocations involving 16q22 and 17p13 in solid variant and extraosseous forms of aneurysmal bone cyst. Genes Chromosom Cancer. 2000;28:233–4.
16. Karkuzhali P, Bhattacharyya M, Sumitha P. Multiple soft tissue aneurysmal cysts: an occurrence after resection of primary aneurysmal bone cyst of fibula. Indian J Orthop. 2007;41:246–9.
17. Lopez-Barea F, Rodriguez-Peralto JL, Burgos-Lizaldez E, Alvarez-Linera J, Sanchez-Herrera S. Primary aneurysmal cyst of soft tissue. Report of a case with ultrastructural and MRI studies. Virchows Arch. 1996;428:125–9.
18. Nielsen GP, Fletcher CD, Smith MA, Rybak L, Rosenberg AE. Soft tissue aneurysmal bone cyst: a clinicopathologic study of five cases. Am J Surg Pathol. 2002;26:64–9.
19. Petrik PK, Findlay JM, Sherlock RA. Aneurysmal cyst, bone type, primary in an artery. Am J Surg Pathol. 1993;17:1062–6.
20. Riccioni L, Foschini MP. Extraosseous aneurysmal bone cyst. Tumori. 1996;82:485–7.
21. Rodriguez-Peralto JL, Lopez-Barea F, Sanchez-Herrera S, Atienza M. Primary aneurysmal cyst of soft tissues (extraosseous aneurysmal cyst). Am J Surg Pathol. 1994;18:632–6.
22. Shannon P, Bedard Y, Bell R, Kandel R. Aneurysmal cyst of soft tissue: report of a case with serial magnetic resonance imaging and biopsy. Hum Pathol. 1997;28:255–7.
23. D'Costa GF, Hastak MS, Patil YV. Primary aneurysmal cyst: bone type in the breast. Indian J Surg. 2007;69:248–50.
24. Della Libera D, Redlich G, Bittesini L, Falconieri G. Aneurysmal bone cyst of the larynx presenting with hypoglottic obstruction. Arch Pathol Lab Med. 2001;125:673–6.
25. Ellison DA, Sawyer JR, Parham DM, Nicholas R Jr. Soft-tissue aneurysmal bone cyst: report of a case with t(5;17)(q33;p13). Pediatr Dev Pathol. 2007;10:46–9.
26. Fellig Y, Oliveira AM, Margolin E, Gomori JM, Erickson-Johnson MR, Chou MM, et al. Extraosseous aneurysmal bone cyst of cerebello-pontine angle with USP6 rearrangement. Acta Neuropathol. 2009;118:579–81.
27. Lopez LV, Rodriguez MG, Siegal GP, Wei S. Extraskeletal aneurysmal bone cyst: report of a case and review of the literature. Pathol Res Pract. 2017;213:1445–9.
28. Pietschmann MF, Oliveira AM, Chou MM, Ihrler S, Niederhagen M, Baur-Melnyk A, et al. Aneurysmal bone cysts of soft tissue represent true neoplasms: a report of two cases. J Bone Joint Surg Am. 2011;93:e45.
29. Sahu A, Gujral SS, Gaur S. Extraosseous aneurysmal cyst in hand: a case report. Cases J. 2008;1:268.
30. Kao YC, Sung YS, Zhang L, Chen CL, Huang SC, Antonescu CR. Expanding the molecular signature of ossifying fibromyxoid tumors with two novel gene fusions: CREBBP-BCORL1 and KDM2A-WWTR1. Genes Chromosom Cancer. 2017;56:42–50.
31. Sukov WR, Franco MF, Erickson-Johnson M, Chou MM, Unni KK, Wenger DE, et al. Frequency of USP6 rearrangements in myositis ossificans, brown tumor, and cherubism: molecular cytogenetic evidence that a subset of "myositis ossificans-like lesions" are the early phases in the formation of soft-tissue aneurysmal bone cyst. Skelet Radiol. 2008;37:321–7.
32. Oliveira AM, Perez-Atayde AR, Dal Cin P, Gebhardt MC, Chen CJ, Neff JR, et al. Aneurysmal bone cyst variant translocations upregulate USP6 transcription by promoter swapping with the ZNF9, COL1A1, TRAP150, and OMD genes. Oncogene. 2005;24:3419–26.
33. Bekers EM, Eijkelenboom A, Grünberg K, Roverts RC, de Rooy JWJ, van der Geest ICM, et al. Myositis ossificans—another condition with USP6 rearrangement, providing evidence of a relationship with nodular fasciitis and aneurysmal bone cyst. Ann Diagn Pathol. 2018;34:56–9.
34. Flucke U, Bekers EM, Creytens D, van Gorp JM. COL1A1 is a fusionpartner of USP6 in myositis ossificans—FISH analysis of six cases. Ann Diagn Pathol. 2018. https://doi.org/10.1016/j.anndiagpath.2018.06.009.

Chapter 7

Low-grade central fibroblastic osteosarcoma may be differentiated from its mimicker desmoplastic fibroma by genetic analysis

This chapter is based on the publication: **Song W**, van den Berg E, Kwee TC, et.al. Low-grade central fibroblastic osteosarcoma may be differentiated from its mimicker desmoplastic fibroma by genetic analysis. Clin Sarcoma Res. 2018 Aug 23;8:16.

Low-grade central fibroblastic osteosarcoma may be differentiated from its mimicker desmoplastic fibroma by genetic analysis

Wangzhao Song[1], Eva van den Berg[2], Thomas C. Kwee[3], Paul C. Jutte[4], Anne-Marie Cleton-Jansen[5], Judith V. M. G. Bovée[5] and Albert J. Suurmeijer[1*]

Abstract

Background: We studied two cases of rare fibrous bone tumors, namely desmoplastic fibroma (DF) and low-grade central osteosarcoma (LGCOS) resembling desmoplastic fibroma (DF-like LGCOS). As the clinical presentation, imaging features and histopathology of DF and DF-like LGOS show much overlap, the objective of this study was to investigate the value of cytogenetic analysis, molecular pathology and immunohistochemistry in discrimination of these two mimickers.

Case presentation: A mutation in *CTNNB* (S45F) and nuclear beta-catenin immunostaining were observed in DF. DF-LGCOS had amplification of *CDK4* and showed strong nuclear expression of CDK4 by IHC. Moreover, the karyotype of DF-LGCOS showed an interstitial heterozygous deletion of the long arm of chromosome 13 (q12q32), associated with loss of the *RB1* tumor suppressor gene.

Conclusions: Karyotyping and molecular genetic analysis may contribute to a conclusive diagnosis.

Keywords: Bone sarcoma, Desmoplastic fibroma, Low-grade osteosarcoma, CDK4, RB1

Background

The histopathological diagnosis of bone tumors is usually rather straightforward, since the most common bone tumors show differentiation along osteoblastic or chondroblastic lines, and form bone matrix or cartilage, which usually can be easily detected in routinely stained tissue sections.

In the past decades, advances in the field of immunohistochemistry (IHC) and molecular pathology have allowed a precise diagnosis in difficult cases. Examples are IHC for *SATB2* to confirm a tentative diagnosis of osteosarcoma, molecular DNA analysis for nonrandom gene translocations to differentiate Ewing sarcoma from other round cell sarcomas, and detection of *H3F3A* mutations to accurately diagnose giant cell tumor of bone.

However, for fibrous tumors of bone the incremental value of IHC and DNA methods over standard basic histology is rather limited. This category of fibrous tumors of bone includes the desmoplastic fibroma (DF)—a rare, locally aggressive tumor—and fibrosarcoma—a tumor once considered to be very common, but currently a diagnosis of exclusion, that one is only allowed to make after having ruled out other spindle cell tumors, e.g. low grade myofibroblastic sarcoma, myoepithelial tumors, follicular dendritic cell tumors, synovial sarcoma, and, last but not least, a rare variant of low-grade central osteosarcoma (LGCOS) resembling desmoplastic fibroma (DF-like LGCOS).

By co-incidence, two patients with these rare bone tumors (DF and DF-LGCOS) were treated in our

*Correspondence: a.j.h.suurmeijer@umcg.nl
[1] Department of Pathology and Medical Biology, University Medical Center Groningen, University of Groningen, P.O. Box 30.001, 9700 RB Groningen, The Netherlands
Full list of author information is available at the end of the article

sarcoma center in the same week. In addition to IHC, we decided to apply classic cytogenetics and next generation sequencing (NGS), which proved to be very helpful in discriminating these two morphologic mimickers.

Case presentation

Case 1: a 10-year-old girl, with a history of distal radius fracture 3 years earlier, presented with a firm, nontender swelling in the same right distal forearm. Her wrist function was unimpaired. As shown in Fig. 1, X-ray examination revealed a large lobulated, compartmentalized, osteolytic, expansive tumor mass in the metadiaphysis of the distal radius. On MRI, the tumor measured $35 \times 46 \times 47$ mm and had a well-defined boundary, but no sclerotic margin. Starting from the distal radius, there was cortical destruction, an extensive soft tissue component, and impression and bowing of the distal ulna. There were no imaging signs of invasive growth, necrosis or fluid-liquid mirrors. Bone scintigraphy did not show increased uptake at the location of the lesion. These imaging features were consistent with a destructive tumor that originated from the distal radius, grew slowly, and then broke through the cortex of the radius into the adjacent soft tissue. The tumor was excised intralesionally. Grossly, the largest tumor fragment measured $6 \times 5 \times 3$ cm. On cut surface the tumor tissue was pale and fibrous.

Tumor histology was reminiscent of desmoid fibromatosis and consistent with desmoplastic fibroma, as it showed a lesion composed of bundles of moderately cellular, collagenous tumor tissue with fibroblastic spindle cells with oval, monomorphic nuclei with bland, finely granular chromatin, small nucleoli and ample cytoplasm. Mitoses were not found (Fig. 2a).

Cytogenetic analysis revealed a normal female karyotype in 18 cells, with trisomy 8 detected in 2 cells (Fig. 2b).

The cancer hotspot NGS analysis revealed a CTNNB1 hotspot class 5 pathogenic variant in exon 3: p.Ser45Phe and, using IHC, the fibroblastic tumor cells showed more than focal nuclear staining for beta-catenin (Fig. 2c), in support of a diagnosis of desmoplastic fibroma.

Case 2: a 24-year-old woman presented with progressive pain in the right hip region that had existed for 1 year. X-ray images showed an osteolytic tumor in the metadiaphysis of the right distal femur with cortical bone destruction on the dorsolateral side. The central part of the tumor had no matrix calcification. On MRI, the tumor destroyed the cortex and extended to the surrounding soft tissues. There was strong tumor enhancement after administration of intravenous gadolinium (Fig. 3a). A resection of the right distal femur was performed. The tumor in the distal femur measured 12×4 cm. On cut surface the tumor was pale and fibrous. There was extension to surrounding soft tissue (Fig. 3b).

Tumor histology strongly resembled the desmoplastic fibroma diagnosed in case 1, however, with some differences. As shown in Fig. 4a, this tumor also consisted of bundles of moderate cellular tissue, with fibroblast-like, spindle cells in abundant collagenous stroma. However, there was evidence of invasive growth in trabecular bone and surrounding skeletal muscle tissue. Although nuclear chromatin was bland, few normal mitoses were found. Osteoid or trabecular bone was absent.

As depicted in Fig. 4b, cytogenetic analysis showed an abnormal karyotype: 47~49,XX,del(13) (q12q32),+1~2r,+1~2mar,1dmin [cp17]/46,XX [2]. This encompasses an interstitial deletion of the long arm of chromosome 13 (q12q32), consistent with heterozygous loss of the *RB1* tumor suppressor gene. With cancer hotspot NGS analysis we found amplification of *CDK4* (NM_000075.3) and an imbalance of the *RB1* gene on chromosome 13.

With IHC, tumor cells exhibited strong nuclear staining for CDK4 (Fig. 4c) and moderate nuclear staining for SATB2. RB1 expression was heterogeneous, not completely lost.

In this case a conclusive diagnosis of DF-LGOS could be made, based on histologic features (an invasive fibroblastic tumor with mitotic activity), karyotyping (heterozygous loss of *RB1*) and molecular genetics/IHC (*CDK4* amplification).

Discussion and conclusions

We have presented the clinical presentation, imaging studies, gross and microscopic pathology, IHC, cytogenetics and molecular genetics (cancer hotspot analysis) of DF and DF-LCOS, two very rare bone tumors, which closely resemble each other.

DF is very rare indeed. Among 4692 benign bone tumors treated in the Birmingham Royal Orthopedic Hospital, Evans et al. [1] identified 13 cases of DF, an incidence of 0.003%. Böhm et al. [2] reviewed 189 cases of DF reported in the literature up to 1996 and observed that, although DF occurs at all ages, children and young adults are most commonly affected, three-quarter of patients being younger than 31 years. Sex distribution is almost equal. DF most commonly presents in the mandible (22%), but also in pelvic bones (13%), and long bones—femur (15%), radius (12%), and tibia (9%). Notably, pathologic fracture of a long bone was reported in 12% of patients. Thus, the clinical presentation of our DF case as a tumor in the distal radius of a 10-year-old girl, who had experienced a radius fracture 3 years earlier, matches data from the literature.

Fig. 1 Conventional AP and lateral radiographs (top left and top middle) show an expansive bubbly lytic bone lesion in the diaphysis-metaphysis of the right distal radius with a narrow zone of transition, nonsclerotic margins, cortical thinning and destruction, and an accompanying large soft-tissue mass which appears to compress the distal ulna with bowing of the latter. Bone scintigraphy (top right) shows no increased uptake at the location of the lesion. MRI with coronal T1-weighted (bottom left) and gadolinium-enhanced T1-weighted (bottom middle) images, and axial T2-weighted and gadolinium-enhanced fat-suppressed T1-weighted images (bottom right) are in keeping with the conventional radiographic findings, and also demonstrate no signs of invasion in surrounding muscles or ulna. Remarkably, in the center of the lesion there is low signal on all sequences (arrows), most strikingly on the T2-weighted sequence. Because the combined imaging features suggest a slow-growing (most likely benign) process with fibrotic components, the differential diagnostic considerations include desmoplastic fibroma, and (less likely) giant-cell tumor or fibrous dysplasia

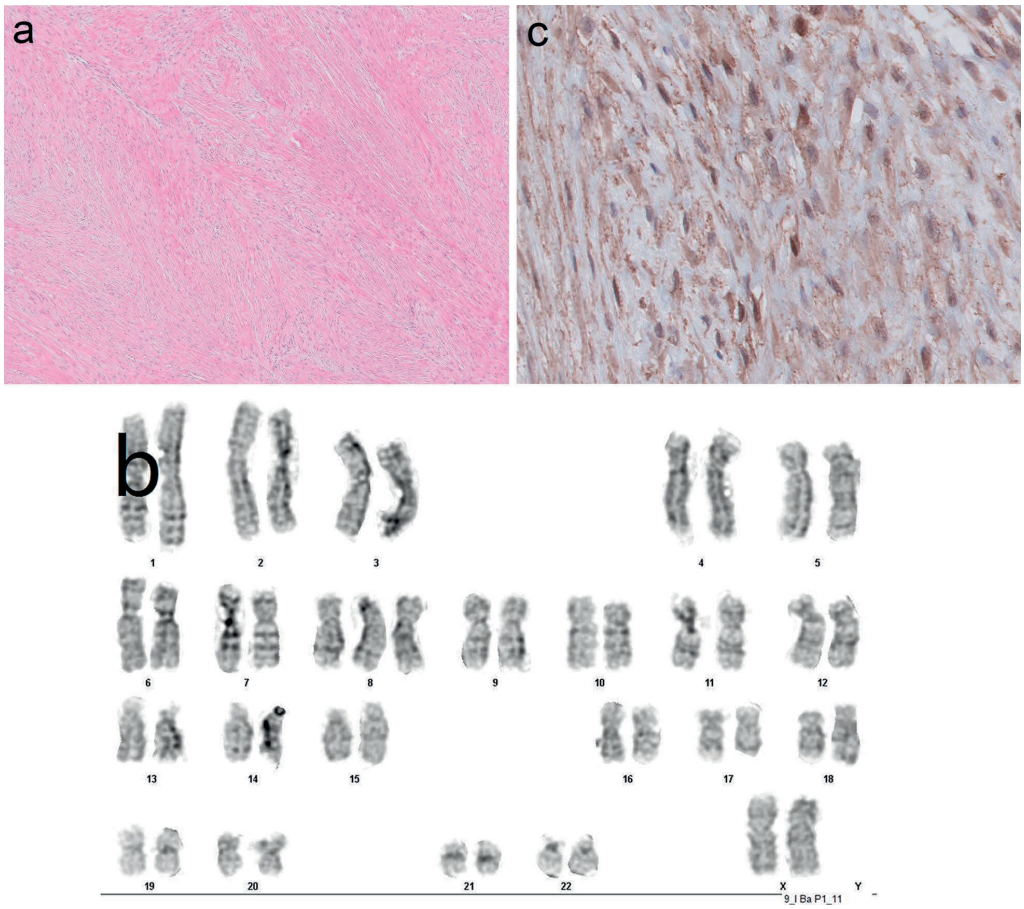

Fig. 2 Histology, karyotype and beta-catenin nuclear expression in DF. **a** Histology showing a fibroblastic tumor with little or no nuclear atypia or mitotic activity (H&E, original magnification × 200). As such, the histology of DF resembles that DF-LGCOS shown in Fig. 4a. **b** DF karyotype: 47,XX,+8[2]/46,XX[18]. **c** IHC expression of beta-catenin in several tumor cell nuclei of DF (original magnification × 400)

It is well appreciated that DF has a high recurrence rate after intralesional excision [1, 2], but since DF is a benign tumor that does not metastasize, we choose to remove the radius tumor of this young girl intralesionally, in order to preserve arm and wrist function. Unfortunately, a recurrence has occurred 12 months after surgery.

As our case illustrates, DF may present as a slowly progressive but locally aggressive tumor. As reviewed by Nedopil et al. [3] by imaging studies, DF can show cortical breakthrough and extension in surrounding soft tissue.

Moreover, infiltrative tumor growth may be seen by microscopy. Mitoses are only rarely found, an important criterion to discriminate DF from DF-LCOS or low-grade fibrosarcoma [4].

Cytogenetic analysis of our DF case revealed a normal female karyotype in 18 cells, with a trisomy 8 detected in 2 cells. To our knowledge, only two papers have been published on the cytogenetics and molecular genetics of DF. Bridge et al. [5] found trisomies 8 and 20 in a single case of DF, but again, these cytogenetic abnormalities were also detected in other fibro-osseous bone tumors,

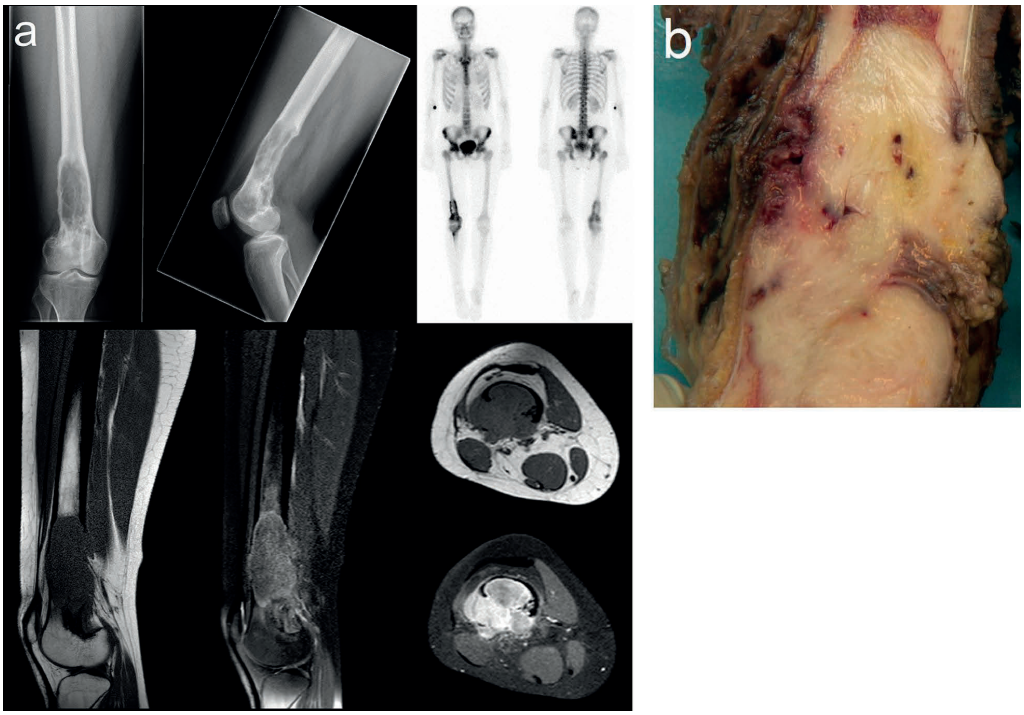

Fig. 3 Conventional AP, lateral radiographs and gross morphology of DF-LGCOS. **a** Conventional AP, lateral radiographs (top left and top middle) show an expansive osteolytic lesion in the diaphysis-metaphysis of the right distal femur with an ill-defined border and cortical destruction. Bone scintigraphy (top right) demonstrates increased uptake at the location of the lesion, but no suspicious uptake elsewhere. MRI with sagittal T1-weighted (bottom left) and fat-suppressed proton density-weighted (bottom middle) images, and axial T1-weighted and gadolinium-enhanced fat-suppressed T1-weighted images (bottom right) show the T1 hypointense, T2 hyperintense, and vividly enhancing lesion in the right distal femur as a large soft-tissue mass with cortical breakthrough and extra-osseous expansion. The combined imaging features are highly suggestive of an aggressive malignant lesion, with osteosarcoma, Ewing sarcoma, and chondrosarcoma being the main differential diagnostic considerations. **b** Gross specimen of DF-LGCOS, showing a white, fibrous tumor of the distal femur with cortical breakthrough and invasion of soft tissue. As such, the gross appearance of DF-LGCOS resembles DF

by which these are noncontributory to a certain DF diagnosis.

An abnormal karyotype 46,XX,del(11)(q13q23),der(19)t(11;19)(q13;p13)del(11)(q23) was reported by Trombetta et al. [6] in a DF occurring in the femur of a 20-year-old female patient. It was hypothesized that loss of a genomic region in 11q, an area containing the genes *RBM14, RBM4, RBM4B, SPTBN2,* and *C11orf80* may be of pathogenic significance.

Using IHC, others and we have noticed nuclear staining of beta-catenin in DF [3, 4, 7–11]. However, although nuclear expression of beta-catenin supports a diagnosis of DF, one has to be aware that nuclear immunostaining of beta-catenin also occurs in other fibro-osseous bone tumors [9] or fibrous soft tissue tumors [12]. Moreover, IHC for beta-catenin is not specific for *APC/CTNNB1* mutations in fibro-osseous bone tumors. *CTNNB1* mutations are a rare molecular event in the few cases of DF that have been analyzed [7–9]. In fact, Flucke et al. [8] found a p.T41A *CTNNB1* mutation in 1 out of 2 cases of DF arising in the mandible, Horvai and Jordan [9] found an *APC* mutation, but no *CTNNB1* mutation in a single DF analyzed, and Hauben et al. [7] found no *CTNNB1* mutation in six DF cases. Using NGS, we detected a *CTNNB1* hotspot class 5 pathogenic variant in exon 3: p.S45F, which is a gain of function mutation. Clearly, to be able to estimate the real frequency of *CTNNB1* mutations in DF, more cases have to be studied, preferably

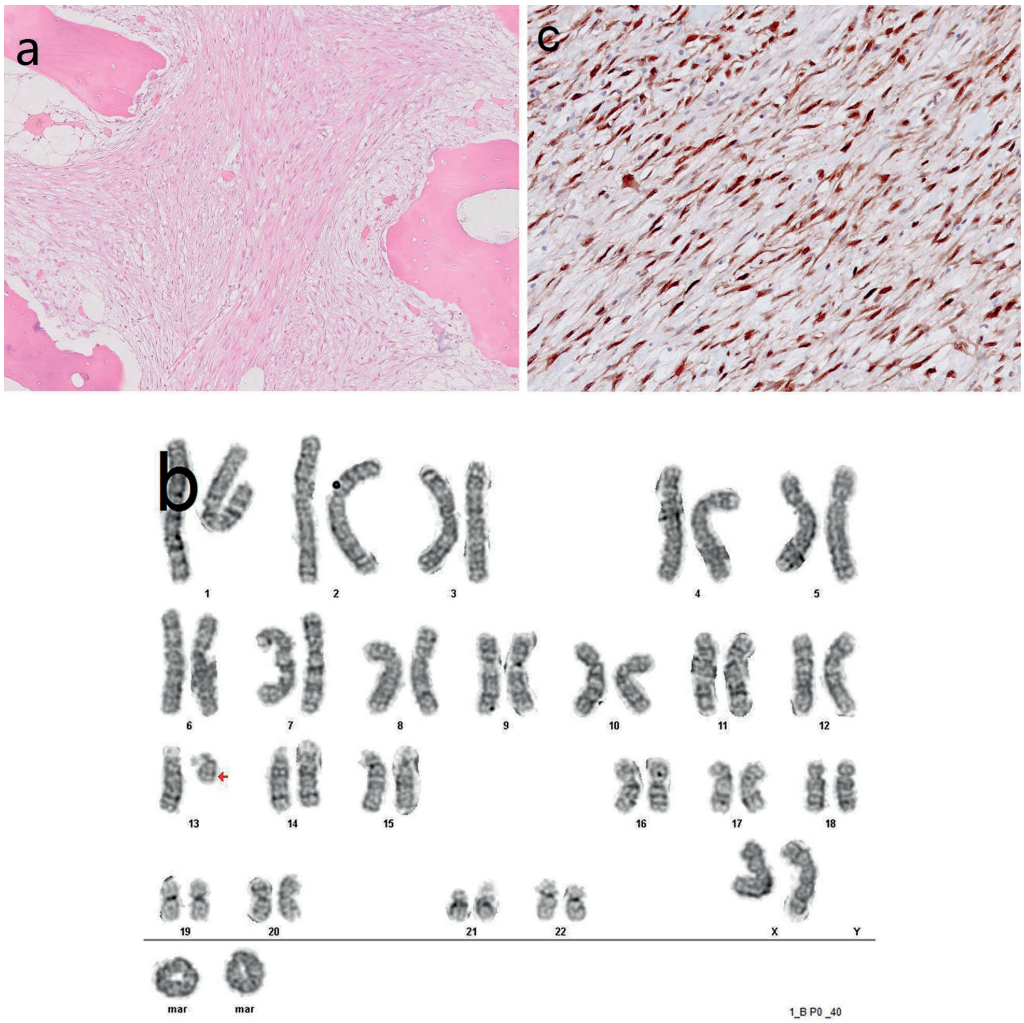

Fig. 4 Histology, karyotype and CDK4 expression in DF-LGOS. **a** Histology showing a fibroblastic tumor with permeative invasive growth (H&E, original magnification × 100). As such, the histology of DF-LGCOS resembles that of DF, shown in Fig. 2a. **b** DF-LGOS karyotype: 47~49,XX,del(13)(q12q32),+1~2r,+1~2mar,1dmin[cp17]/46,XX[2]. **c** Diffuse nuclear expression of CDK4 in cell nuclei of DF-LGCOS (original magnification × 200)

using NGS, since NGS has a higher sensitivity compared with traditional DNA sequencing methods in picking up *CTNNB1* mutations [13] Interestingly, the S45F *CTNNB* mutation also occurs in desmoid fibromatosis, in particular in aggressive and recurrent lesions [14]. However, it remains to be proven that DF is the bony counterpart of desmoid fibromatosis of soft tissue. In this respect, one may argue whether our case 1 represents a soft tissue tumor that had invaded bone. However, given the imaging features, in particular the bubbly compartmentalized appearance of the radius tumor and the bowing of the distal ulna without bone invasion (see Fig. 1), we regarded the radius tumor in this girl as a slow growing primary bone tumor with soft tissue extension, a clinical presentation consistent with a histopathologic diagnosis of desmoplastic fibroma of bone.

The majority of central osteosarcomas are high-grade conventional osteosarcomas, in which the tumor cells show severe nuclear atypia and produce a variable amount of cartilaginous or osteoid matrix. High grade osteosarcomas with severe nuclear atypia, but little or no matrix formation can be confirmed by SATB2 immunohistochemistry [15, 16].

Our DF-LGCOS case is part of another subset of low grade central osteosarcomas namely the ones that resemble DF and have little or no osteoid matrix deposition. So far, this very rare OS subtype has only been described in case reports and small series [17, 18]. Most likely these rare DF-LCOS have been included in the histological spectrum of fibrosarcomas of bone [4]. We agree with Horvai and Jordan [9], who stated that it seems logical that at least a subset of fibrosarcomas of bone are actually osteosarcomas with little or no osteoid or bone formation. Surprisingly, in the 2013 WHO classification of tumors of soft tissue and bone, fibrosarcomas of bone are defined as intermediate to high grade spindle cell tumors that lack any line of differentiation other than fibroblastic, leaving little room for the recognition of low grade variants, also excluding DF- LGCOS.

Strong and diffuse SATB2 nuclear IHC staining reflects an osteoblastic line of differentiation. To date, only one Chinese study investigated SATB2 expression in low grade osteosarcoma and desmoplastic fibroma. Th ese authors found that low-grade osteosarcoma and fibrous dysplasia are positive for SATB2, while desmoplastic fibroma, low-grade fi brosarcoma and other fib rous tumors are negative [19].

The notion that DF-LGCOS is an osteosarcoma variant is also supported by the cytogenetics and molecular genetics of our second case. DF-LGCOS had a karyotype with interstitial deletion of the long arm of chromosome 13 (q12q32), consistent with loss of the *RB1* tumor suppressor gene, a genetic abnormality found in a substantial number of osteosarcomas. Notably, cancer hotspot NGS analysis revealed amplification of *CDK4* and IHC showed overexpression of CDK4.

The prototypical LGCOS (which resembles parosteal osteosarcoma) usually produces abundant bone matrix and contains trabecular woven bone. The fi broblastic stromal cells of the prototypical LGCOS show slight nuclear atypia and mitosis are not easily discerned. This subset of LGCOS often has gain or amplification of the *MDM2* and/or *CDK4* genes, which can be visualized by their nuclear expression by IHC [19]. By IHC, CDK4 is positive in the majority of LGOS, and, when combined with MDM2 immunostaining, the sensitivity and specificity for LGOS is 100% and 97.5%, respectively [20].

The c linical p resentation, i maging s tudies a nd g ross morphology of DF-LGCOS shows much overlap with DF. Both are fibrous tumors of bone with are slowly progressive and locally aggressive showing cortical breakthrough. DF and DF-LGCOS consist of bundles of moderately cellular collagenous tumor tissue with spindled fibroblast-like cells. The two cases reported herein show that karyotyping and molecular genetic analysis may contribute to a conclusive diagnosis, DF showing *CTNNB1* S45F mutation and DF-LGCOS showing *CDK4* amplification.

Abbreviations

DF: desmoplastic fibroma; DF-like LGCOS: low-grade central osteosarcoma (LGCOS) resembling desmoplastic fibroma; NGS: next generation sequencing; IHC: immunohistochemistry; LGCOS: low-grade central osteosarcoma; CC1: cell conditioning buffer 1.

Authors' contributions

WS observed pathology specimens, participated in the study design and drafted the manuscript. EB and AMCJ performed classic cytogenetics and next generation sequencing, respectively. TCK interpreted imaging features. PCJ performed the surgery, managed the patient and completed the clinical data collection. JVMGB conceived of the study, participated in its design. AJS conceived, designed and supervised this article. All authors read and approved the final manuscript.

Author details

[1] Department of Pathology and Medical Biology, University Medical Center Groningen, University of Groningen, P.O. Box 30.001, 9700 RB Groningen, The Netherlands. [2] Department of Genetics, University Medical Center Groningen, University of Groningen, P.O. Box 30.001, 9700 RB Groningen, The Netherlands. [3] Department of Radiology, Nuclear Medicine and Molecular Imaging, University Medical Center Groningen, University of Groningen, P.O. Box 30.001, 9700 RB Groningen, The Netherlands. [4] Department of Orthopedic Surgery, University Medical Center Groningen, University of Groningen, P.O. Box 30.001, 9700 RB Groningen, The Netherlands. [5] Department of Pathology, Leiden University Medical Center, Leiden, The Netherlands.

Acknowledgements

We want to acknowledge Tom van Wezel and Dina Ruano Neto (Pathology, LUMC) for setting up the NGS pipeline.

Competing interests

The authors declare that they have no competing interests.

Availability of data and materials

The dataset supporting the conclusions of this article is included within the article.

Consent for publication

Written informed consent for publication of their clinical details and/or clinical images was obtained from the patient. A copy of the consent form is available for review by the Editor of this journal.

Ethics approval and consent to participate

All procedures performed in studies involving human participants were in accordance with the ethical standards of the institutional and/or national research committee and with the 1964 Helsinki declaration and its later amendments or comparable ethical standards. The study met the criteria of the code of conduct for responsible use of human tissue that is used in the Netherlands (Dutch federation of biomedical scientific societies; http://www.federa.org).

Funding

Wangzhao Song receives funding from the China Scholarship Council (CSC) program (Grant No: 201606940023).

Publisher's Note

Received: 18 May 2018 Accepted: 23 July 2018
Published online: 23 August 2018

References

1. Evans S, Ramasamy A, Jeys L, et al. Desmoplastic fibroma of bone: a rare bone tumour. J Bone Oncol. 2014;3:77–9.
2. Bohm P, Krober S, Greschniok A, et al. Desmoplastic fibroma of the bone. A report of two patients, review of the literature, and therapeutic implications. Cancer. 1996;78:1011–23.
3. Nedopil A, Raab P, Rudert M. Desmoplastic fibroma: a case report with three years of clinical and radiological observation and review of the literature. Open Orthop J. 2013;8:40–6.
4. Saito T, Oda Y, Tanaka K, et al. Low-grade fibrosarcoma of the proximal humerus. Pathol Int. 2003;53:115–20.
5. Bridge JA, Swarts SJ, Buresh C, et al. Trisomies 8 and 20 characterize a subgroup of benign fibrous lesions arising in both soft tissue and bone. Am J Pathol. 1999;154:729–33.
6. Trombetta D, Macchia G, Mandahl N, et al. Molecular genetic characterization of the 11q13 breakpoint in a desmoplastic fibroma of bone. Cancer Genet. 2012;205:410–3.
7. Hauben E, Jundt G, Cleton-Jansen AM, et al. Desmoplastic fibroma of bone: an immunohistochemical study including beta-catenin expression and mutational analysis for beta-catenin. Hum Pathol. 2005;36:1025–30.
8. Flucke U, Tops BB, van Diest PJ, et al. Desmoid-type fibromatosis of the head and neck region in the paediatric population: a clinicopathological and genetic study of seven cases. Histopathology. 2014;64:769–76.
9. Horvai A, Jordan R. Fibro-osseous lesions of the craniofacial bones: β-catenin immunohistochemical analysis and CTNNB1 and APC mutation analysis. Head Neck Pathol. 2014;8(3):291–7.
10. Woods TR, Cohen DM, Islam MN, et al. Desmoplastic fibroma of the mandible: a series of three cases and review of literature. Head Neck Pathol. 2015;9:196–204.
11. Okubo T, Saito T, Takagi T, et al. Desmoplastic fibroma of the rib with cystic change: a case report and literature review. Skeletal Radiol. 2014;43:703–8.
12. Carlson JW, Fletcher CD. Immunohistochemistry for beta-catenin in the differential diagnosis of spindle cell lesions: analysis of a series and review of the literature. Histopathology. 2007;51:509–14.
13. Colombo C, Urbini M, Astolfi A, et al. Novel intra-genic large deletions of CTNNB1 gene identified in WT desmoid-type fibromatosis. Genes Chromosomes Cancer. 2018. https://doi.org/10.1002/gcc.22644.
14. van Broekhoven DL, Verhoef C, Grünhagen D, et al. Prognostic value of CTNNB1 gene mutation in primary sporadic aggressive fibromatosis. Ann Surg Oncol. 2015;22:1464–70.
15. Conner JR, Hornick JL. SATB2 is a novel marker of osteoblastic differentiation in bone and soft tissue tumours. Histopathology. 2013;63:36–49.
16. Davis JL, Horvai AE. Special AT-rich sequence-binding protein 2 (SATB2) expression is sensitive but may not be specific for osteosarcoma as compared with other high-grade primary bone sarcomas. Histopathology. 2016;69:84–90.
17. Kurt AM, Unni KK, McLeod RA, et al. Low-grade intraosseous osteosarcoma. Cancer. 1990;65:1418–28.
18. Bertoni F, Bacchini P, Fabbri N, et al. Osteosarcoma. Low-grade intraosseous-type osteosarcoma, histologically resembling parosteal osteosarcoma, fibrous dysplasia, and desmoplastic fibroma. Cancer. 1993;71:338–45.
19. Chen CY, Zhang HZ, Jiang ZM, et al. Value of MDM2, CDK4 and SATB2 immunohistochemistry in histologic diagnosis of low-grade osteosarcoma. Zhonghua Bing Li Xue Za Zhi. 2016;45:387–92.
20. Yoshida A, Ushiku T, Motoi T, et al. Immunohistochemical analysis of MDM2 and CDK4 distinguishes low-grade osteosarcoma from benign mimics. Mod Pathol. 2010;23:1279–88.

Chapter 8

Summary, general discussion and future perspectives

Chapter 8

Summary, general discussion and future perspectives

To achieve an accurate and histopathological diagnosis of STB tumors is by no means easy. In daily pathology practice, STB tumors often show overlapping morphologic features and nonspecific or absent IHC marker expression, which makes it difficult to render an objective diagnosis[1-3], in particular when one is dealing with small (needle biopsy) specimens. Molecular genetic abnormalities define different STB tumors and allow a more precise diagnosis in a significant number of cases. It is well appreciated that even expert pathologists in the sarcoma field may misinterpret a significant number of STB tumors when relying on morphology and immunohistochemistry. Italiano et al.[4] reported that the initial histological diagnosis was refined by the molecular findings in 53/384 cases (14%). This thesis consists of two parts. First, we explored novel technologies to diagnose STB tumors, namely the Cellient™ cell block method and the Nanostring FusionPlex hybridization assay. Second, we studied the significance of novel molecular methods for diagnosing rare STB tumors, in particular myoepithelial tumors, ossifying fibromyxoid tumor, soft tissue aneurysmal bone cyst, and desmoplastic fibroma of bone. Given the relative rarity of these uncommon STB tumors, the study of larger series may profit from national or international collaboration. For the studies included in this thesis, data were shared by colleagues from Leiden University Medical Center, Radboud Medical Center Nijmegen, and Memorial Sloan Kettering Cancer Center (MSKCC, New York).

Part 1: Novel technology in diagnosis soft tissue and bone tumors

A. The Cellient™ automated cell block technology

Cytology is rarely applied for the diagnosis of STB tumors. Prompted by promising results obtained in other tumor types[5,6], we studied 20 STB tumors (8 primary lesions and 12 secondary or metastases) using the Cellient™ cell block method (Chapter 2). Compared with traditional cell block methods, this fully

automatic method produces a cell block within 1 hour, thus the diagnosis can be made on the same day. We noted that the morphological details of tumor cells could be well appreciated in small tumor tissue fragments (so-called minibiopsies). After optimization of the IHC protocols, we could apply 14 diagnostically relevant antibodies for diagnosing STB tumors. The IHC results provided clinically important information in all cases, for instance, GIST was positive for CD117 and DOG-1 and a PEComa showed positive IHC staining for actin, desmin and HMB-45. In the group of 12 secondary tumors, SATB2 was visualized in metastatic osteosarcoma, whereas expression of S-100 was present in two secondary chondrosarcomas. Metastatic chordoma could be confirmed by brachyury expression. Two metastatic alveolar rhabdomyosarcomas were myf4 positive, a metastasis of a gynecologic leiomyosarcoma was positive for actin and ER and a recurrent dermatofibrosarcoma protuberans expressed CD34. In addition, high quality DNA and RNA were preserved by this methanol-based method, allowing the use of molecular techniques. For instance, as shown in a previous publication by our group, using FISH, a SS18 break apart signal allowed a definitive diagnosis of a synovial sarcoma[5]. More recently, using NanoString nCounter FusionPlex, we were able to detect an *EWSR-WT1* fusion in a desmoplastic small round cell tumor processed by Cellient™ , using an RNA input concentration of 77ng/ul (personal observation). In selected cases, Cellient processing of fine-needle aspiration (FNAC) material and body fluids, is a good alternative for molecular studies that can be applied with tumor cell material with limited amounts of DNA and RNA. This requires further study.

B. The NanoString hybridization assay

Molecular technologies continue to improve and become cheaper and user-friendlier. We evaluated the NanoString nCounter FusionPlex hybridization assay by using 174 unique specific probes for gene fusion detection in 22 different soft tissue tumors (Chapter 3). The sensitivity and specificity of the NanoString assay, using an alternative molecular method as a gold standard, was 85% and 100%, respectively. By combining our results with those of the initial study by Chang et al.[7], we concluded that the NanoString assay is a promising screening tool with an excellent diagnostic coverage for the detection of fusion

transcripts in five sarcomas, including Ewing sarcoma, synovial sarcoma, myxoid liposarcoma, alveolar rhabdomyosarcoma, and desmoplastic small round cell tumor. The cost effectiveness and short turn-around time of a NanoString analysis is a strong argument for the replacement of FISH and RT-PCR as the initial screening test for these particular sarcoma types. Moreover, we showed that the relative value of the NanoString assay was strongly associated with the level of diagnostic evidence in daily practice, indicating that the method is best applied with tumors with typical morphology and IHC profile. Its diagnostic yield for rare soft tissue tumors is limited and might require additional or alternative testing, e.g. next generation sequencing. Further improvement of the assay can likely extend its diagnostic value to other sarcoma subtypes.

Part 2: Applying molecular techniques in diagnostic pathology

Chapter 4 contains a literature review of myoepithelial tumors (METs) of bone (BMETs), a rare but distinct tumor entity. BMETs have a wide age range, may involve any part of the skeleton, and have a variable spindle cell and epithelioid morphology with myxohyaline stroma. By IHC, BMETs often express cytokeratins and/or EMA together with S100, GFAP or calponin. Nearly half of the BMETs harbor recurrent *EWSR1* (and rare *FUS*) gene fusions. Several different fusion partners have been described, including *POU5F1, PBX1, PBX3, and KLF17*. Additional fusion partners detected in soft tissue tumor METs are *ZNF444* and *ATF1*. In a recent collaborative study of a large series of 66 genetically confirmed MET of soft tissue and bone[8], it appeared that *EWSR1-POU5F1* occur with predilection in malignant MET in children and young adults and these tumors have a nested epithelioid morphology and clear cytoplasm. In contrast, *EWSR1/FUS-PBX1/3* fusions are associated with benign and sclerotic spindle cell morphology, whereas MET with *EWSR1-KLF17* show a chordoma-like morphology. Importantly, these molecular abnormalities may allow discrimination of MET from ossifying fibromyxoid tumors (OFMT), as discussed in Chapter 5.

Ossifying fibromyxoid tumor (OFMT) is an uncommon mesenchymal neoplasm of uncertain differentiation and intermediate malignant potential. Recurrent *PHF1* gene rearrangements are detected in up to 80% of OFMTs. We describe the clinicopathologic features of five OFMTs harboring a novel *PHF1-TFE3* fusion. In two cases, RNA sequencing identified a fusion transcript composed of *PHF1* exon 11 fused to *TFE3* exon 3, whereas in a third case *PHF1* exon 12 was fused to *TFE3* exon 7. A FISH break-apart assay revealed rearrangements in both *PHF1* and *TFE3* genes in all cases. The cohort included three males and two females with a median age of 64 years. One OFMT originated in the scapula, while four occurred in the deep soft tissues. Two OFMTs had typical features, whereas three were classified as malignant. Despite uniform cytologic features and fibromyxoid stroma compatible with an OFMT diagnosis, none showed a peripheral shell of lamellar bone. S100 expression was focally present in only one case, while desmin was positive in three cases. All tumors showed strong nuclear immunopositivity for TFE3. All three malignant OFMTs developed metastases, either regionally or to the lung. One patient died of disease 1 year after diagnosis, while the remaining two are alive with disease.

Aneurysmal bone cysts (ABC) rarely present in soft tissue locations (STABC). The 30 cases of STABC reported in the English literature were reviewed. Six new cases, retrieved from the files of the Netherlands Committee on Bone Tumors, were compared to the six cases described in the radiological literature (Chapter 6). On imaging, the six STABC presented as a solid or multicystic intramuscular soft tissue mass, usually with thin peripheral mineralized bone shell. On MRI, perilesional edema was visualized in nearly all cases. Fluid-fluid levels were observed in one case. All lesions had the distinct histologic features of STABC. In three cases suitable for NGS, a *COL1A1–USP6* fusion gene confirmed the diagnosis of STABC. In one additional case, FISH detected *USP6* gene rearrangement. After marginal excision, none of the six STABC recurred after a mean follow-up period of 50 months (range, 39– 187 months). On imaging, it can be difficult to discriminate between STABC and myositis ossificans. The presence of a thin bony shell and fluid-fluid levels can be helpful in discriminating these two entities. STABC is readily

diagnosed after histopathologic examination of the resection specimen. STABC belongs to the spectrum of tumors with USP6 rearrangements, which includes ABC, myositis ossificans, and nodular fasciitis.

Two cases of rare fibrous bone tumors, namely desmoplastic fibroma (DF) and low-grade central osteosarcoma (LGCOS) resembling desmoplastic fibroma (DF-like LGCOS) arrived in our lab in the same week and were studied by IHC, cytogenetics, and molecular genetics, as described in Chapter 7. It is well known that the clinical presentation, imaging features and histopathology of DF and DF-like LGOS show much overlap. Both are fibrous tumors of bone with are slowly progressive and locally aggressive, showing cortical breakthrough. Using NGS, we detected a *CTNNB1* hotspot class 5 pathogenic variant in exon 3: p.S45F, which is a gain of function mutation. Clearly, to be able to estimate the real frequency of *CTNNB1* mutations in DF, more cases have to be studied with this technique. The notion that DF-LGCOS is an osteosarcoma variant was supported by the cytogenetics and molecular genetics of our case. DF-LGCOS had a karyotype with interstitial deletion of the long arm of chromosome 13 (q12q32), consistent with loss of the *RB1* tumor suppressor gene, a genetic abnormality found in a substantial number of osteosarcomas. Moreover, cancer hotspot NGS analysis revealed amplification of *CDK4* and IHC showed overexpression of CDK4.

Future perspectives

So far, about 150 different fusion transcripts have been identified in around one-third of soft tissue tumors, 10% of which are shared by bone tumors[9]. A large proportion of STB tumors have not been explored for possible gene defining fusions or other molecular aberrations. This is mainly due to two factors[9,10]. First, many STB tumors are extremely rare. Therefore, molecular studies of larger series of rare STB tumors can only be performed by collaboration between national and international sarcoma centers[11]. Second, more information is to be gained in the group of genetically complex STB tumor types, e.g. by the use of whole genome or exome sequencing. To date only few laboratories worldwide apply RNA-sequencing, but it is to be expected that new sophisticated molecular techniques with broader coverage will gradually replace traditional molecular assays for detection of gene fusions, gene mutations or gene amplifications[11].

Importantly, in the past decade, the cost of RNA-sequencing has decreased substantially. Thus, one may expect that future techniques may become more affordable and accessible for research and diagnosis. Finally, (publicly available) gene expression profiles obtained from RNA-seq methods may be analyzed by deep learning methods (artificial intelligence), which may give more insight into signaling networks involved in STB tumors and possibly identify therapeutic targets that may benefit patients with these rare diseases[12,13].

Inarguably, the importance of molecular pathology in the diagnosis of STB tumors should not be underestimated. In the near future, it is to be expected that new molecular data and sophisticated analysis of gene expression data will provide more insight into the complex landscape of this heterogeneous group of tumors.

References

1. Lam SW, Cleton-Jansen AM, Cleven AHG, et al. Molecular Analysis of Gene Fusions in Bone and Soft Tissue Tumors by Anchored Multiplex PCR-Based Targeted Next-Generation Sequencing. *J Mol Diagn.* 2018;20(5):653-663.
2. Lam SW, van IDGP, Cleton-Jansen AM, Szuhai K, Bovee J. Molecular Pathology of Bone Tumors. *J Mol Diagn.* 2019;21(2):171-182.
3. Puls F, Niblett AJ, Mangham DC. Molecular pathology of bone tumours: diagnostic implications. *Histopathology.* 2014;64(4):461-476.
4. Italiano A, Di Mauro I, Rapp J, et al. Clinical effect of molecular methods in sarcoma diagnosis (GENSARC): a prospective, multicentre, observational study. *Lancet Oncol.* 2016;17(4):532-538.
5. van Hemel BM, Suurmeijer AJ. Effective application of the methanol-based PreservCyt() fixative and the Cellient() automated cell block processor to diagnostic cytopathology, immunocytochemistry, and molecular biology. *Diagn Cytopathol.* 2013;41(8):734-741.

6. Montgomery E, Gao C, de Luca J, Bower J, Attwood K, Ylagan L. Validation of 31 of the most commonly used immunohistochemical antibodies in cytology prepared using the Cellient((R)) automated cell block system. *Diagn Cytopathol.* 2014;42(12):1024-1033.
7. Chang KTE, Goytain A, Tucker T, et al. Development and Evaluation of a Pan-Sarcoma Fusion Gene Detection Assay Using the NanoString nCounter Platform. *J Mol Diagn.* 2018;20(1):63-77.
8. Suurmeijer AJH, Dickson BC, Swanson D, et al. A morphologic and molecular reappraisal of myoepithelial tumors of soft tissue, bone, and viscera with EWSR1 and FUS gene rearrangements. *Genes Chromosomes Cancer.* 2020.
9. Mertens F, Antonescu CR, Mitelman F. Gene fusions in soft tissue tumors: Recurrent and overlapping pathogenetic themes. *Genes Chromosomes Cancer.* 2016;55(4):291-310.
10. Marino-Enriquez A, Bovee JV. Molecular Pathogenesis and Diagnostic, Prognostic and Predictive Molecular Markers in Sarcoma. *Surg Pathol Clin.* 2016;9(3):457-473.
11. Dickson BC, Swanson D. Targeted RNA sequencing: A routine ancillary technique in the diagnosis of bone and soft tissue neoplasms. *Genes Chromosomes Cancer.* 2019;58(2):75-87.
12. Van IJzendoorn DGP, Szuhai K, Briaire-de Bruijn IH, Kostine M, Kuijjer ML, Bovee J. Machine learning analysis of gene expression data reveals novel diagnostic and prognostic biomarkers and identifies therapeutic targets for soft tissue sarcomas. *PLoS Comput Biol.* 2019;15(2):e1006826.
13. Mathews JC, Pouryahya M, Moosmuller C, Kevrekidis YG, Deasy JO, Tannenbaum A. Molecular phenotyping using networks, diffusion, and topology: soft tissue sarcoma. *Sci Rep.* 2019;9(1):13982.

Appendix

Chapter 9

Nederlandse samenvatting

Nederlandse samenvatting

Hoofdstuk 1 is een algemene inleiding in de pathologie van weke delen- en bottumoren (WDBT), waarbij het belang van moleculaire pathologie bij de diagnostiek van deze zeldzame tumoren wordt benadrukt.

Cytologie kan in bepaalde omstandigheden behulpzaam zijn bij de diagnostiek van deze tumoren. In **hoofdstuk 2** hebben we 20 WDBT (8 primaire tumoren en 12 secundaire tumoren of metastasen) bestudeerd met behulp van de Cellient^{TM} celblok methode. We merkten op dat de morfologische details van tumorcellen in kleine tumorfragmenten goed werden gevisualiseerd. Na optimalisatie van immunohistochemie (IHC) protocollen konden we 14 diagnostisch relevante antilichamen toepassen. De IHC-resultaten gaven in alle gevallen klinisch belangrijke informatie. Bovendien bleken het DNA en RNA van het tumorweefsel goed te zijn geconserveerd met de toegepaste methanol fixatie, waardoor het gebruik van moleculaire technieken mogelijk was.

Hoofdstuk 3 beschrijft de betrouwbaarheid van NanoString als diagnostische methode. We hebben de NanoString nCounter FusionPlex-hybridisatietest geëvalueerd met behulp van 174 unieke specifieke probes voor genfusie detectie in 22 verschillende weke delen tumoren. Vergeleken met een andere diagnostische moleculaire methode als gouden standaard, waren de sensitiviteit en specificiteit van de NanoString-test respectievelijk 85% en 100%. Door onze resultaten te combineren met die van de oorspronkelijke studie van Chang et al., concluderen we dat de NanoString-test een veelbelovende screenings tool, die bij uitstek geschikt is voor de detectie van fusietranscripten in vijf sarcomen, te weten Ewing-sarcoom, synoviaal sarcoom, myxoid liposarcoom, alveolair rabdomyosarcoom en desmoplastische kleincellige rondcellige tumor. Bovendien toonden we aan dat de relatieve waarde van de NanoString-test geassocieerd was met het niveau van diagnostisch bewijs in de dagelijkse praktijk. De methode kan het best worden toegepast bij WDBT met typische morfologie en bijpassend IHC-profiel.

Hoofdstuk 4 bevat een literatuuroverzicht van myoepitheliale tumoren (MET's) van het bot (BMET's), een zeldzame tumorentiteit. Vanwege de zeer variabele morfologie en weinig specifieke immunoprofiel, is

de differentiële diagnose van BMET's breed. Bijna de helft van de BMET's bevat kenmerkende *EWSR1* (en zeldzame *FUS*) genfusies. Door het aantonen van deze moleculaire afwijkingen kunnen MET worden onderscheiden van andere tumoren, bijvoorbeeld ossificerende fibromyxoïde tumoren (OFMT), een tumor die wordt bestudeerd in hoofdstuk 5.

Ossificerende fibromyxoïde tumor (OFMT) is een zeer zeldzame mesenchymale tumor met onduidelijke cellulaire differentiatie en intermediaire kwaadaardige potentie. In **hoofdstuk 5** van dit proefschrift beschrijven we de klinisch-pathologische kenmerken van vijf OFMTs gekenmerkt door een nieuwe *PHF1-TFE3* genfusie, aangetoond met RNA-sequencing (RNA seq) en/of FISH. Ondanks uniforme cytologische kenmerken en fibromyxoid stroma compatibel met een OFMT-diagnose, bevatte geen van deze tumoren een perifere schaal van lamellair bot. Slechts één OFMT toonde S100 expressie, terwijl alle sterke nucleaire aankleuring voor TFE3 lieten zien.

In **hoofdstuk 6** bespreken we zes gevallen van een zeldzame aneurysmatische botcyste ontstaan in de weke delen (STABC). Alle tumoren hadden de typische histologische kenmerken van STABC. Met NGS vonden we in drie gevallen een *COL1A-USP6* fusiegen en FISH detecteerde *USP6* genherrangschikking in één extra geval. Bij beeldvormend onderzoek overlappen de kenmerken van STABC met die van myositis ossificans. Echter, STABC kan goed worden gediagnosticeerd met histopathologisch onderzoek van het resectiepreparaat. STABC behoort tot het spectrum van tumoren met *USP6* herschikkingen, waaronder ABC, myositis ossificans en nodulaire fasciitis.

In **hoofdstuk 7** gaan we dieper in op de differentiële diagnose van twee bottumoren namelijk het desmoplastisch fibroom (DF) van het bot en het laaggradig centraal osteosarcoom (LGCOS). De klinisch-pathologische kenmerken en histologische kenmerken van DF en LGCOS tonen sterke overeenkomsten. Met behulp van NGS hebben we een *CTNNB1* p.S45F mutatie gevonden in de DF casus. De LGCOS casus had een karyotype met interstitiële deletie van de lange arm van chromosoom 13 (q12q32), hetgeen gepaard gaat met verlies van het *RB1* tumorsuppressorgen, een genetische afwijking die o.a. in osteosarcomen wordt aangetroffen. Bovendien werd met NGS-analyse amplificatie van *CDK4* in de

LGCOS aangetoond, hetgeen zich vertaalt in CDK4 overexpressie met IHC, hetgeen tamelijk kenmerkend is voor deze tumor.

Hoofdstuk 8 bevat een samenvatting en discussie van dit proefschrift. Hierin wordt tevens een toekomstperspectief van moleculaire pathologie bij de weefseldiagnostiek van WDBT geschetst.

Chapter 10

Acknowledgements

Acknowledgements

These past four years have flown by, and I can't believe they are coming to an end and I am marching to the defence of my thesis. I wouldn't have achieved this success without the support and help I have received. Appreciation is a wonderful thing and I would like to acknowledge mine.

First, I would like to thank my supervisor Prof. Albert Suurmeijer. I still remember the first time we met each other. You said to me: "if you have any questions, just come to my office and ask me". Following your "instruction", in the past four years, I have stepped into your office without an appointment for a hundred times. Thank you for always keeping an open door for me and the problems that challenged me during my study, therefore, have been dealt with promptly and properly. It is one of the reasons why our projects can progress smoothly. I have enjoyed all the projects I worked together with you. Personally, you are not only my supervisor but also my mentor of life and a good friend. I enjoyed very much the sharing and talking when we drove to Leiden. Thanks for your invaluable input and for always encouraging me to be the best I can be.

I also want to express my sincere gratitude to my second supervisor, Prof. Judith Bovée. Your expertise amazes me all the time. It has been a nice experience of working together on the desmoplastic fibroma and soft tissue ABC article. You've helped me to achieve my ambition. Thank you!

Dear Prof. Haary Hollema, Prof. Paul van der Valk and Prof. Winand Dinjens, thank you so much for taking time out of your busy schedule to read my thesis and provide insightful remarks.

I would like to extend my sincere gratitude to my paranymphs Goek Wee and Pei. Thank you for being the support at this special moment. I wish all the best for you, I am looking forward to celebrating your defense ceremony in the coming future.

My deepest gratitude also goes to Prof. Anke van den Berg, Dr. Lydia Visser, Dr. Joost Kluiven and Dr. Lotteke Swier. Thank you for including me as a group member and inviting me to the group activities. Your continuous support and encouragement have given me strength throughout my study.

I wish to thank each of my co-authors and colleagues for helping me with my articles, Dr. Bettien van Hemel, Teus Ruitenbeek, Inge, Léon, Jolanda Haarsma, Dr. Thomas C. Kwee, Dr. Paul C. Jutte, Dr. Sanne Molenkamp and Henk Buikema. Without your help, it would not have been possible for me to achieve my PhD degree.

I would like to extend my gratitude to all PhD students from the department of pathology, Yichen Liu, Pei Meng, PeiJia Jiang, Fubiao Niu, Goek Wee, Mathilde, Myra, Sofia, Xin Zhao, Melanie, Johanna, Yuan Ye, and Jiacong Wei. I will never forget the delicious homemade food from each of you. Keep it up, and achieve the best chef among the PhD's.

To my dear colleagues, thank you for your assistance during the past three years, Dr. Jan Doff, Dr. Erwin Geuken , Dr. NK de Boer, Dr. Stefano Rosati, Dr. Gilles Diercks, Dr. Corry-Anke Brandsma, Dr. Evert van den Broek, Dr. Marcel Dijkstra, and Marco Abma.

I would love to express my gratitude to my previous supervisors back in China who inspired me to pursue a scientific career, Prof. Wenfeng Cao and Prof. Lisha Qi. In addition, a big thank you goes to my previous colleagues Lingmei Li l and Lu Cao, who added fuel to this pursuit during my master study time.

I am also deeply indebted to my friend, my language partner Tijskte. We have been knowing each other for about 2 years. I really appreciate you sharing your stories with me. Thank you for helping me improve my Dutch skills. I have this image of you as always being cheerful and optimistic, even in difficult situations. I wish all the best to you and Jurjen.

A big thank-you to my dear friends for continuous support. Haoqi Chen, Lin Chen, Elias, Haritt, Huimin Ke, Jing Wu, Yufang Zhang, Wenjun Tao, Hailun Zhou, Xiao Zhao. Special thank you goes to Lu Wang and Min Wang, thank you for always being there for me.

My heartfelt gratitude goes to my friend André, thank you for helping me through the difficult time. I can't thank you enough for your constant unconditional support and encouragement both in my career and my life as well.

In the end, I wish to thank my parents. Dear mama and baba, I am eternally grateful for your unconditional support and wholehearted encouragement. The parenting roles you have plaid in my life is invaluable. I can never thank you enough for guiding me to the right direction. Success is in my stride because I have parents like you by my side. (最后，我要感谢我的父母，谢谢你们无条件的鼓励和支持. 在我成长过程中你们所给于我的教育是无价的，在人生观的树立中，再多的感激也道不尽在树立正确人生观上给我指导。正是有了你们这样的父母，在前进的路上我从不会感觉孤单.)

It would be impossible to list all the names who showed their kindness to me, I just want to say thank you to all the people who helped me in various ways.

Chapter 11

Curriculum vitae and list of publications

Curriculum vitae

Name: Wangzhao Song

Birth: 03/16/1989

EDUCATION:

Novem.2016- Novem.2020 PhD training of Medical Science, Major in pathology, University of Groningen, Groningen, The Netherlands

Sept.2013-Jun.2016 Master of Medical Science, Major in pathology, Tianjin Medical University, Tianjin, China.

Sept.2007-Jun.2012 Bachelor of Medical Science, Major in Clinical Medicine, Henan University of Science and Technology, Luoyang, China.

RESEARCH EXPERIENCE:

Projects during the PhD. study (supervised by Prof. A.J.H. Suurmeijer and Prof. J.V.M.G. Bovée):

Molecular Diagnostics of Uncommon Soft Tissue and Bone Tumors.

Projects during the master study (supervised by Prof. Wenfeng Cao and Prof. Lisha Qi):

1. The mechanisms of FGF-induced epithelial-mesenchymal transition in lung adenocarcinoma.
2. Based on Next-generation sequencing to identify the driven-gene of endometrial cancer that guided personalized therapy
3. The effect of acidic microenvironment regulatory protein ATP6L in tumor angiogenesis and the relevant mechanism.

CONFERENCES AND COURSUS:

2020 ESMO Sarcoma and GIST Symposium 2020. Milan, Italy.

2019 31st European Congress of Pathology. Nice, France.

2019 A multidisciplinary approach to the diagnosis of bone tumours. Leiden, The Netherland.

2019 ESMO Advanced Course on NTRK Gene Fusion: A new target in precision treatment of cancer. Barcelona, Spain.

2019 ESMO Advanced Course on Biomarkers for Precision Medicine. Zurich, Switzerland.

2018 The Connective Tissue Oncology Society 2018 Annual Meeting. Rome, Italy.

List of publications

Bekers EM, **Song W**, Suurmeijer AJ, et.al. Myxoid liposarcoma of the foot: a study of 8 cases. Annals of Diagnostic Pathology, 2016 Dec;25:37-41.

Song W, Flucke U, Suurmeijer AJH, et.al. Myoepithelial Tumors of Bone. Ann Diagn Pathol. 2016 Dec;25:37-41.

Song W, van Hemel BM, Suurmeijer AJH. Suitability of the Cellient™ cell block method for diagnosing soft tissue and bone tumors. Diagn Cytopathol. 2018 Apr;46(4):299-305.

Stevenson MG, Hoekstra HJ, **Song W**, et.al. Histopathological tumor response following neoadjuvant hyperthermic isolated limb perfusion in extremity soft tissue sarcomas: Evaluation of the EORTC-STBSG response score. Eur J Surg Oncol. 2018 Sep;44(9):1406-1411.

Song W, Kwee TC, Suurmeijer AJ. Macrodactyly with a complex glomuvenous malformation in congenital lipomatous overgrowth with vascular malformations, epidermal naevi and skeletal anomalies (CLOVES) syndrome. Histopathology. 2018 Oct;73(4):705-708.

Song W, Suurmeijer AJH, Bollen SM, et.al. Soft tissue aneurysmal bone cyst: six new cases with imaging details, molecular pathology, and review of the literature. Skeletal Radiol. 2019 Jul;48(7):1059-1067.

Song W, van den Berg E, Kwee TC, et.al. Low-grade central fibroblastic osteosarcoma may be differentiated from its mimicker desmoplastic fibroma by genetic analysis. Clin Sarcoma Res. 2018 Aug 23;8:16.

Suurmeijer AJH, **Song W**, Sung YS, et.al. Novel recurrent *PHF1-TFE3* fusions in ossifying fibromyxoid tumors. Genes Chromosomes Cancer. 2019 Sep;58(9):643-649

Wangzhao Song, Inge Platteel, Albert J. H. Suurmeijer et.al. Diagnostic yield of NanoString nCounter FusionPlex profiling in soft tissue tumors. Genes Chromosomes Cancer, 2020 May; 59(5): 318–324.